University of Salerno

Department of Chemistry and Biology
"Adolfo Zambelli"

PhD Course in Chemistry

XXXIV Cycle

Thesis on

Synthesis of New Naphthol-Based Macrocycles for Supramolecular Applications

Tutor:
Prof. Carmine Gaeta
Co-Tutor:
Prof. Aldo Spinella

PhD Student
Rocco Del Regno
8800100047

PhD Coordinator:
Prof. Claudio Pellecchia

Academic Year 2021-2022

Abstract

Nature has always inspired supramolecular chemists who, with the aim to mimic the structural features of the natural receptors, have designed artificial systems with amazing functions and properties. Therefore, in the last two decades, macrocyclic compounds based on naphthalene or anthracene units have been reported, with the aim of obtaining new supramolecular hosts embedding deep π-electron-rich aromatic cavity.[a]

Prompted by these considerations, during this PhD project, I focused my efforts on the synthesis of novel naphthol-based macrocycles. Thus, prismarenes[b] (**a** in **Figure**) and the calix[2]naphtha[2]arene[c] (**b** in **Figure**) have been obtained and their supramolecular properties were investigated.

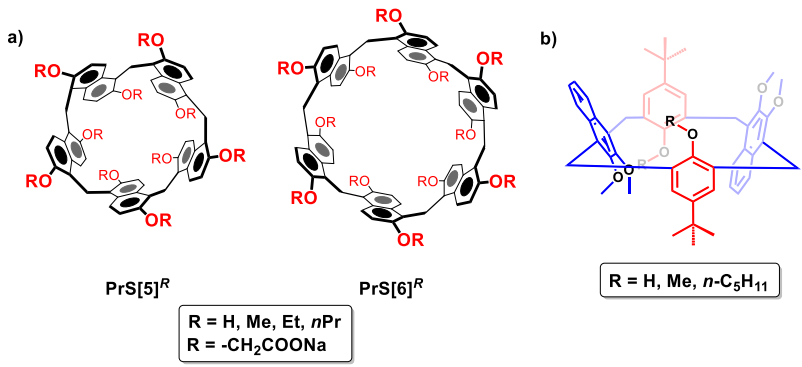

Figure. (a) Chemical drawing of prism[n]arenes; (b) Chemical drawing of the calix[2]naphtha[2]arene.

[a] Yao, H.; Jiang, W. *Naphthol-Based Macrocycles*, in Handbook of Macrocyclic Supramolecular Assembly, Springer, Singapore, **2019.**

Methoxy-based prism[n]arenes (n = 5 and 6),[b] were formed by exploiting thermodynamic intermolecular templating effects with alkylammonium-guests. [b] Differently, the formation of prismarenes bearing longer alkyl chains,[d] such as ethyl or propyl groups, was obtained by a thermodynamic intramolecular self-templating effect due to the alkyl chains, which drive the macrocyclization toward the formation of the hexameric derivatives.[d]
Prismarenes were found to be interesting for their molecular recognition properties: in fact, their π-electron rich deep cavities can host ammonium guests by cation···π and $^{+}$NC−H···π interactions.[b,d]
We have also investigated a procedure for the synthesis of *per*–hydroxylated prism[n]arenes **PrS[n]*OH*** (n = 5 and 6).[e] In details, **PrS[5]*Me*** can be efficiently demethylated by a supramolecularly assisted reaction in the presence of tetramethylammonium iodide. **PrS[n]*OH*** can be considered as useful synthetic precursors to obtain novel hosts with intriguing supramolecular properties. In fact, starting by *per*–hydroxylated prism[n]arenes **PrS[n]*OH*** (n

[b] Della Sala, P.; Del Regno, R.; Talotta, C.; Capobianco, A.; Hickey, N.; Geremia, S.; De Rosa, M.; Spinella, A.; Soriente, A.; Neri, P.; Gaeta, C. *J. Am. Chem. Soc.* **2020**, *142*, 1752-1756. Highlighted in: Yang, L.-P.; Jiang, W. *Angew. Chem. Int. Ed.* **2020**, *59*, 15794-15796.
[c] Del Regno, R; Della Sala, P.; Spinella, A.; Talotta, C.; Iannone, D.; Geremia, S.; Hickey, Neal; Neri, P.; Gaeta, C. *Org. Lett*. **2020** , *22,* 6166–6170.
[d] Della Sala, P.; Del Regno, R.; Di Marino, L.; Calabrese, C.; Palo, C.; Talotta, C.; Geremia, S.; Hickey, N.; Capobianco, A.; Neri, P.; Gaeta, C. *Chem. Sci.* **2021**, *12*, 9952-9961.
[e] Del Regno, R.; Della Sala, P.; Picariello, D.; Talotta, C.; Spinella, A.; Neri, P.; Gaeta, C. *Org. Lett.* **2021**, *23*, 8143–8146.

= 5 and 6), water-soluble prism[n]arenes (n = 5 and 6) bearing carboxylato anionic groups were obtained.[f]
Carboxylato-prism[*n*]arenes (*n* = 5 and 6), **PrS[5]^{COONa}** and **PrS[6]^{COONa}** were able to form complexes with organic ammonium cations **G^{n+}@PrS[n]$^{COO-}$** (n = 5 and 6) in water as confirmed by NMR titration experiments. ITC studies showed that the complexation processes, are driven by different thermodynamic factors depending on prismarene size and cation charge.
Finally, we obtained a new class of phenol−naphthalene hybrid macrocycles, named calix[2]naphth[2]arenes.[c] X-ray studies show that calix[2]naphth[2]arene adopts a rare 1,2-alternate conformation (**b** in **Figure**). Moreover, this conformation is also observed when alkali metal cations are added to the solution of host.

[f] Del Regno, R.; Santonoceta, G. D. G.; Della Sala, P.; De Rosa, M.; Soriente, A.; Talotta, C.; Spinella, A.; Neri, P.; Sgarlata, C.; Gaeta, C. *Org. Lett.* **2022**, *24*, 2711-2715.

Table of Contents

1.0 Introduction

1.1 Supramolecular Chemistry

Supramolecular chemistry was defined by Jean-Marie Lehn as: *"……the chemistry of the intermolecular bond, covering the structures and functions of the entities formed by the association of two or more chemical species."* [1] It deals with complex systems resulting by the chemical association of two or more molecules held together by secondary interactions. [2] The key feature in supramolecular chemistry is the *selectivity* with which the different molecular components bind to form supramolecular complexes, namely *molecular recognition.*[3]

Molecular recognition plays a crucial role in all biological processes and in supramolecular chemistry and may provide basic prototypes for some of the problems in the fields of biomedical science, catalysis, materials science, and environmental science.[4]

In molecular recognition processes we make a basic distinction between the two components, named host and guest, the larger molecule and the smaller one,

---

[1]Lehn, J. M. *Supramolecular Chemistry*, *Concepts and Perspectives*, Wiley-VCH, Weinheim, **1995**.

[2] (a) Lehn, J.-M. *Proc. Natl. Acad. Sci*. **2002**, *99*, 4763 – 4768; (b) Klärner, F. G.; Schrader, T. *Acc. Chem. Res*. **2013**, *46*, 967–978; (c) Wang, D.-X.; Zheng, Q.-Y.; Wang, Q.-Q.; Wang, M.-X. *Angew. Chem. Int. Ed.* **2008**, *47*, 7485-7488.

[3] Cram, D. J. *Angew. Chem. Int. Ed. Engl*., **1988**, *27*, 1009-1020.

[4] (a) Yang, L.-P.; Wang, X.; Yao, H.; Jiang, W. *Acc. Chem. Res.* **2020**, *53*, 198−208; (b) Heid, C.; Sowislok, A.; Schaller, T.; Niemeyer, F.; Klärner, F.-G.; Schrader, T. *Chem. Eur. J.* **2018**, *24*, 11332–11343.

respectively, which are associated by secondary interactions[2]. Molecular recognition is the basis of many biological processes such as, substrate@enzyme recognition, immunological antigen@antibody association, translation and transcription of the genetic code, signal transmission through neurotransmitters and cellular recognition.[5]

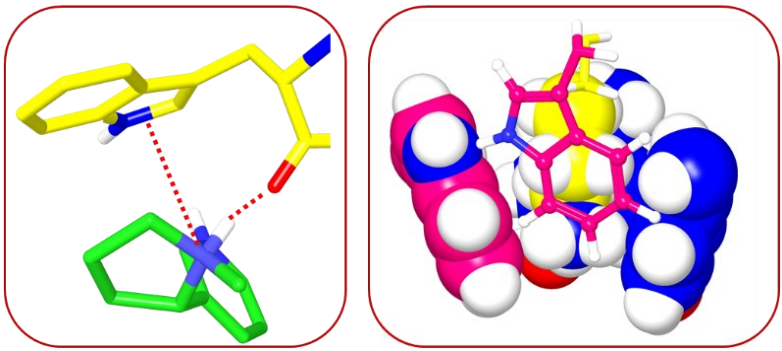

Figure 1. (Left) Particular of the interaction of nicotine (green) with the TrpB residue (yellow) in the X-ray structure of the complex between nicotine and acetylcholine binding protein.[6b] (Right) Particular of the four cation−π interactions observed in the glucoamylase X-ray structure[6c].

Thus, for example, α4β2[6a] neuronal receptor shows an aromatic cavity constituted by Trp and Tyr residues, which has high affinity for the nicotine substrate due to cation−π

[5] Nelson, D. L.; Cox, M. *Lehninger Principles of Biochemistry: Int. Ed.*, WH Freeman, **2017**.

[6] (a) Xiu, X.; Puskar, N. L.; Shanata, J. A. P.; Lester, H. A.; Dougherty D. A. *Nature* **2009**, *458*, 534−538; (b) Celie, P. H.; Van Rossum-Fikkert, S. E.; Van Dijk, W. J.; Brejc, K.; Smit, A. B.; Sixma, T. K. *Neuron* **2004**, *41*, 907–914; (c) Aleshin, A. E.; Stoffer, B.; Firsov, L. M.; Svensson, B.; Honzatko, R. B. *Biochemistry* **1996**, *35*, 8319-8328.

interactions between the positively charged nicotine $^{+}$NH group and the aromatic rings - **Figure 1**, **left**.[6b]
Finally, another interesting example is the glucoamylase X-ray structure in which four cation−π interactions (**Figure 1, right**) have been observed between a residue of lysine (yellow) and four aromatic rings of tryptophane.[6c]

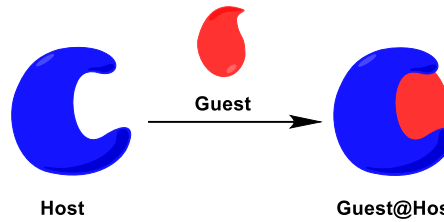

Figure 2. Host-Guest Complexation.

The binding of a guest with its host leads, then, to the formation of a supramolecular host-guest complex by a molecular recognition process (**Figure 2**).[2]
Host-guest recognition processes can be described through an association constant which is given by the following equation:

$$H + G \rightleftharpoons (H@G)$$

$$K = \frac{[Guest@Host]}{[Host]x[Guest]}$$

The ability of a host H to discriminate between two G_1 and G_2 guests, is called **selectivity (S)**,[7] and is given by the ratio of the association constants $S = K_1/K_2$:

[7] Steed, J.W.; Turner, D. R.; Wallace, K. J. in *Core concepts in Supramolecular Chemistry and Nanochemistry*, Chapter 1, WILEY, West Sussex - UK, **2007**.

$$H + G_1 \longrightarrow HG_1 \qquad K_1 = \frac{HG_1}{[H]\,x\,[G_1]}$$

$$S = \frac{K_1}{K_2}$$

$$H + G_2 \longrightarrow HG_2 \qquad K_2 = \frac{HG_2}{[H]\,x\,[G_2]}$$

A good host can recognize its specific guest with high thermodynamic stability (high *K* values) and good selectivity (high S values).

In supramolecular chemistry, macrocycles play a crucial role in the development of new hosts. Macrocyclic hosts, show peculiar structural properties that make them particularly versatile in molecular recognition processes. First, taking inspiration by natural bioreceptors, macrocycles possess internal cavities that embedded binding sites complementary to the guest. The cyclic structure ensures a good conformational stability, namely macrocyclic hosts are more **preorganized**[8] than the linear analogues. The preorganization permits to the host to interact with the guest without significant conformational changes, and this aspect plays a crucial role for the thermodynamic and kinetic stability of the supramolecular complexes. In fact, macrocyclic hosts, form more stable host-guest complexes if compared to their linear analogous (podands).[7] In detail, a free podand host can assume many linear conformations, while upon complexation with the guest only a conformation can be adopted in which the guest is centrally wrapped. As a result, a great loss of degrees of freedom will occur ($\Delta S<0$). Instead, macrocyclic hosts have a cavity already

[8] (a) Cram, D. J. *Angew. Chem., Int. Ed. Engl.,* **1986**, *25*, 1039-1134. (b) Cram, D. J. *Science* **1988**, *240*, 760-767.

preorganized for complexation with the guest, and consequently the ΔS of binding is more favourable. This aspect, strongly connected to preorganization, is named as "**macrocycle effect**", which plays a fundamental role for the thermodynamic stability of the complexes- **Figure 3**.[9]

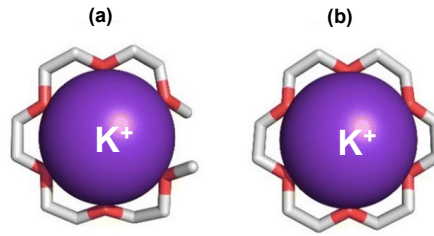

Figure 3. The macrocycle effect: (a) K^+@Pentaglyme (the podand analogue of [18]-Crown-6); (b) K^+@[18]-Crown-6.[10]

However, the presence of a preorganized system with a large contact area is not sufficient to ensure optimal secondary interactions. Accordingly, a high recognition is also related to the steric and electronic **complementarity** between interacting surfaces, which ensure a high selectivity in the molecular recognition.[11]

Based on these considerations, we can conclude that, in molecular recognition processes, macrocyclic hosts

[9] Cabiness, D. K.; Margerum, D. W. *J. Am. Chem. Soc.* **1969**, *91*, 4092-4093.

[10] Meisel, J. W.; Hamilton, A. D. in *Supramolecular Protein Chemistry: Assembly, Architecture and Application*, Chapter 1, Monographs in Supramolecular Chemistry; Crowley, P. B. Ed; Royal Society of Chemistry: Cambridge, **2020**.

[11] Atwood, J. L.; Steed, J. W. in *Encyclopedia of Supramolecular Chemistry*, CRC Press, **2004**.

ensure higher thermodynamic and kinetic stabilities than the analogous podands.

1.2 Macrocycles in Supramolecular Chemistry

In the last decades particular attention has been focused on cyclophane macrocycles such as, calix[n]arenes[12], resorcinarenes[13], and pillar[n]arenes[14], which have shown interesting applications as sensors[15], materials[16], catalysts[17], pharmaceutical[18] and molecular machines[19].

---

[12] Neri, P; Sessler J. L.; Wang M.-X. (Eds.), *Calixarenes and Beyond*, Springer, Dordrecht, **2016**.

[13] Cram, D. J.; Cram J. M. in *Container Molecules and Their Guests*, Monographs in Supramolecular Chemistry; Stoddart, J. F. Ed; Royal Society of Chemistry: Cambridge, **1994.**

[14] Ogoshi, T.; Gale, P.; Steed, J.; *Pillararenes*, The Royal Society of Chemistry: Cambridge, **2016**.

[15] a) Bell, T. W.; Hou, Z.; Luo, Y.; Drew, M. G. B.; Chapoteau, E.; Czech, B. P.; Kumar, A. *Science*, **1995**, *269*, 671- 674. (b) Lavigne, J. J.; Anslyn, E. V. *Angew. Chem. Int.*, **1999**, *38* (24), 3666-3669. (c) Chen, J.-F.; Cheng, X.-B.; Li, H.; Lin, Q.; Yao, H.; Zhang, Y.-M.; Wei, T.-B. *New J. Chem.*, **2017**, ***41***, 2148-2153.

[16] Hong, B. H.; Bae, S. C.; Lee, C. W.; Jeong, S.; Kim, K. S. *J. Am. Chem. Soc*. **2002**, *124*, 14268-14279.

[17] La Manna, P.; Talotta, C.; Floresta, G.; De Rosa, M.; Soriente, A.; Rescifina, A.; Gaeta, C.; Neri, P. *Angew. Chem.* **2018**, *130*, 5521 – 5526.

[18] Webber, M. J.; Langer, R. *Chem. Soc. Rev.*, **2017**, *46*, 6600-6620.

[19] Balzani, V.; Credi, A.; Venturi, M. *Molecular Devices and Machines*, WILEY-VCH Verlag GmbH & Co. KGaA: Weinheim, **2003**.

1.2.1 Cyclophanes

The family of the cyclophanes,[12-14,20] include macrocyclic compounds constituted of aromatic units linked by aliphatic bridges. As an example, calix[n]arenes[12], resorcinarenes[13] and pillar[n]arenes[14] (**Figure. 4**), are obtained by a reversible acid- or base-catalysed condensation of the respective monomers with an aldehyde. These macrocycles show bowl-shaped structures embedded with a central deep cavity which looks like to a prototype of enzymatic active site. In addition, thanks to the presence of aromatic units, the cyclophanes show higher synthetic versatility if compared to crown-ethers,[21] cryptands[22] and spherands[23].

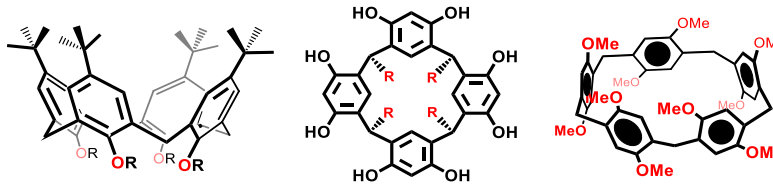

Figure 4. (a) Calix[4]arene[12], (b) Resorcin[4]arene[13], (c) Pillar[5]arene[14].

[20] Diederich, F. N. *Cyclophanes*; Royal Society of Chemistry: London, **1991**.

[21] Pedersen, C. J. *J. Am. Chem. Soc.* **1967,** *89,* 2495-2496.

[22] Lehn, J. M. *Acc. Chem. Res.* **1978**, *11*, 49–57.

[23] Dijkstra, P. J.; Brunink, J. A. J.; Bugge, K.-E.; Reinhoudt, D. N.; Harkema, S.; Ungaro, R.; Ugozzoli, F.; Ghidini, E. *J. Am. Chem. Soc.* **1989**, *111*, 7567–7575.

1.2.1.1 Calix[n]arenes

Calix[*n*]arenes[12,24] are macrocycles in which *p*-substituted phenolic units are linked together via methylene bridges. These derivatives are synthesized starting by *p*-tert-butylphenol and a source of formaldehyde, in acidic or basic conditions.[12,24]

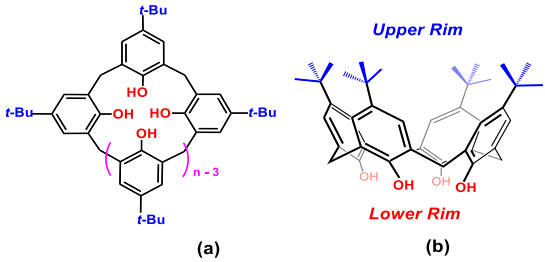

Figure 5. Structures of Calix[*n*]arenes (n = 4 - 20).[12]

The family of the calix[n]arenes consists of cyclic oligomers in which the number of phenolic units *n* ranging from 4 to 20, but the most studied are constituted by 4-8 aromatic units. [12,24]

In the last decades, many interest has been focused on bowl-shaped calixarene macrocycles, making them ubiquitous in several areas of supramolecular chemistry, where numerous interesting applications have been

[24] (a) Gutsche, C. D.; Dhawan, B.; No, K. H.; Muthukrishnan, R. *J. Am. Chem. Soc.* **1981**, *103*, 3782-3792. (b) Vicens, J.; Harrowfield, J. *Calixarenes in the Nanoworld*, Springer: Dordrecht, **2007**; (c) Gutsche, C. D. *Calixarenes Revisited*, Royal Society of Chemistry: Cambridge, **1998**; (d) Bohmer, V. *The Chemistry of Phenols*, Wiley: Chichester, **2003**; (e) Gutsche, C. D. *Calixarenes, An Introduction*, Royal Society of Chemistry: Cambridge, **2008**.

reported. This interest is undoubtedly related to their facile synthesis and conformational and synthetic versatility.[12]

1.2.1.2 Resorcin[n]arenes

Resorcin[n]arenes[13] also belong to the family of cyclophane compounds. They were synthesised in 1989 by Cram[25] starting by resorcinol in the presence of aldehyde and an acid catalyst.
Tetrameric derivative can be easily obtained under these conditions, generally using an aliphatic or aromatic aldehydes and HCl, as acid catalyst, in ethanol as solvent - **Scheme 1**.[13,25,26]

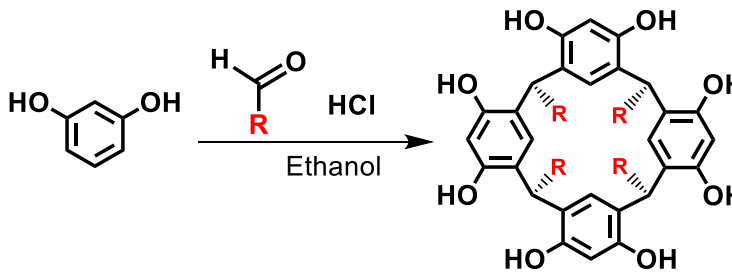

Scheme 1. Synthesis of the resorcin[4]arene developed by Cram.[25]

The resorcin[4]arene adopts, both in solution and in the solid state, a cone conformation, stabilized by intramolecular hydrogen bonds between the OH groups.[13] Particularly interesting are the self-assembly capabilities in the solid state and in solution of the resorcin[4]arene

[25] Cram, D. J. *J. Org. Chem. ,***1989**, *54,* 1305-1312.
[26] Della Sala, P.; Gaeta, C.; Navarra, W.; Talotta, C.; De Rosa, M.; Brancatelli, G.; Geremia, S.; Capitelli, F.; Neri, P. *J. Org. Chem.* **2016**, *81*, 5726-5731.

derivative, which forms, in the presence of 8 water molecules, a hexameric capsule stabilised by 60 hydrogen bonds.[27] This is still a widely studied system in the field of catalysis[17, 28, 29] and molecular storage.

1.2.1.3 Pillar[n]arenes

Pillar[n]arenes[14] (**Figure 6**), reported by Ogoshi in 2008,[30] are macrocycles consisting of 1,4-dialkoxybenzene units connected by methylene bridges at the *para* positions.[14,30] Pillar[n]arenes adopt a very peculiar pillar-shape structure.[14]

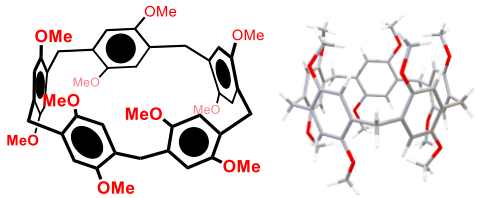

Figure 6. Chemical drawing of the Pillar[5]arene (Left); Solid state structure of the *per*-methylated Pillar[5]arene (Right).[14]

Per-methylated pillar[5]arene was obtained in 71 % of yield[31] starting by 1,4-dimethoxybenzene in the presence

[27] MacGillivray, L. R.; Atwood, J. L. *Nature* ,**1997**, *389*, 469-472.
[28] Gambaro, S.; Talotta, C.; Della Sala, P.; Soriente, A.; De Rosa, M.; Gaeta, C.; Neri, P. *J. Am. Chem. Soc.* **2020**, *142*, 14914–14923.
[29] La Manna, P.; De Rosa, M.; Talotta, C.; Gaeta, C.; Soriente, A.; Floresta, G.; Rescifina, A.; Neri, P. *Org. Chem. Front.*, **2018**, *5*, 827–837.
[30] Ogoshi, T.; Kanai, S.; Fujinami, S.; Yamagishi, T.; Nakamoto, Y. *J. Am. Chem. Soc.* **2008**, *130*, 5022-5023.
[31] Ogoshi, T.; Aoki, T.; Kitajima, K.; Fujinami, S.; Yamagishi, T.-a.; Nakamoto, Y. *J. Org. Chem.* **2011**, *76*, 328–331.

of paraformaldehyde and BF_3, as a Lewis acid catalyst, in 1,2-dichloroethane. [14,30]

The solvent plays a crucial role for the formation of pillar[5]arene. In fact, Szumna[32] investigated the effect of the solvent on this synthesis, showing that it templates the macrocyclization of the pillar[5]arene. In particular, the linear pentamer wraps itself around a solvent molecule, by promoting the macrocyclization reaction in high yields - **Figure 7a**.[14]

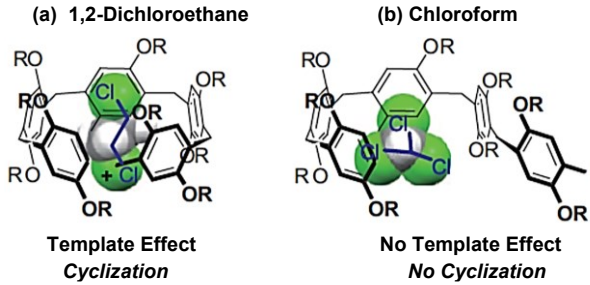

Figure 7. (a) Dichloroethane acts as template for the pillar[5]arene. (b) Chloroform does not act as a template for the cyclic pentamer.[14]

In contrast, solvents, such as chloroform, do not promote macrocyclization, leading to a complex mixture of different cyclic adducts – **Figure 7b**.[14]

In recent years a plethora of supramolecular applications of the pillararenes[14] has been reported in literature, ranging from biomedical[33] to supramolecular polymers[34],

[32] Boinski, T.; Szumna, *Tetrahedron*, **2012**, *68*, 9419-9422.
[33] Si, W; Li, Z.-T.; Hou, J.-L. *Angew. Chem.,* **2014**, *53*, 4578-4581.
[34] Zhang, Z.; Luo, Y.; Chen, J.; Dong, S.; Yu, Y.; Ma, Z.; Huang, F., *Angew. Chem.,* **2011**, *50*, 1397–1401.

which can be applied for drug delivery,[35] photovoltaic devices, [36] porous membranes, [37] and self-healing materials[38].[14]

1.2.2 Naphthalene-Based Macrocycles

Nature continually inspires scientists, who, by studying the *modus operandi* of natural systems, have obtained artificial systems with amazing functions and properties.[4a] However, the recognition ability of synthetic receptors is far from satisfactory, particularly compared with that of bioreceptors. In the last two decades several macrocyclic hosts have been reported able to form stable host−guest complexes. Nevertheless, high-performing artificial receptors are still very rare, and more are urgently needed in the field of supramolecular chemistry and beyond. In fact, usually, bioreceptors possess deep cavities that embedded binding sites. Thus, for example, the complex between HDAC2 (Histone deacetylase 2) and SAHA (Suberoylanilide hydroxamic acid) [39] confirms this structural feature (**Figure 8, Left**), in which SAHA is in the

[35] Huang, X.; Du, X., A*CS Appl. Mater. Interfaces,* **2014**, *6*, 20430–20436.

[36] Wu, Y.; Li, H.; Yan, Y.; Shan, X.; Zhao, M.; Zhao, Q.; Liao, X.; Xie, M., *ACS Macro Lett.* **2019**, *8*, 1588–1593.

[37] Ogoshi, T.; Takashima, S.; Yamagishi, T.-a., *J. Am. Chem. Soc.* **2015**, *137*, 10962–10964.

[38] Zhao, M.; Li, C.; Shan, X.; Han, H.; Zhao, Q.; Xie, M.; Chen, J.; Liao, X., *Molecules*, **2021**, *26*, 2191-2201.

[39] Lauffer, B. E. L.; Mintzer, R.; Fong, R.; Mukund, S.; Tam, C.; Zilberleyb, I.; Flicke, B.; Ritscher, A.; Fedorowicz, G.; Vallero, R.; Ortwine, D. F.; Gunzner, J.; Modrusan, Z.; Neumann, L.; Koth, C. M.; Lupardus, P. J.; Kaminker, J. S.; Heise, C. E.; Steiner, P. *J. Biol. Chem.*, **2013**, *288*, 26926-26943.

deep cavity of the active site of HDAC2, inhibiting its functions; finally, another example regards the avidin that can accommodate the biotin in a deep cavity (**Figure 8, Right**)[40].

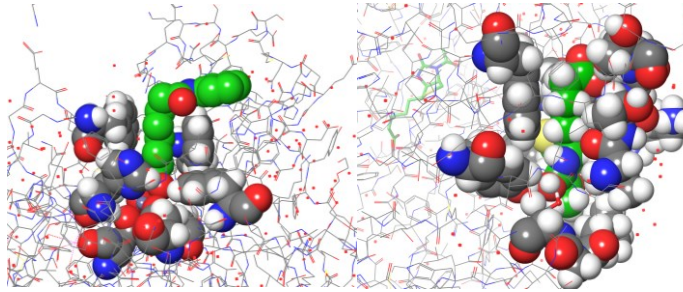

Figure 8. Structure of Human SAHA@HDAC2 complex (Left)[39]; Structure of biotin@avidin complex (Right)[40].

Learning the lesson from biological systems, we can envision that with the aim to improve the recognition ability of synthetic receptors, we need a more rigorous mimicking of the structural features of the natural cavities. Prompted by these considerations, many scientists in the last decades, were attracted by design of synthetic macrocycles incorporating deep π-electron-rich aromatic cavity. [41] Thus, macrocyclic compounds based on naphthalene[41] or anthracene units have been reported

[40] Terai, T.; Maki, E.; Sugiyama, S.; Takahashi, Y.; Matsumura, H.; Mori, Y.; Nagano, T. *Chemistry & Biology*, **2011**, *18*, 1261–1272.

[41] (a) Yao, H.; Jiang, W. *Naphthol-Based Macrocycles*, in Handbook of Macrocyclic Supramolecular Assembly, Springer, Singapore, **2019**; (b) Wang, X.; Jia, F.; Yang, L.-P.; Zhou, H.; Jiang, W. *Chem. Soc. Rev.,* **2020**, *49*, 4176–4188.

such as, oxatub[n]arene [42] , naphthocage [43] , and naphthotubes[4a,44,45], prismarenes[46,47], pagodarenes[48] and saucerarens[49], which have shown interesting recognition and structural properties.

1.2.2.1 Oxatubarenes

Oxatubarenes reported by Wei Jiang in 2015,[42] shows a deep π-electron-rich aromatic cavity, capable to form very stable host-guest complexes by cation···π and π···π interactions. Oxatubarene is conformationally flexible and can adopts four conformations: zigzag (I), disrupted zigzag (II), 1,2-alternate (III), and 1,3-alternate (IV)- **Figure 9**.[42]

---

[42] Jia F.; He, Z.; Yang, L. P.; Pan, Z. S.; Yi, M.; Jiang, R. W.; Jiang, W. *Chem. Sci.,* **2015***, 6,* 6731- 6738.

[43] Jia, F.; Hupatz, H.; Yang, L. P.; Schröder, H. V.; Li, D.-H.; Xin, S.; Lentz, D.; Witte, F.; Xie, X.; Paulus, B.; Schalley, C. A.; Jiang, W. *J. Am. Chem. Soc.* **2019**, *141*, 4468–4473.

[44] Shorthill, B.J.; Avetta, C.T.; Glass, T.E. *J. Am. Chem. Soc.* **2004**, *126*, 12732-12733.

[45] Yang, L.; Liu, W.; Jiang, W. *Tetrahedron Lett*. **2016**, *57*, 3978-3985.

[46] Della Sala, P.; Del Regno, R.; Talotta, C.; Capobianco, A.; Hickey, N.; Geremia, S.; De Rosa, M.; Spinella, A.; Soriente, A.; Neri, P.; Gaeta, C. *J. Am. Chem. Soc.* **2020**, *142*, 1752-1756.

[47] Della Sala, P.; Del Regno, R.; Di Marino, L.; Calabrese, C.; Palo, C.; Talotta, C.; Geremia, S.; Hickey, N.; Capobianco, A.; Neri, P.; Gaeta, C. *Chem. Sci.* **2021**, *12*, 9952-9961.

[48] (a) Han, X.- N.; Han, Y.; Chen, C. - F. *J. Am. Chem. Soc.* **2020**, *142* (18), 8262–8269; (b) Han, X.- N.; Zong, Q.– S.; Han, Y.; Chen, C.- F. *CCS Chem.* **2022**, *4*, 318–330.

[49] Li, J.; Zhou, H.-Y.; Han, Y.; Chen, C.-F. *Angew. Chem. Int. Ed.* **2021**, *60*, 21927-2193.

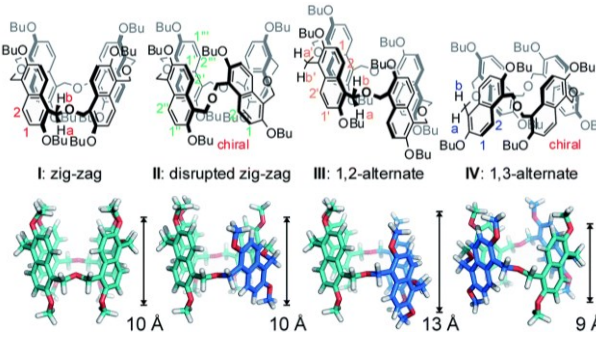

Figure 9. Chemical structures of four representative conformers of oxatub[4]arene.[42]

However, these conformers undergo quick interconversion at room temperature, in the NMR time scale.[42]

The identification of the different conformers of the oxatubarene (**Figures 9** and **10**) was possible thanks to their different molecular recognition properties. Thus, four different guests were identified, each capable to stabilize a different conformation-**Figure 10**.[42]

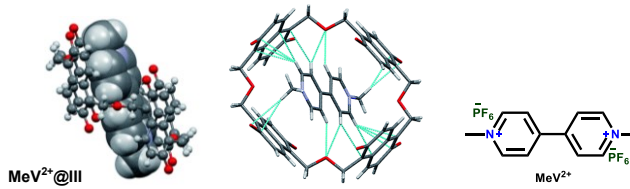

Figure 10. (Left) Single crystal structures of **MeV^{2+}@III**; (Right) Chemical structure of the guest involved.[42]

In all four complexes, C–H···O hydrogen bonds are detected, between the oxygen atoms of CH_2–O–CH_2 and CH of guest, supporting a role for these linkers. In addition, C–H···π and cation···π interactions are also observed.[42]

1.2.2.2 Naphthotubes

The macrocyclic hosts discussed here have a deep hydrophobic and an electron-rich cavity. However, unlike common natural bioreceptors, they do not have functional groups within the cavity. This often results in a clear difference in molecular recognition properties between synthetic and naturally receptors. For this reason, naphthotubes[4a] were designed and synthesised. These are tubular-shaped synthetic macrocycles reminiscent of enzyme binding sites, consisting of naphthol units linked by bridges appropriately functionalised with polar groups. The first example of a naphthotube was reported in the literature by Glass (**Figure 11**).[44] It is constituted by bis-naphthalene dimers bridged by amide groups.

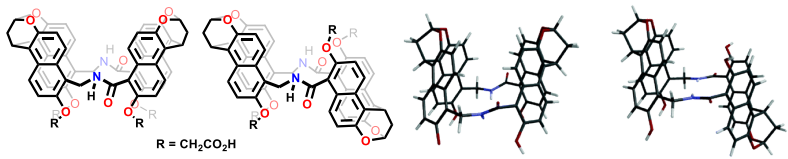

Figure 11. Representations of two napthotubes.[44]

Taking inspiration by this result,[44] Wei Jiang reported the naphthotubes (**Figure 12**) bearing functionalised bridges.[4] Jiang reported the synthesis of variously functionalized naphthotubes with ureidic [50] and thioureidic [51] groups

[50] Huang, G.; He, Z.; Cai, C.; Pan, F.; Yang, D.; Rissanen, K.; Jiang, W. *Chem. Commun.* **2015**, *51*, 15490-15493.
[51] Huang, G.; Valkonen, A.; Rissanen, K.; Jiang, W. *Chem. Commun.* **2016**, *52*, 9078-9081.

(**Figure 12a**), amine [52] groups (**Figure 12b**), ether [53] groups (**Figure 12c**) and ester[54] groups (**Figure 12d**).

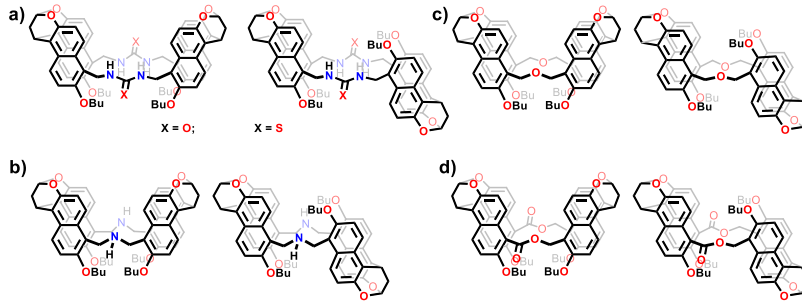

Figure 12. Naphthotubes synthesised by Wei Jiang.[4a]

The host-guest properties of the naphthotubes in **Figure 12** were studied, obtaining extremely interesting results. At this regard, naphthotubes show a deep π-electron rich aromatic cavities adorned with polar functions, which exhibits very peculiar supramolecular properties.[4a]
In fact naphthotubes that are functionalised with hydrogen bond donor groups, such as amide or ureidic groups exhibit good affinity towards neutral molecules in water, such as 1,4-dioxane (**Figure 13**) pyrazine, dimethoxymethane, ethyl acetate, 2-methyl-1,3-dioxolane, thiazole and benzene.[55]

---

[52] Cui, J.; Ba, Q.; Ke, H.; Valkonen, A.; Rissanen, K.; Jiang, W. *Angew. Chem. Int. Ed.* **2018**, *57*, 7809-7814.
[53] Ma, Y.; Ke, H.; Valkonen, A.; Rissanen, K.; Jiang, W. *Angew. Chem. Int. Ed.* **2018**, *57*, 709-713.
[54] Chai, H.; Yang, L.; Ke, H.; Pang, X.; Jiang, W. *Chem. Commun.* **2018**, *54*, 7677-7680.
[55] Yao, H.; Ke, H.; Zhang, X.; Pan, S.-J.; Li, M.-S.; Yang, L.-P.; Schreckenbach, G.; Jiang, W. *J. Am. Chem. Soc.* **2018**, *140*, 13466-13477.

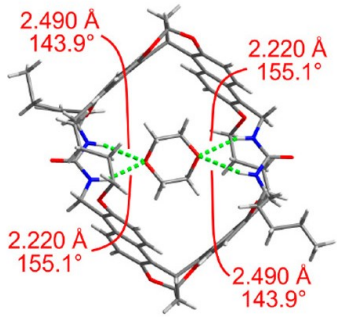

Figure 13. Single-crystal X-ray structure of the complexes of macrocycle with 1,4-Dioxane.[55]

In these complexations, the hydrophobic effect of the cavity plays a crucial role, together with the hydrogen-bonding interactions between the hydrophilic molecules and the amide groups of the macrocycle.[55]

2.0 Prism[n]arene Macrocycles: A New Tool in Supramolecular Chemistry[46]

2.1 Prism[n]arenes: A New Class of Macrocyclic Hosts[46]

Oxatub[n]arenes[42], naphthocages[43] and naphthotubes[4] show intriguing structural properties and amazing supramolecular functions. Taking inspiration by this class of supramolecular hosts, during the first year of my PhD project, the synthesis of a novel class of macrocycles, named prismarenes has been studied. Prism[n]arene are macrocycles constituted by 1,5-methylene-bridged 2,6-dialkoxynaphthalene units and show a deep π-electron rich aromatic cavity and a prism-like shape, which inspired the name prism[n]arene. [46]

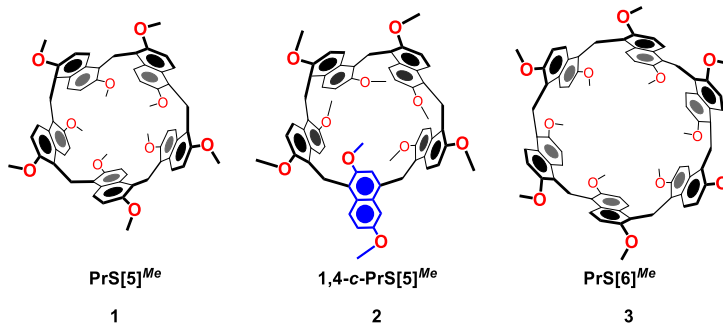

Figure 14. Chemical drawing of prism[n]arenes. [46]

[46] Della Sala, P.; Del Regno, R.; Talotta, C.; Capobianco, A.; Hickey, N.; Geremia, S.; De Rosa, M.; Spinella, A.; Soriente, A.; Neri, P.; Gaeta, C. *J. Am. Chem. Soc.* **2020**, *142*, 1752-1756. Highlighted in: Yang, L.-P.; Jiang, W. *Angew. Chem. Int. Ed.* **2020**, *59*, 15794-15796.

In detail, when 2,6-dimethoxynaphthalene in 1,2-dichloroethane (1,2-DCE, 2.5 mM) and paraformaldehyde (1.2 equiv) were reacted in the presence of TFA (15 equiv) at 70 °C, after 22 h, (**1,4-*confused*-PrS[5]^{Me}**) **2** was the favoured product (40 %), while **PrS[5]^{Me} 1** was isolated in 0.3 % yield, - **Scheme 2**. [46]

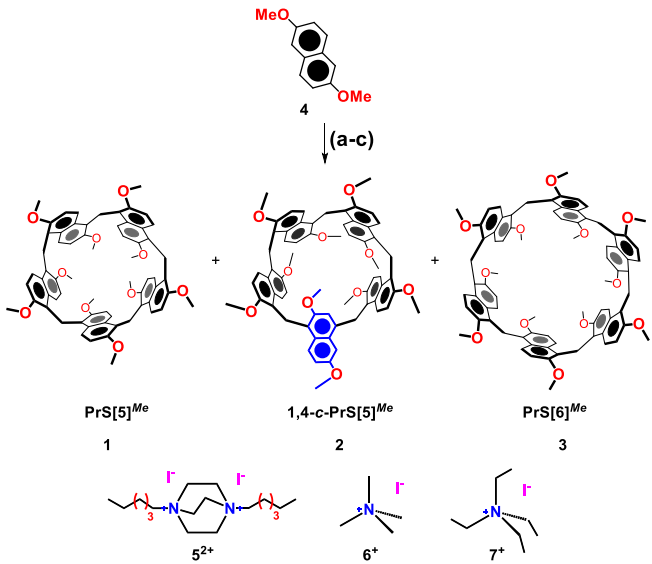

Scheme 2. The synthesis of **PrS[n]^{Me} 1-3**. Reagents and conditions: a) 1,2-DCE, TFA, 70 °C, 22 h: **1** (0.3 %), **2** (40%). b) **5^{2+}·2I^-**, 1,2-DCE, TFA, 70 °C, 22 h: **1** (47%), **2** (16 %). c) **6^+·I^-**, 1,2-DCE, TFA, 70 °C, 22 h: **1** (32%), **2** (8%). d) **7^+·I^-**, 1,2-DCE, TFA, 70 °C, 72 h: **1** (0.3 %), **2** (6%), **3** (20%).[46]

In order to investigate the possible role of the solvent for the formation of prism[n]arenes, it was found that **1,4-*c*-PrS[5]^{Me}** was obtained in lower yield in solvents such as *o*-dichlorobenzene or chloroform - **Table 1**. Furthermore, when the reaction was carried out at room temperature, **2** was isolated in 11% yield. [46]

Solvent	Temperature	Yield of **1**	Yield of **2**
o-dichlorobenzene	70 °C	----	9.4 %
Chloroform	Reflux	----	9.6 %
1,1,2 - trichloroethane	70 °C	----	----
1,1,2,2- tetrachloroethane	70 °C	----	18 %
1,2 - dichloroethane	25 °C	----	11%

Table 1. Yields of **1** and **2** in the presence different solvents.[46]

An exhaustive 1D and 2D NMR study evidenced that 4/5 of the naphthalene rings of **2** were bridged through their 1,5-positions, while one naphthalene unit showed a 1,4-bridging pattern.

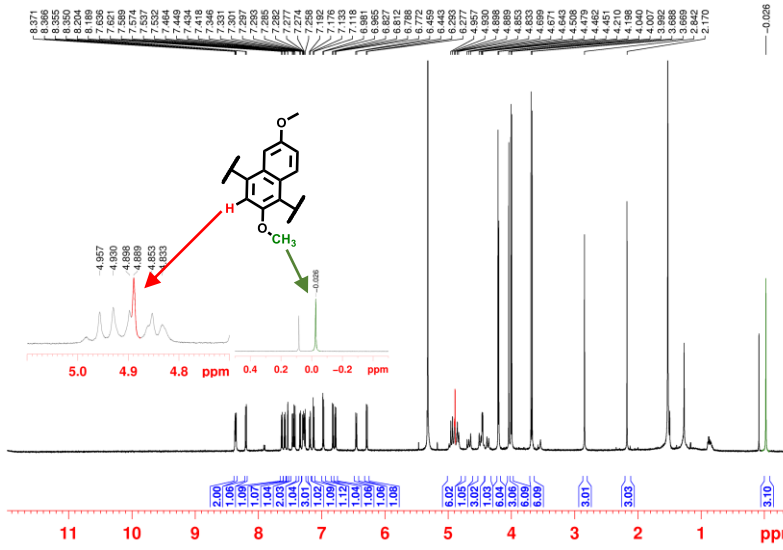

Figure 15. ^{1}H NMR spectrum of **2** (CD_2Cl_2, 600 MHz, 298 K).[46]

In fact, the aromatic H-atom on position 3 of the *confused* 1,4-bridged naphthalene ring, was up-field shielded at 4.89 ppm (singlet) in its ^{1}H NMR spectrum (**Figure 15**) and showed a ^{1}J correlation in the HSQC experiment with a

carbon resonance at 116.7 ppm (See **Figure 25**, paragraph **2.4.2**). Analogously, a strong shielding was also experienced by the OMe group in position 2 of the *confused* ring, which resonated at –0.026 ppm. These data clearly suggest that **2** adopts a conformation in which the 1,4-confused-naphthalene ring is coplanar to the methylene mean plane, with its OMe group pointing inside the aromatic cavity.[46]

The HR-ESI mass spectrum confirmed the molecular mass of **2** (found: 1000.4218 m/z, calculated for [M]+ 1000.4186).[46]

1,4-*c*-PrS[5]*Me* macrocycle was able to form endo-cavity supramolecular complex in the presence of 1,4-dihexyl-DABCO cation $\mathbf{5^{2+}}$ (See **Figure 20**, paragraph **2.2**). When the barfate ($BArF^-$) salt of $\mathbf{5^{2+}}$ was added to a CD_2Cl_2 solution of **2**, the formation of the supramolecular complex $\mathbf{5^{2+}@2}$ was ascertained by the appearance of shielded ^1H NMR signals at negative value of chemical shifts (from 0 to −2 ppm, see **Figure 30b**, paragraph **2.4.3**) attributable to the protons of the guest $\mathbf{5^{2+}}$ hosted inside the aromatic cavity of **2**. An association constant value of 470 M^{-1} was obtained by integration of the slowly exchanging ^1H NMR signals of the host free and host complexed. [46]

Previously, Scarso[56] and Leclaire[57] showed that the yields of macrocyclization of pillararene derivatives was improved in the presence of ammonium cations that acted as templates.

---

[56] (a) da Pian, M.; de Lucchi, O.; Strukul, G.; Fabris, F.; Scarso, A. *RSC Adv.* **2016,** *6*, 48272–4827; (b) Da Pian, M.; Schalley, C. A.; Fabis, F.; Scarso, A. *Org. Chem. Front*. **2019**, *6*, 1044–1051.

[57] Dumartin, M.; Septavaux, J.; Donnier-Marechal, M.; Jeamet, E.; Dumont, E.; Perret, F.; Vial, L; Leclaire, J. *Chem. Sci.*, **2020**, *11*, 8151–8156.

Prompted by these considerations, we envisioned to perform the synthesis in **Scheme 2** in the presence of $\mathbf{5}^{2+}$ as iodide salt, with the aim to investigate its probable template effect for the synthesis of prism[n]arenes. Surprisingly, by adding $\mathbf{5}^{2+}$ as iodide salt in the reaction mixture (**Scheme 2**), **PrS[5]*Me*** was isolated in 47 % of yield after 22 h. When the tetramethylammonium cation $\mathbf{6}^{+}$, was added to the reaction mixture in Scheme 2, analogously **PrS[5]*Me*** was the favored product (32% of yield).[46]

^{1}H NMR spectrum of **1** (CD_2Cl_2, 600 MHz, 298 K) showed the presence of an AX system in the aromatic region of the spectrum at 7.96 and 6.92 ppm (J = 9.4 Hz) and attributable to the H-atoms of the naphthalene rings. In addition, two singlets were present at 4.68 and 3.63 ppm attributable to the methylene-bridge and methoxy groups of **1**, in accord with the D_5 symmetry of **1** - **Figure 16**.[46]

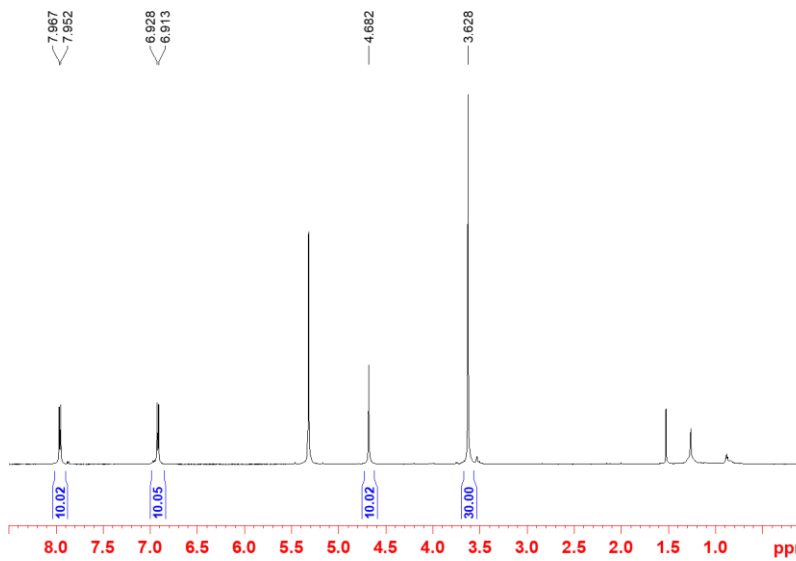

Figure 16. ^{1}H NMR spectrum of **1** (CD_2Cl_2, 600 MHz, 298 K).[46]

Finally, by adding **7**$^{+}$ as iodide salt in the reaction mixture (**Scheme 2**), the hexamer **PrS[6]**^{Me} was obtained in 20 % yield after 22 h, in addition, **2** and **1** were isolated in very low yields, 6 % and in 0.3 % respectively. [46]

In conclusion, we can say that it is possible to obtain a specific macrocycle by using an appropriate ammonium templating agent which acts by a thermodynamic control.[46]

In literature are known examples of reversible acid or base catalyzed macrocyclization reactions, under thermodynamic conditions, in which is possible to isolate a specific macrocycle from the equilibrium-mixture by adding an appropriate complementary guest.[56, 57,58]In this way, the specific formation of the host-guest complex stabilizes the complementary host component, thus altering the equilibrium distribution in its favour (**Figure 17**), at the expense of other members. This process was defined by Jeremy Sanders as "*Supramolecular templating in thermodynamically controlled synthesis*".[58]

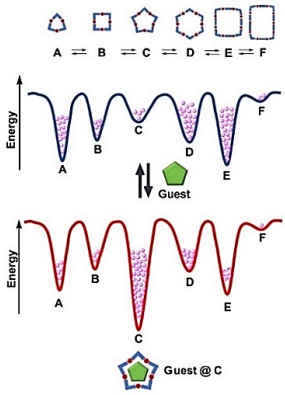

Figure 17. Templation in a thermodynamically controlled synthesis: (top in blue) schematic representation of the free energy landscape of a reversible macrocyclization, in which different cyclooligomers are in equilibrium; (bottom in red) alteration of the equilibrium composition caused by the addition of a guest able to bind a specific component.

[58] Furlan, R. L. E.; Otto, S.; Sanders, J. K. M. *Proc. Natl. Acad. Sci.* USA 94, **2002**, *99*, 4801 – 4804.

To investigate this possible thermodynamically templated process, we performed a series of experiments to study a probable interconversion process between the prismarene derivatives - **Figure 18**. [46]

In detail, when the **PrS[5]*Me*** was reacted with TFA in 1,2-DCE at 70 °C, a complete conversion to its isomer **1,4-*c*-PrS[5]*Me*** was observed after 16 h. In contrast, when **2** was treated in the presence of $\mathbf{5}^{2+}$ in 1,2-DCE at 70 °C for 22 h, a mixture of **1,4-*c*-PrS[5]*Me*** and **PrS[5]*Me*** in 4/1 ratio was obtained. Finally, the conversion of the **PrS[6]*Me*** to **1,4-*c*-PrS[5]*Me*** in the presence of TFA in 1,2-DCE at 70°C, was completed after 16 h -**Figure 18**.[46]

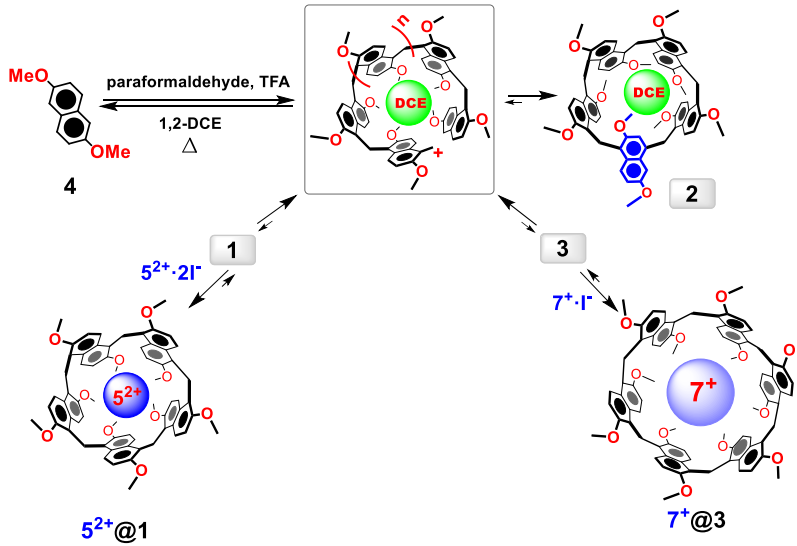

Figure 18. Thermodynamically controlled templated synthesis of prismarenes.[46]

Furthermore, density functional theory (DFT) calculations have shown that **PrS[5]*Me*** is less stable than its confused-isomer by 5.1 kcal/mol, but this energy decreases to 2.6

kcal/mol when considering the equilibrium geometries of **1** and **2** with 1,2-DCE within their cavity.

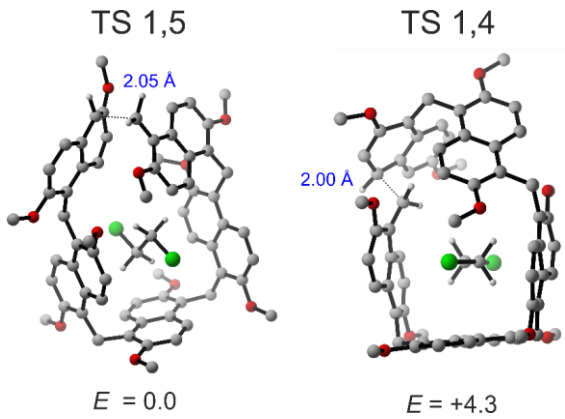

Figure 19. The most stable transition states for the macrocyclization step leading to 1,5 and 1,4 products. Noncritical hydrogen atoms have been omitted for clarity. Relative energy is expressed in kcal/mol, the forming bond distances (Å) are highlighted in blue.[46]

In the case of the equilibrium geometries of the transition states (TS), it was seen that the TS for the 1,4 attack is predicted to lie 3.3 kcal/mol above that involved in the 1,5 attack. This energy difference increases to 4.3 kcal/mol when considering 1,2-DCE inside the cavity – **Figure 19**.[46] In conclusion, these studies confirmed that **1,4-*c*-PrS[5]^{Me}** is the thermodynamic product, while **PrS[5]^{Me}** and **PrS[6]^{Me}** are the kinetic ones. In fact, HPLC analysis of the reaction mixture showed that after 270 min of reaction, **PrS[5]^{Me}** was the favoured product, while after 330 min the 1,4-*c*-isomer prevailed. In addition, HPLC analysis confirmed the crucial role played by the ammonium guests. In fact, when the reaction was conducted in the presence of **5^{2+}**, the HPLC evidenced that prism[5]arene **PrS[5]^{Me}** was the favoured product over time. In summary,

these results indicate that the formation of prism[n]arenes occurs through a thermodynamically controlled templated process.[46]

In details, the selectivity towards a specific prismarene cyclooligomer can be driven by template effect (**Figure 18**) of the halogenated solvent or appropriate ammonium guests. Thus, the pentameric prism[5]arene **PrS[5]*Me*** and the hexameric prism[6]arene **PrS[6]*Me*** were selectively isolated from the equilibrium mixture by using their complementary guests, respectively, 1,4-dihexyl-DABCO (**5**$^{2+}$) and tetraethylammonium cation (**7**$^{+}$). Differently, the formation of the 1,4-confused-prism[5]arene ***c*-PrS[5]*Me*** was observed by template effect of the halogenated solvent 1,2-dichloroethane (1,2-DCE)- **Scheme 2**.[46]

2.2 Molecular Recognition Properties of Prismarenes [46]

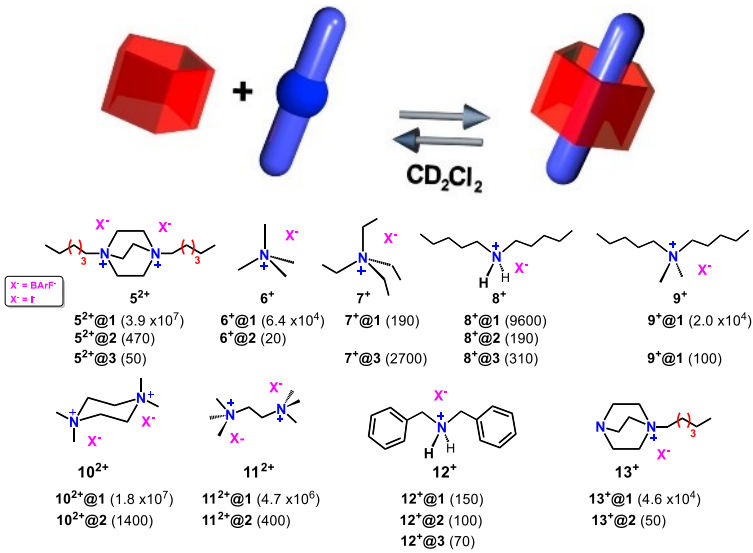

Figure 20. Schematic complexation equilibrium of the prism[5]arene **1** with guests **5^{2+}- 13^{+}.** (Bottom) Binding constant values of their host−guest complexes with the prism[n]arenes **1−3**, determined by ^{1}H NMR experiments in CD_2Cl_2 Errors <15% calculated as mean values of three measures. [46]

Prism[n]arenes present an extended π–electron rich aromatic cavity.[46] In fact, at this point our attention focused on the recognition ability of derivatives **1-3** toward ammonium guests - **Figure 20**. The data in **Figure 20** indicated that the thermodynamic affinities of prismarenes toward ammonium guests is driven by the structural features and charges of the differently guests. The complexation of double-charged cations **5^{2+}** and **10^{2+}** for **PrS[5]*Me*** showed very high binding affinities, with constant values of $3.9x10^{7}$ $M^{-1}$and $1.8x10^{7}$ M^{-1},

respectively. **PrS[5]*Me*** has a higher affinity for the tetramethylammonium **6**$^{+}$ than the bigger tetraethylammonium **7**$^{+}$ with a high selectivity ratio (S = $K_{6+@1}/K_{7+@1}$= 64000/190 = 337). The stronger binding affinity of **PrS[5]*Me*** for double-charged guests suggests that C-H---π, cation---π interactions play a crucial role for the stabilisation of the complexes.

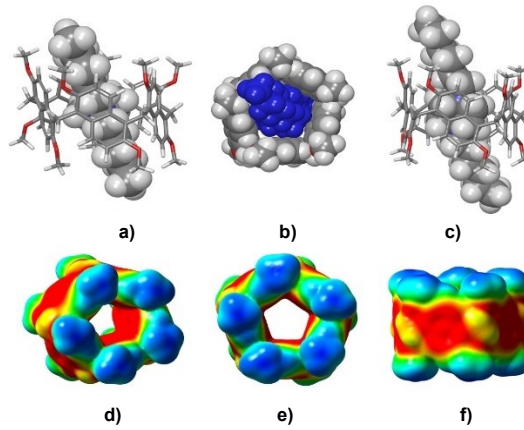

Figure 21. (a-c) DFT-optimized structures (B97D3/SVP/SVPFIT) of the: a) **9**$^{+}$**@1** complex. The methyl groups of **9**$^{+}$ are involved in C–H··· π interactions with an average C–H··· $\pi^{centroids}$ distance of 2.45 Å and an average C–H··· $\pi^{centroids}$ angle of 160°. b,c) Different views of the **5**$^{2+}$**@1**. 12 C–H··· π interactions were detected between the ethylene groups $^{+}NCH_2CH_2N^{+}$ and the aromatic walls of **1** with an average C–H··· $\pi^{centroids}$ distance of 2.72 Å. d-f) Different views of the ESPs mapped onto electron density isosurfaces (ρ = 0.004) for the prism[5]arene **1**.[46]

In fact, derivative **PrS[5]*Me*** (**1**) forms a pseudo[2]rotaxane stabilised by $^{+}$NC-H---π and cation---π interactions with the **5**$^{2+}$ cation, as observed by DFT-optimized structures[46] - **Figure 21**. The supramolecular complex between **5**$^{2+}$ and **PrS[5]*Me*** also has an association constant value much

higher than that observed for the analogous complexation of $\mathbf{5^{2+}}$ with the isomer ***c*-PrS[5]^{Me}(2)** (470 M^{-1}) and **PrS[6]^{Me}** (**3**) (50 M^{-1}) - **Figure 20**. This difference of affinity could be attributed to the lower $\mathbf{5^{2+}}$/ **PrS[6]^{Me}** complementarity, due to the larger size of the hexamer cavity that causes a scarce steric fit with $\mathbf{5^{2+}}$.

Further confirmation of the crucial role of $^{+}$NC-H---π interactions is also obtained for the pseudo[2]rotaxane $\mathbf{9^{+}@1}$, which shows a constant of $2.0x10^{4}$ M^{-1}, significatively higher than that calculated for the formation of the $\mathbf{8^{+}@1}$ of 9600 M^{-1}.[46]

Finally, the association constants values (**Figure 20**) obtained for the ammonium@PrS[6]^{Me} complexes are all lower than the values reported for the corresponding **PrS[5]^{Me}** complexes, except for the tetraethylammonium $\mathbf{7^{+}}$ that shows a higher **PrS[6]^{Me}/PrS[5]^{Me}** selectivity ratio ($S = \boldsymbol{K}_{7+@3}/\boldsymbol{K}_{7+@1} = 2700/90 = 30$).[46] This difference of affinity could be attributed to the larger size of the hexamer cavity that causes a scarce steric fit with the guests.[46]

2.3 Conclusions[46]

In conclusion, during the first year of this PhD project, we have obtained a novel naphthalene-based macrocycles, named Prism[n]arenes, by a templated approach of a thermodynamically controlled synthesis. In detail, the pentameric prism[5]arene **1** or the hexameric prism[6]arene **3** are selectively caught from the equilibrium mixture by using the appropriate ammonium templating agent. Furthermore, the prism[n]arenes present an extended π–electron rich aromatic cavity that show a good affinity for ammonium guests though cation···π, $^{+}$NC−H···π interactions.

2.4 Experimental Section

2.4.1 General Section

HR MALDI mass spectra were recorded on a Bruker Solarix FT-ICR mass spectrometer equipped with a 7T magnet. The samples recorded in MALDI were prepared by mixing 10 µL of analyte in dichloromethane (1 mg/mL) with 10 µL of solution of 2,5-dihydroxybenzoic acid (10 mg/mL in Methanol). The mass spectra were calibrated externally, and a linear calibration was applied. All reaction solvents were dried by activated 3 Å molecular sieves[59]. All chemical reagents grade was used without further purification and were used as purchased. Reaction temperatures were measured externally. Reactions were monitored by TLC silica gel plates (0.25 mm) and visualized by UV light 254 nm, or by spraying with H_2SO_4−$Ce(SO_4)_2$. NMR spectra were recorded on a Bruker Avance-600 [600 (^{1}H) and 150 MHz (^{13}C)], Avance-400 [400 (^{1}H) and 100 MHz (^{13}C)], Avance-300 MHz [300 (^{1}H) and 75 MHz (^{13}C)] or Avance-250 MHz [250 (^{1}H) and 62.5 MHz (^{13}C)] spectrometers. Chemical shifts are reported relative to the residual solvent peak [60]. Standard pulse programs, provided by the manufacturer, were used for 2D COSY-45, 2D HSQC and 2D NOESY experiments.

[59] Williams, D. B. G.; Lawton, M. *J. Org. Chem*. **2010**, *75*, 8351-8354.
[60] Fulmer, G. R.; Miller, A. J. M.; Sherden, N. H.; Gottlieb, H. E.; Nudelman, A.; Stoltz, B.M.; Bercaw, J.E.; Goldberg, K.I. *Organometallics* **2010**, *29*, 2176–2179.

2.4.2 General Procedure for the Synthesis of PrS[n]^{Me} and Copies of NMR Spectra[46]

Procedure A. A solution of 2,6-dimethoxynaphthalene (250 mg, 1.33 mmol), paraformaldehyde (48 mg, 1.60 mmol, 1.2 equiv) in 530 mL of dry 1,2-dichloroetane was heated to 70° C, then trifluoroacetic acid (1.5 mL, 0.02 mol, 15 equiv) was added. The solution was stirred for 22 h at 70° C and subsequently the solvent evaporated under reduced pressure. The residue was dissolved in CH_2Cl_2 (30 mL) and the mixture was washed with an aqueous saturated solution of $NaHCO_3$ (30 mL). Finally, the organic layer was washed with brine (2x20 mL), and the organic phases were dried over sodium sulfate and concentrated to give a solid light brown. The crude product was purified by chromatographic column on silica gel (hexane/dichloromethane = 1/9). Macrocycle **1** was obtained in 0.3 % of yield (1 mg) and macrocycle **2** was obtained as a white solid (106 mg, 40 %).

Procedure B. A solution of 2,6-dimethoxynaphthalene (250 mg, 1.33 mmol), paraformaldehyde (48 mg, 1.60 mmol, 1.2 equiv), and templating agent, $\mathbf{5^{2+}\cdot 2I^-}$, $\mathbf{6^{+}\cdot I^-}$ or $\mathbf{7^{+}\cdot I^-}$ (1.33 mmol, 1.0 equiv) in 530 mL of dry 1,2-dichloroetane was heated to 70° C, then trifluoroacetic acid (1.5 mL, 0.02 mol, 15 equiv) was added. The solution was stirred for 22 h at 70° C and subsequently the solvent evaporated under reduced pressure. The residue was dissolved in CH_2Cl_2 (30 mL) and the mixture was washed with an aqueous saturated solution of $NaHCO_3$ (30 mL). Finally, the organic layer was washed with brine (2x20 mL), and the organic phases were dried over sodium

sulfate and concentrated to give a solid light brown. The crude product was purified by chromatographic column on silica gel (hexane/dichloromethane = 1/9).

Template synthesis in presence of $5^{2+}\cdot 2I^-$ salt: The macrocycle **1** was obtained in 47 % yield (125 mg) and the macrocycle **2** in 16 % yield (42 mg).

Template synthesis in presence of $6^{+}\cdot I^-$ salt: The macrocycle **1** was obtained in 32% of yield (85 mg) and the macrocycle **2** in 8% of yield (21 mg).

Template synthesis in presence of $7^{+}\cdot I^-$ salt: The macrocycle **1** was obtained in 0.3 % yield (1 mg), the macrocycle **2** in 6 % yield (16 mg) and the macrocycle **3** was obtained in 20 % yield (54 mg).

Derivative 1:
M.p.: >374 °C dec; **^{1}H NMR** (CD_2Cl_2, 600 MHz, 298 K, **Figure 16**): δ 7.95 (*d*, 10H, Ar-*H, J* = 9.4 Hz), 6.92 (*d*, 10H, Ar-*H, J* = 9.4 Hz), 4.68 (*s*, 10H, ArC*H*$_2$Ar), 3.63 (*s*, 30H, O*Me*); **^{13}C NMR** {^{1}H} (CD_2Cl_2, 150 MHz, 298 K): δ 153.1, 129.8, 125.0, 123.7, 113.9, 56.8, 21.8; **HRMS** (MALDI) m/z $[M]^+$ calcd for $C_{65}H_{60}O_{10}$: 1000.4186. found: 1000.4227.

Derivative 2:
M.p.: >385 °C dec; **^{1}H NMR** (CD_2Cl_2, 600 MHz, 298 K, **Figure 15**): δ 8.37-8.35 (*overlapped*, 2H, Ar-*H*), 8.19 (d, 1H, Ar-*H*, *J* = 9.4 Hz), 7.63 (d, 1H, Ar-*H*, *J* = 9.3 Hz), 7.58 (d, 1H, Ar-*H*, *J* = 9.4 Hz), 7.53 (d, 1H, Ar-*H*, *J* = 2.6 Hz), 7.46 (d, 1H, Ar-*H*, *J* = 9.4 Hz), 7.43 (d, 1H, Ar-*H*, *J* = 9.4

Hz), 7.34 (d, 1H, Ar-*H*, *J* = 9.4 Hz), 7.30-7.27 (*overlapped*, 2H, Ar-*H*), 7.26 (s, 1H, Ar-*H*), 7.18 (d, 1H, Ar-*H*, *J* = 9.4 Hz), 7.12 (d, 1H, Ar-*H*, *J* = 9.4 Hz), 6.97 (d, 1H, Ar-*H*, *J* = 9.4 Hz), 6.82 (d, 1H, Ar-*H*, *J* = 9.4 Hz), 6.78 (d, 1H, Ar-*H*, *J* = 9.4 Hz), 6.45 (d, 1H, Ar-*H*, *J* = 9.4 Hz), 6.29 (d, 1H, Ar-*H*, *J* = 9.4 Hz), 4.96-4.83 (*overlapped*, 6H, ArC*H*$_2$Ar and Ar-*H*), 4.70-4.64 (*overlapped*, 1H, ArC*H*$_2$Ar), 4.51-4.45 (*overlapped*, 3H, ArC*H*$_2$Ar), 4.20 (d, 1H, ArC*H*$_2$Ar), 4.21 (s, 3H, O*Me*), 4.20 (s, 3H, O*Me*), 4.04 (s, 3H, O*Me*), 4.01 (s, 3H, O*Me*), 4.00(s, 3H, O*Me*), 3.69 (s, 3H, O*Me*), 3.67 (s, 3H, O*Me*), 2.84 (s, 3H, O*Me*), 2.17 (s, 3H, O*Me*), -0.03 (s, 3H, O*Me*); **^{13}C NMR** {^{1}H} (CD_2Cl_2, 150 MHz, 213 K): *δ* 155.6, 153.1, 152.7, 152.0, 151.6, 151.5, 151.4, 151.1, 150.9, 150.5, 134.4, 129.2, 128.8, 128.7, 128.6, 128.2, 128.0, 127.9, 127.5, 125.1, 124.9, 124.7, 124.3, 124.0, 123.9, 123.7, 123.6, 123.4, 123.0, 122.8, 122.4, 120.9, 119.8, 117.9, 117.2, 116.9, 115.4, 112.5, 112.2, 111.7, 111.6, 110.9, 110.7, 102.1, 56.7, 56.5, 56.2, 56.1, 56.0, 55.8, 55.6, 55.2, 54.7, 53.3, 26.6, 23.4, 21.6, 20.3, 20.1; **HRMS** (MALDI) m/z [M]$^+$ calcd for $C_{65}H_{60}O_{10}$: 1000.4186. found: 1000.4218.

Derivative 3:

M.p.: >352 °C dec; **^{1}H NMR** (TCE-*d*$_2$, 300 MHz, 393 K): *δ* 7.64 (*d*, 12H, Ar-*H, J* = 9.3 Hz), 6.72 (*d*, 12H, Ar-*H, J* = 9.3 Hz), 4.61 (*s*, 12H, ArC*H*$_2$Ar), 3.27 (*s*, 36H, O*Me*); **^{13}C NMR** {^{1}H} (TCE-*d*$_2$, 75 MHz, 298 K): *δ* 152.1, 129.2, 123.9, 123.7, 114.1, 56.5, 29.6; **HRMS** (MALDI) m/z [M]$^+$ calcd for $C_{78}H_{72}O_{12}$: 1200.5024. found: 1200.5117.

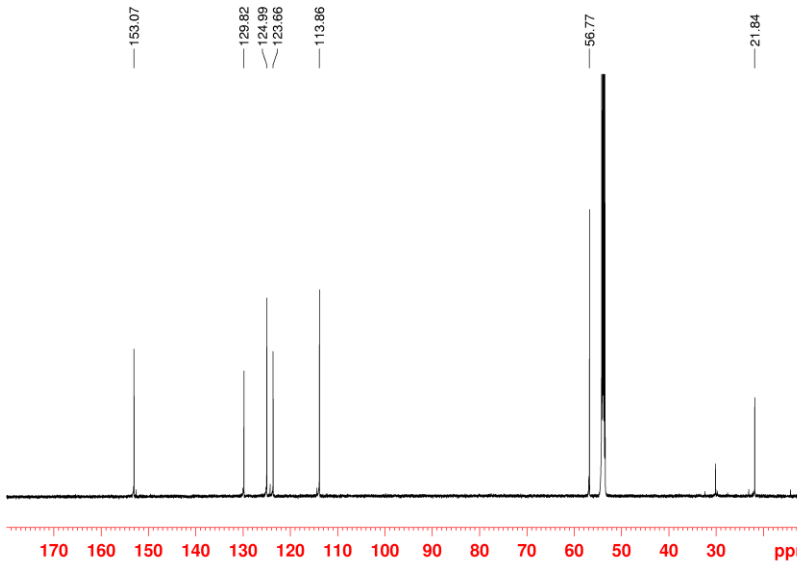

Figure 22. ^{13}C NMR spectrum of **1** (CD_2Cl_2, 150 MHz, 298 K).

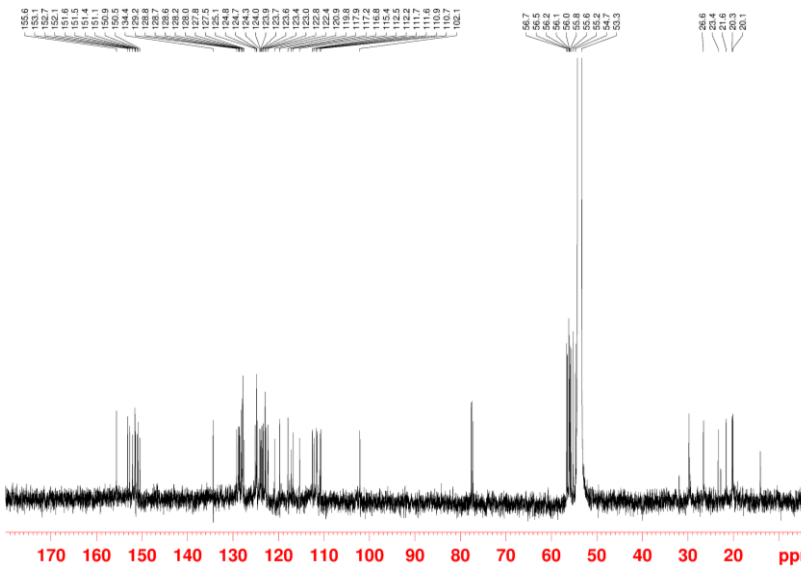

Figure 23. ^{13}C NMR spectrum of **2** (CD_2Cl_2, 150 MHz, 213 K).

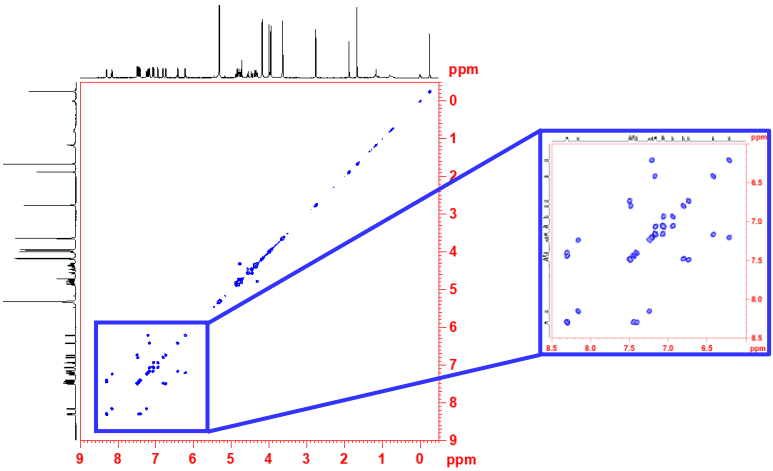

Figure 24. 2D-DQF COSY spectrum of **2** (CD_2Cl_2, 600 MHz, 213 K).

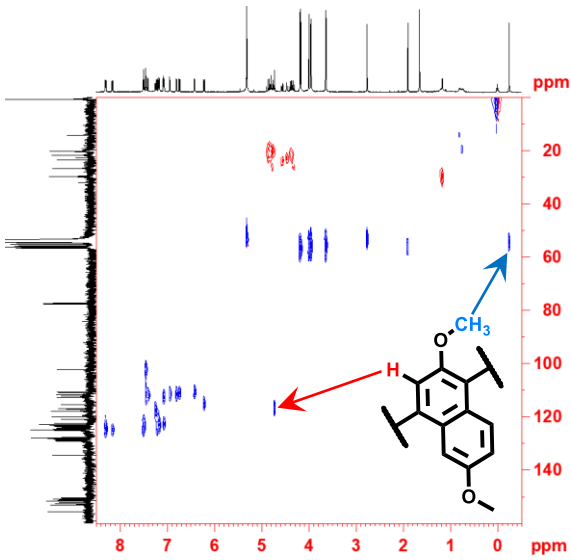

Figure 25. Significant portion of 2D-HSQC spectrum of **2** (CD_2Cl_2, 600 MHz, 213 K).

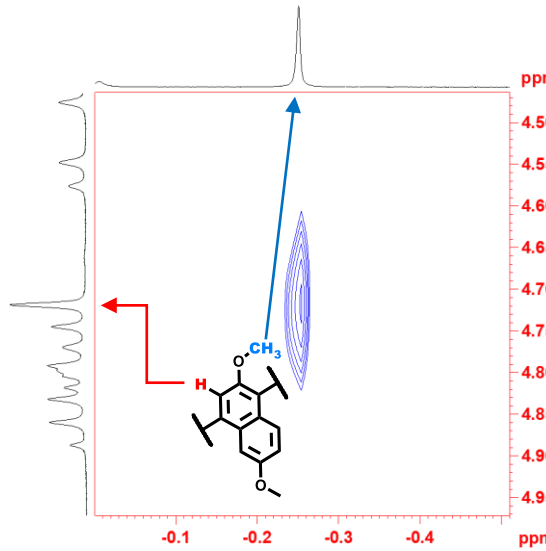

Figure 26. Significant portion of NOESY spectrum of **2** (CD_2Cl_2, 600 MHz, 213 K).

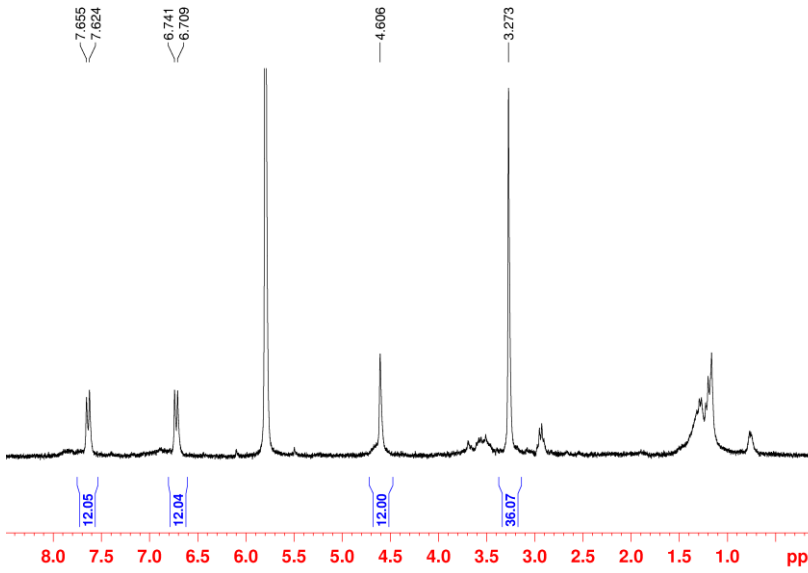

Figure 27. ^{1}H NMR spectrum of **3** (TCE-d_2, 300 MHz, 393 K).

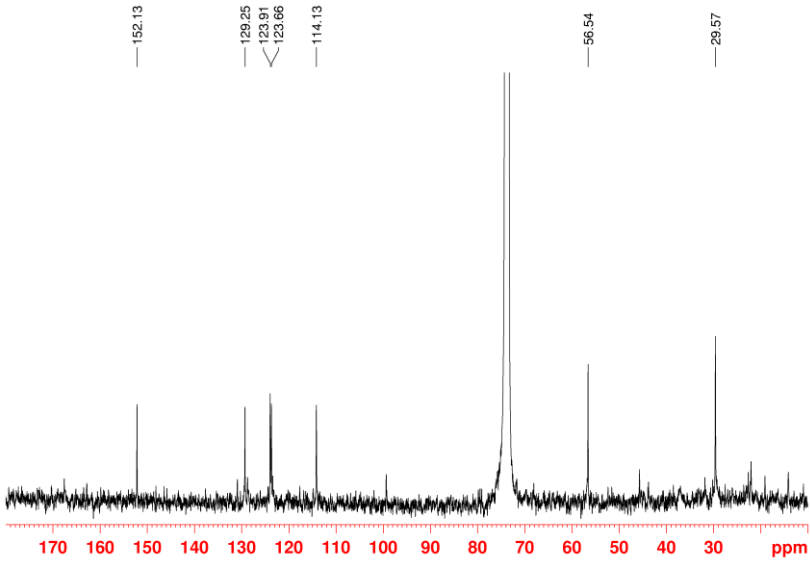

Figure 28. ^{13}C NMR spectrum of **3** (TCE-d_2, 75 MHz, 298 K).

2.4.3 Copies of 1D NMR Spectra of PrS[n]^{Me} Complexes[46, 61]

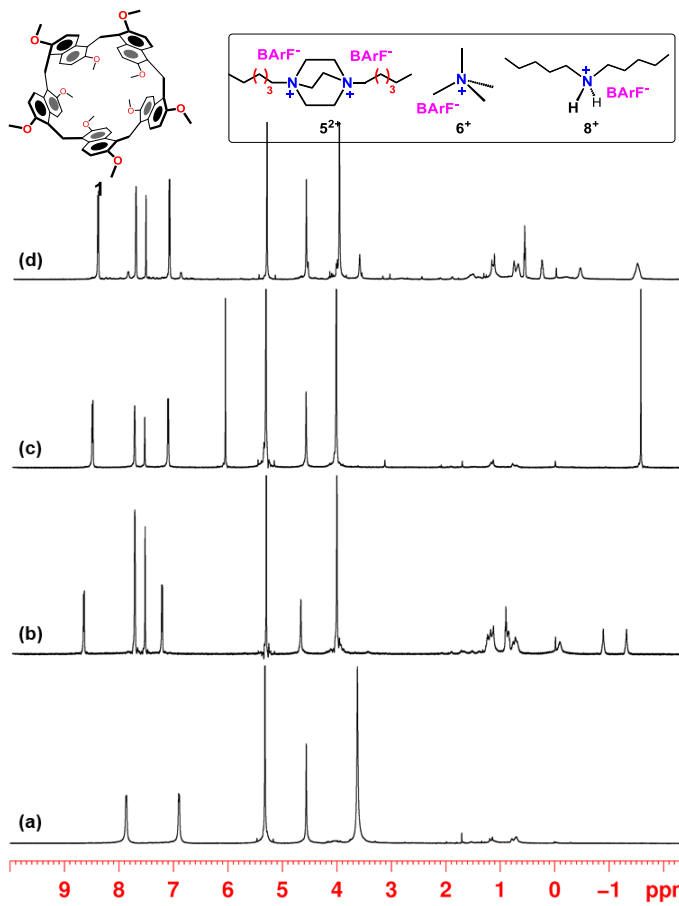

Figure 29. ^{1}H NMR spectra in CD_2Cl_2, 600 MHz at 183 K of: (a) **1**; 1:1 mixture (2.85 mM) of **1** and, respectively: (b) **5^{2+}· 2BArF^{-}**, (c) **6^{+}· BArF^{-}**, (d) **8^{+}· BArF^{-}**.

[61] For all 1D and 2D NMR spectra of prismarenes complexes see: Della Sala, P.; Del Regno, R.; Talotta, C.; Capobianco, A.; Hickey, N.; Geremia, S.; De Rosa, M.; Spinella, A.; Soriente, A.; Neri, P.; Gaeta, C. *J. Am. Chem. Soc.* **2020**, *142*, 1752-1756.

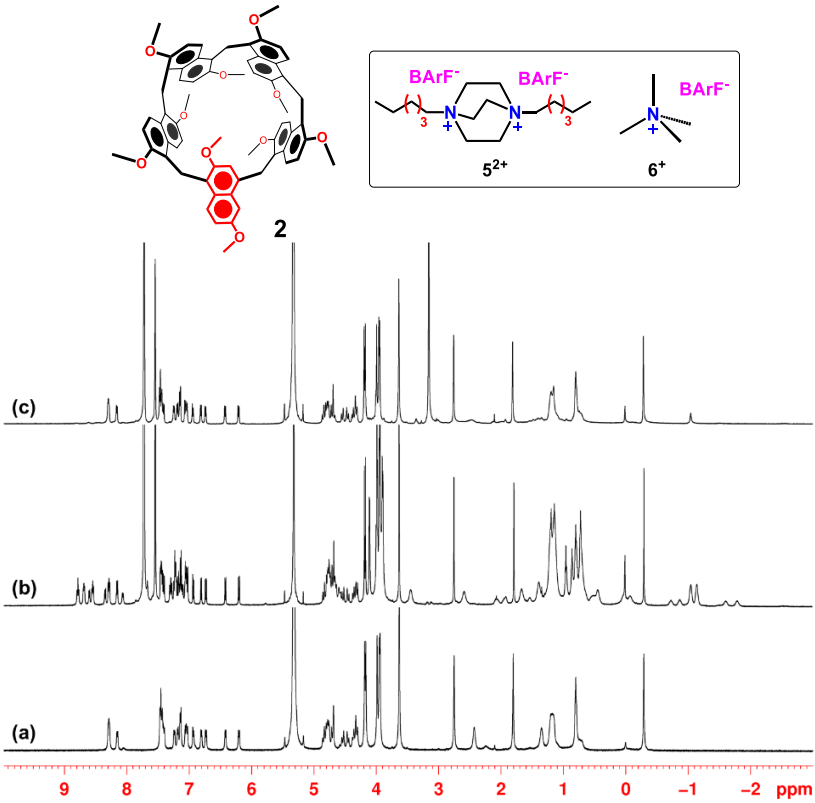

Figure 29. ^{1}H NMR spectra in CD_2Cl_2, 600 MHz at 183 K of: (a) **2**; 1:1 mixture (2.85 mM) of **2** and, respectively: (b) $\mathbf{5^{2+}\cdot\ 2BArF^{-}}$, (c) $\mathbf{6^{+}\cdot\ BArF^{-}}$

.

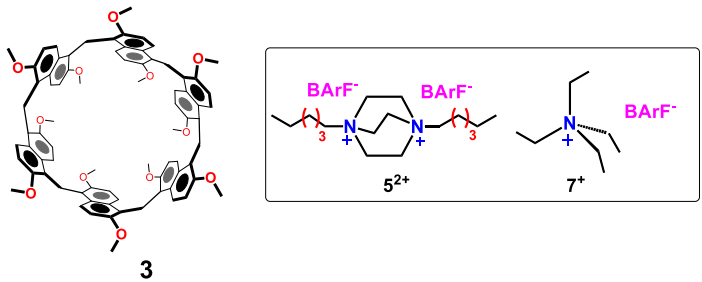

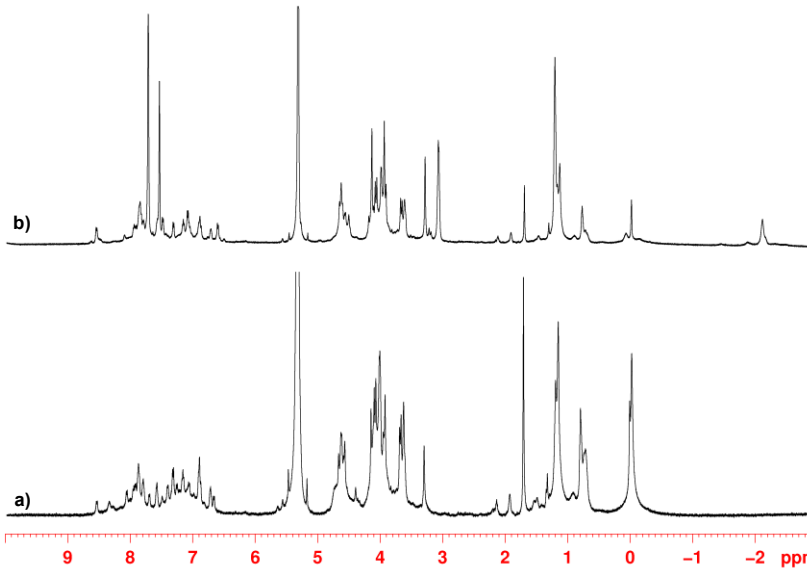

Figure 31. ^{1}H NMR spectra (600 MHz, CD_2Cl_2, 183 K) of: (a) a solution of **3** (b) an equimolar solution of **3** and **7**$^{+\cdot}$ **BArF**$^{-}$ (2.85 mM).

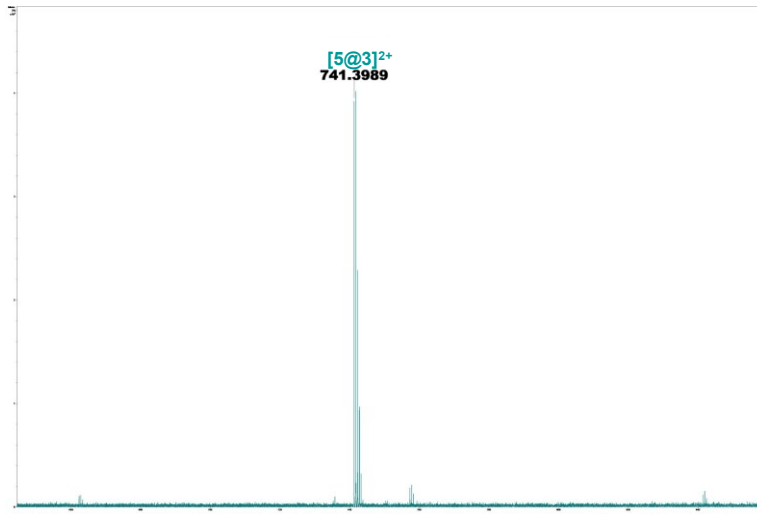

Figure 32. Significant portion of the HR ESI FT-ICR mass spectrum of **[5@3]**$^{2+}$.

2.4.4 ^{1}H NMR Determination of K_{ass} Values[46, 62, 63]

The association constant values of complexes were calculated by means of three methods:

a) Integration of free and complexed ^{1}H NMR signals of host or guest. In this case, an equimolar solution (2.85 mM) of hosts and guests was solubilized in CD_2Cl_2 and equilibrated in a NMR tube after mixing for 24 h at 40 °C.
b) ^{1}H NMR competition experiments. In this case, was performed an analysis of a 1:1:1 mixture of host, and two guests in an NMR tube using 0.7 mL of CD_2Cl_2 as solvent.
c) Quantitative ^{1}H NMR experiments using TCE as the internal standard[64]. In this case, ^{1}H NMR experiments were carried out on a 1:1 mixture of host and guest in 0.7 mL of CD_2Cl_2 containing 1 µL or 0.5 µL of 1,1,2,2-tetrachloroethane (d= 1.59 g/mL) as internal standard.

[a]Calculated by quantitative ^{1}H NMR spectroscopy at 298 K analysis using TCE as internal standard, the calculated

[62] Gaeta, C.; Troisi, F.; Neri, P. *Org. Lett.* **2010**, *12*, 2092-2095.
[63] For all 1D NMR spectra of the experiments for the calculation of K_{ass} values see: Della Sala, P.; Del Regno, R.; Talotta, C.; Capobianco, A.; Hickey, N.; Geremia, S.; De Rosa, M.; Spinella, A.; Soriente, A.; Neri, P.; Gaeta, C. *J. Am. Chem. Soc.* **2020**, *142*, 1752-1756.
[64] Bakić, M. T.; Iuliano, V.; Talotta, C.; Geremia, S.; Hickey, N.; Spinella, A.; De Rosa, M.; Soriente, A.; Gaeta, C.; Neri, P. *J. Org. Chem.* **2019**, *84*, 11922-11927.

K_{ass} value was confirmed by competition experiment. [b]Calculated by competition experiment at 298 K with **13**$^{+}$. [c]Calculated by competition experiment at 298 K with **11**$^{2+}$. [d]Calculated by competition experiment at 298 K with **10**$^{2+}$. [e]Calculated by quantitative ^{1}H NMR study at 183 K analysis using TCE as internal standard, the calculated K_{ass} value was confirmed by competition experiment. [f]Calculated at 183 K by integration of ^{1}H NMR signals of free and complexed species.[63]

	1	2	3
5^{2+}	$3.9 \cdot 10^{7}$[d]	470[f]	50[f]
6^{+}	$6.4 \cdot 10^{4}$[e]	20[f]	-
7^{+}	90[f]	–	2700[f]
8^{+}	9600[f]	190[f]	310[f]
9^{+}	$2.0 \cdot 10^{4}$[f]	–	100[f]
10^{2+}	$1.8 \cdot 10^{7}$[c]	1400[f]	–
11^{2+}	$4.7 \cdot 10^{6}$[b]	400[f]	–
12^{+}	150[f]	100[f]	70[f]
13^{+}	$4.6 \cdot 10^{4}$[a]	50[f]	-

Table 2. Association constant ($K_{ass,}$ M^{-1}) values for the formation of the complexes between the ammonium **5**$^{2+}$ - **13**$^{+}$ cations as **BArF**$^{-}$ salts and the prism[n]arenes **1**–**3**. Determined by ^{1}H NMR experiments in CD_2Cl_2 (600 MHz). Errors < 15% calculated as mean values of three measures.

3.0 An intramolecularly Self-Templated Synthesis of Prism[n]arene[47]

3.1 Synthesis of Alkoxy-Prismarenes[47]

As previously reported, the first study on prismarenes was focused on the synthesis and recognition properties of methoxy-based prismarenes, obtained by a thermodynamically controlled cyclization process.[46]
In fact, starting by derivative **4a**, in the presence of paraformaldehyde and TFA in 1,2-DCE, we isolated ***c*-PrS[5]^{Me}** in 40% yield. Differently, adding an appropriate complementary templating agent in the reaction mixture, the **PrS[5]^{Me}** or the **PrS[6]^{Me}** was selectively removed from the equilibrium- as reported in **Paragraph 2.1**.[46]

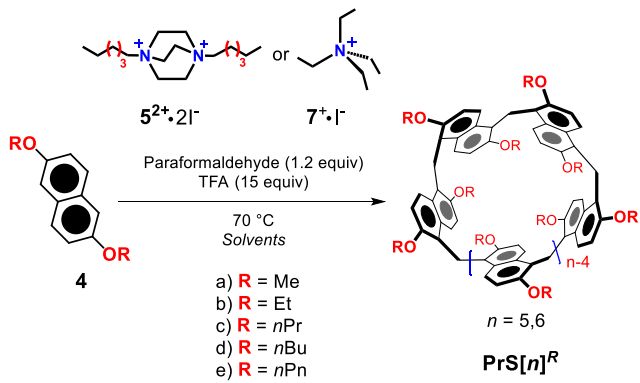

Scheme 3. Synthesis of **PrS[n]^R** prismarenes.[46,47]

[47] Della Sala, P.; Del Regno, R.; Di Marino, L.; Calabrese, C.; Palo, C.; Talotta, C.; Geremia, S.; Hickey, N.; Capobianco, A.; Neri, P.; Gaeta, C. *Chem. Sci.* **2021**, *12*, 9952-9961.

In analogy with this study[46], we decided to explore the synthesis of prism[n]arenes by changing the solvent and alkoxy-chains[47].

In detail, starting by 2,6-diethoxynaphthalene **4b** (in 1,2-dichloroethane, as solvent, paraformaldehyde and in a presence of TFA, as catalyst, at 70 °C - **Scheme 3**) unexpectedly, after 45 min the hexamer **PrS[6]*Et*** was formed in 75% yield - **Table 3**.[47]

Entry[a]	Solvent	Monomer	Time	***c*-PrS[5]*R***	**PrS[5]*R***	**PrS[6]*R***
1	1,2-DCE	**4a**[46]	22 h	40	0.3	–
2	1,2-DCE	**4a**[46, b]	22 h	16	47	–
3	1,2-DCE	**4a**[46, c]	72 h	6.0	0.3	20
4	1,2-DCE	**4b**[a]	45 min	–	–	75
5	1,2-DCE	**4c**[a]	90 min	–	–	65
6	1,2-DCE	**4b**[a, b]	22 h	–	10	35
7	1,2-DCE	**4b**[a, c]	22 h	–	–	60
8	1,2-DCE	**4c**[a, b]	22 h	–	25	25
9	1,2-DCE	**4c**[a, c]	22 h	–	–	55
10	1,2-DCE	**4d**[a]	40 min	-	-	30
11	1,2-DCE	**4e**[a]	12 h	–	–	8
12	Cl-CyHex	**4b**[a]	40 min	–	–	71
13	Cl-CyHex	**4c**[a]	2 h	–	–	64
14	Toluene	**4a**[a]	24 h	11	–	–
15	Toluene	**4b**[a]	3 h	–	–	74
16	Toluene	**4c**[a]	8 h	–	–	57
17	CyHex	**4a**[a]	24 h	7	–	–
18	CyHex	**4b**[a]	30 min	–	–	76
19	CyHex	**4c**[a]	40 min	–	–	65
20	Decaline	**4b**[a]	30 min	–	–	75
21	Decaline	**4c**[a]	45 min	–	–	70

[a] [Monomer] = 5 mM; TFA and paraformaldehyde, 70 °C. [b] In the presence of $\mathbf{5}^{2+}$. [c] In the presence of $\mathbf{7}^{+}$.

Table 3. Solvent and alkoxy-chain effects in the synthesis of **PrS[n]*R***.[47]

Surprisingly, when 2,6-dipropoxynaphthalene **4c** was used, **PrS[6]^{nPr}** was isolated in 65% yield (**Table 3**).[47]
These results were surprising; in fact, from the data previously reported by Ogoshi[65] and by us[46], the 1,2-DCE does not play a template effect in the synthesis of pillar[6]arene or **PrS[6]^{Me}**.
The hexamer **PrS[6]^{Et}** was the favoured product also in the presence of other not-templating solvents, such as chloro-cyclohexane, cyclohexane, toluene, and decaline - **Table 3**.[47]
In addition, analogues results were obtained for the 2,6-dipropoxynaphtalene.[47]
In order to investigate whether **PrS[6]^{Me}** is obtained by using different solvents than 1,2-DCE, we performed the reactions in cyclohexane or toluene (**Scheme 6**, **Table 3**). In these conditions, no hexamer was detected, in contrast the *confused* was formed but in a very low yield (**Table 3**). Moreover, starting by a monomer with longer alkyl chains, such as 2,6-dibutoxynaphthalene and 2,6-dipentoxynaphthalene, the **PrS[6]^{R}** were obtained in lower yield - **Scheme 3**, **Table 3**.[47]
In conclusion, we can argue that the length of the alkyl chains of prismarens plays a crucial role in the synthesis of these macrocycles. In fact, in the presence of ethoxy and propoxy chains, the hexamer is formed in high yields, independent of the nature and size of the solvent, while in the presence of methoxy groups, the hexamer is not formed. In addition, the yields of prism[6]arene decrease with longer alkyl chains than propyl.

[65] T. Ogoshi, T.; Ueshima, N.; Akutsu, T.; Yamafuji, D.; Furuta, T.; Sakakibara F.; Yamagishi, T.-a. *Chem. Commun.*, **2014**, *50*, 5774–5777.

Finally, we investigated the role of the ammonium templates in the synthesis of ethoxy and propoxy derivatives – **Scheme 3**. In particular, when we used the cation $\mathbf{5^{2+}}$ as template and 2,6-diethoxynaphtalene as monomer (**Scheme 3**), the **PrS[6]*Et*** was formed in 35% yield, while the pentamer was obtained in 10% yield – **Table 3**. In addition, using 2,6-dipropoxynaphtalene as monomer and the cation $\mathbf{5^{2+}}$ as template, a mixture of **PrS[5]*nPr*** and **PrS[6]*nPr*** in 1/1 ratio was obtained.[46] While, when we used the cation $\mathbf{7^{+}}$, after 22 h (**Scheme 3**), the yields of **PrS[6]*Et*** and **PrS[6]*nPr*** reached, respectively, a value of 60% and 55%.[47]

These results indicate that, the $\mathbf{5^{2+}}$ cation is less effective as a thermodynamic template in the synthesis of ethoxy and propoxy pentamers. Similarly, we can state that the ammonium cation $\mathbf{7^{+}}$ has no influence on the formation of the prismarene hexamers. In other words, the thermodynamic effect of the host-guest complexation observed in the synthesis of methoxy-based prismarenes **PrS[5]*Me*** and **PrS[6]*Me***,[45] is exceeded by the intramolecular effect of the ethyl and propyl chains.[47]

In fact, the thermodynamically self-templation by the *Et* and *nPr* alkyl chains in the synthesis of prismarene hexamers is testified by the higher yield (65-75%) of product and shorter reaction time, in absence of cations.

To confirm the thermodynamic nature of the hexamers, the **PrS[5]*Et*** or **PrS[5]*nPr*** were heated at 70 °C in 1,2-DCE, in the presence of TFA. Under these conditions, a conversion to **PrS[6]*Et*** and **PrS[6]*nPr*** in 83 % and 85 % yield, respectively, was observed after 22 h, confirming their higher thermodynamic stability[47].

3.2 The Role of the Alkyl Chains in the Synthesis of Ethoxy- and Propoxy-Prismarenes[47]

With these results in hand, we investigated the nature of the self-templation effect by the alkyl chains by detailed X-ray, DFT and 2D NMR studies. The structure of prismarenes were explored, both in solution and in the solid state, by single crystal X-ray diffraction (**Figure 33**), NMR techniques[47] and by DFT calculations (**Figure 34**).[47]

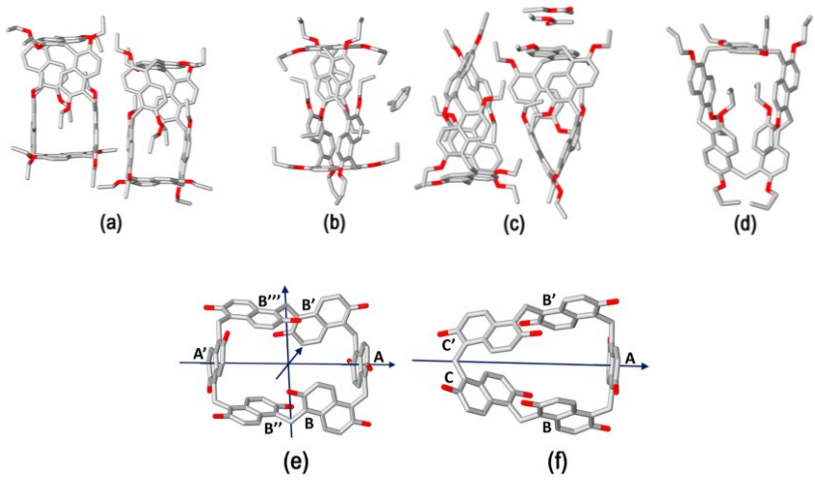

Figure 33. Stick representation of the asymmetric units of a) **PrS[6]**^{Et}, b) **PrS[6]**^{nPr}, c) **PrS[5]**^{Et}, and d) **PrS[5]**^{nPr}. For **PrS[6]**^{nPr} the entire molecule generated by a crystallographic two-fold axis is shown. (e and f) Stick representation of e) the D_2 symmetric **PrS[6]**^{R} and f) the C_2 symmetric **PrS[5]**^{R} scaffolds.[47]

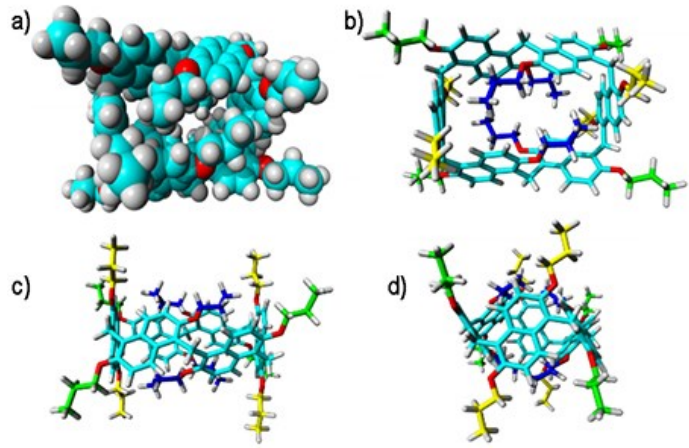

Figure 34. Different views of the DFT optimized structure of **Pr[6]**^{nPr}. Top views of the CPK (a) and tube (b) structure. Side views (c and d). In blue the propoxy chains inward oriented and filling the cavity, in green the propoxy chains outside oriented, and in yellow the propoxy chains on the parallel naphthalene rings.[47]

In particular, it was observed that the prism[6]arenes are folded in a nearly square cuboid-structure (**Figures 33a**, **33b**, **33e** and **34**), in which the two opposite naphthalene rings define the square faces of the macrocycle. In addition, four alkyl chains are oriented inward to the cavity of the macrocycle. These chains establish four C-H$\cdots\pi$ interactions with the aromatic walls - **Figure 34**. Moreover, the X-ray structures (**Figures 35a** and **35b**) show that the terminal methyl group of the chains of **PrS[6]**^{nPr} are outward oriented while the four ethyl groups of **PrS[6]**^{Et} are entirely included inside the cavity of the macrocycle (**Figures 35d** and **35e**), filling the inner space more efficiently than the propyl chains.[47]

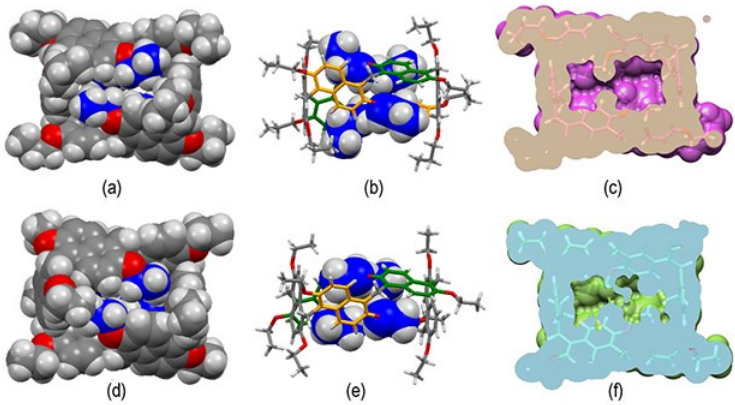

Figure 35. Self-filling of the cavities of prism[6]arenes as obtained by X-ray structures. (a and b) Different views of **PrS[6]^{nPr}** . (d and e) Different views of **PrS[6]^{Et}** . (c and f) Self-filling of the cuboid cavity. Cross-sections of the **PrS[6]^{Et}** (f) and **PrS[6]^{nPr}** (c) molecules. An enclosed internal cavity was obtained from accessible surface area calculations using a 0.4 Å probe. The free cavity volume is 49 Å^3 and 77 Å^3 for **PrS[6]^{Et}** and **PrS[6]^{nPr}**, respectively.[47]

This self-filling of the central cavity of the hexamer is fundamental for the thermodynamic stabilization of the macrocycle; in particularly, it is relevant to the conformational properties in solution and recognition abilities.[47]

The cuboid structure of **PrS[6]^{R}** (R = Et and *n*Pr) is retained also in solution as confirmed by 1D and 2D NMR investigations. In fact, the ^{1}H NMR spectrum at 243 K of the **PrS[6]^{nPr}** (**Figure 36**) in CD_2Cl_2, is in accord with the D_2 symmetry (**Figure 35b**). In detail, the ^{1}H NMR spectrum of **PrS[6]^{nPr}** show three aromatic AX/AB systems at 8.28/7.35 (9.6 Hz), 7.91/7.01 (9.6 Hz), and 7.52/6.35 (9.6 Hz), and two singlets at 4.82 and 4.42 ppm attributable to the methylene-bridged groups. Moreover, the spectrum

shows three diasterotopic AB systems at 4.25/4.23, 4.17/3.95, and 3.00/2.29 ppm, attributable to the O*CH*$_2$ groups. Finally, the signals at negative chemical shift values are attributable to the propyl chains shielded inside the cavity of the macrocycle– **Figure 36** and see **Figure 49**, paragraph **3.6.2**. [47]

Similarly, the 1D NMR spectrum of **PrS[6]*^{Et}*** (see **Figure 46**, paragraph **3.6.2**) show the same features of **PrS[6]*^{nPr}***.[47]

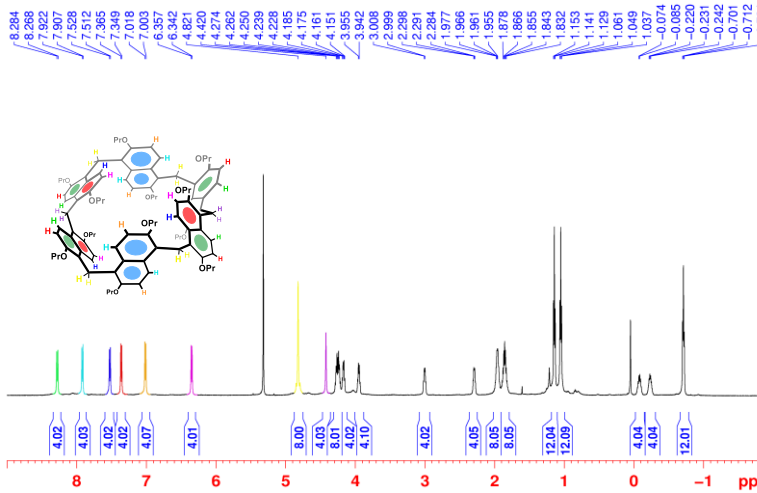

Figure 36. ^{1}H NMR spectrum of **PrS[6]*^{nPr}*** (CD_2Cl_2, 600 MHz, 243 K).[47]

Interestingly the *D*$_2$ cuboid structure of the hexamers, were retained in solution in the presence of solvents, such as chloro-cyclohexane, decaline, and 1,2-DCE, used during the synthesis. In fact, ^{1}H NMR spectra of the **PrS[6]*^{nPr}*** (**Figure 37**),[47] in non-deuterated solvents such as: chloro-cyclohexane, decaline, and 1,2-DCE, showed analogous features than that obtained in dichloromethane.

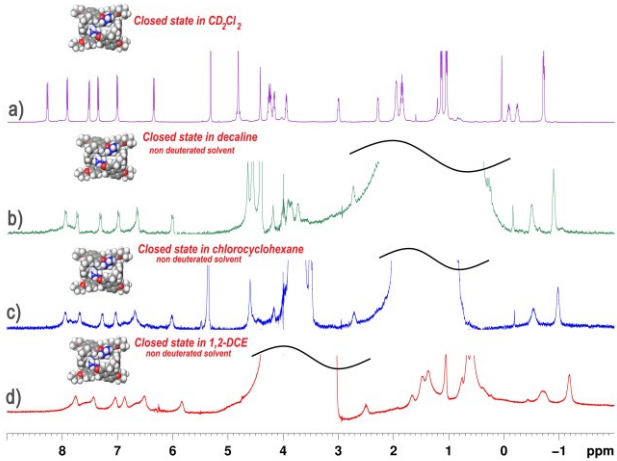

Figure 37. ^{1}H NMR spectra of **Pr[6]^{nPr}** in: (a) CD_2Cl_2 at 243 K (600 MHz); (b) non-deuterated decaline (298 K); (c) non-deuterated chlorocyclohexane; (298 K); (d) non-deuterated 1,2-dichloroethane (298 K).[47]

These results (**Figure 37**) indicates clearly that the solvents used during the synthesis in **Table 3**, were not included inside the cavity of prism[6]arene^R (R = Et and *n*Pr) and consequently didn't act as templated agents. Therefore, we can assume that the nature of the alkyl chains, plays a crucial role in the conformational stabilization of the hexamers and drives the equilibrium toward their formation.[47] Based on these results, an intramolecular thermodynamic self-templating effect was invoked, in which the formation of the prism[6]arene is driven by an "intramolecular self-templation" of the alkyl chains. In other words: the self-filling of the internal cavity of **PrS[6]^{Et}** or **PrS[6]^{nPr}** stabilizes their cuboid structure driving the equilibrium toward their formation.[47]

3.3 Conformational Dynamics of Prism[n]arenes

Analogously to pillararene[14] macrocycles, the prism[n]arenes exhibit planar chirality (**Figure 38**). The hexamers (**PrS[6]^{R}**) show six planes of chirality which are coplanar with the 2,6-dialkoxynaphthalene rings and the bridged-methylene carbons at the 1/5 ring positions. In theory, the **PrS[6]^{R}** can adopt 13 conformers of different planar chirality of which 5 enantiomeric pairs (I-V in **Figure 38**) and 3 meso-forms (VI, VII and VIII in **Figure 38**). The pentamers **PrS[5]^{R}** can adopt 8 conformers of different planar chirality corresponding to 4 enantiomeric pairs (I-IV in **Figure 38**).

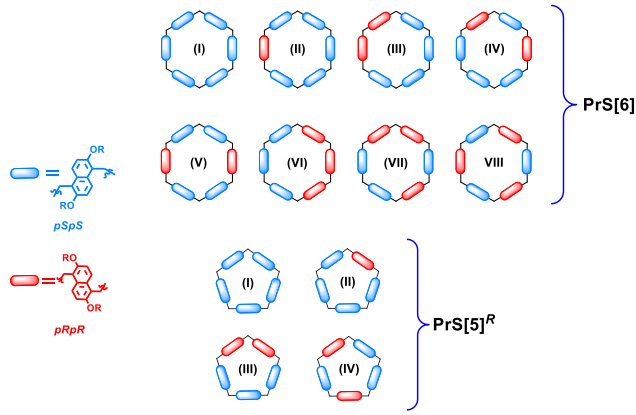

Figure 38. (Top) Schematization of the eight possible conformers (5 enantiomeric forms I-V and 3 meso-forms VI-VIII) of the prism[6]arene**.** *pS*-(I) = *pSpSpSpSpSpS*; (II) = ***pR****pSpSpSpSpS*; (III) = ***pRpR****pSpSpSpS*; (IV) = ***pR****pS****pR****pSpSpS*; (V) = ***pR****pSpS****pR****pSpS*; (VI) = ***pRpRpR****pSpSpS;* (VII) = ***pRpR****pS****pR****pSpS;* (VIII) = ***pR****pS****pR****pS****pR****pS*. (Bottom) Schematization of the four conformers of the prism[5]arene (4 enantiomers)**.** *pS*-(I) = *pSpSpSpSpS*; (II) = ***pR****pSpSpSpS*; (III) = ***pRpR****pSpSpS*; (IV) = ***pR****pS****pR****pSpS*.

The chirality in these conformational isomers of prismarenes can be described with *p*R and *p*S nomenclature (**Figure 38**) as reported for the pillararenes.[14]

The structure assumed by prismarenes were studied theoretically by DFT calculations and experimentally, both in solution and in the solid state, by NMR techniques and single crystal X-ray diffraction, respectively. DFT study were conducted at the B97D3/SVP/SVPFIT level of theory. The calculations indicate the conformations I, all-*p*S (*p*R) (**Figure 38**), as the most stable for **PrS[6]^{nPr}**, while the conformations II–VIII in **Figure 38** are predicted to be less stable than the I by 30-45 kcal/mol (see **Table 6** paragraph **3.6.5**). Analogues result were obtained for the **PrS[5]^{nPr}**, with conformations I, all-*p*S (*p*R) (**Figure 38**), more stable than all the other possible conformations II, III and IV (**Figure 38**) by 11.8, 14.7 and 8.1 kcal/mol (see **Table 7** paragraph **3.6.5**) respectively.

Analogously, the 1D and 2D NMR analysis indicates that the **PrS[6]^{nPr}** (**Figure 36**) adopts also in solution an all-*p*S (*pR*) conformation (I) with a pseudo D_2 point symmetry. This is in agreement with the presence of shielded ^{1}H NMR signals at negative chemical shift values, attributable to the methyl groups of the propoxy-chains (**Figure 36**). The presence of diastereotopic resonances for the OCH_2 groups of **PrS[6]^{nPr}** (see **Figure 49**, paragraph **3.6.2**) is due to the planar chirality of the macrocycle, in agreement with the considerations previously reported for pillar[5]arenes[14]. The diasterotopic OCH_2 signals coalesced at 363 K (see **Figure 53**, paragraph **3.6.3**), and above this temperature a broad signal was detected for the OCH_2 groups. The coalescence of the diastereotopic OCH_2 signals of **PrS[6]^{nPr}** indicates clearly that the *p*S-I is

converted to *p*R-I and *vice versa* (**Figure 39**), by the *oxygen-through-the-annulus* passage of the naphthalene units, which is fast on the NMR time scale at higher temperature. At the coalescence temperature of 363 K a $\Delta G^{\ddagger}$ value of 17.3 kcal/mol was calculated for this process see (**Figure 53**, paragraph **3.6.3**).

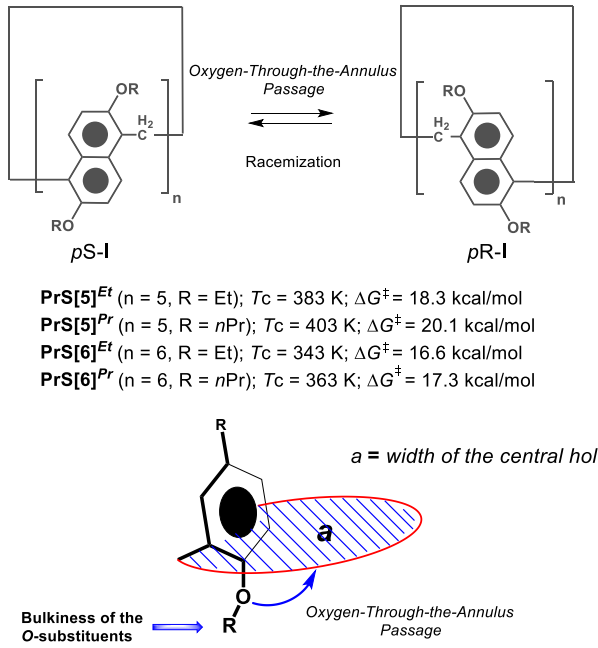

Figure 39. (Top) *Oxygen-through-the-annulus* in prism[*n*]arene derivatives. (Bottom*) O-through-the-annulus* passage in cyclophane macrocycles and factors OR-passage rate determining.

The DFT calculations show that the energies of all the other conformations (II–VIII in **Figure 38**) are much higher (30-45 kcal/mol) than the two I conformations, all-p*S* and all-pR. The comparison of these values with the $\Delta G^{\ddagger}$ value of 17.3 kcal/mol calculated from the coalescence temperature indicates that the interconversion between

all-pS/all-pR should take place by a mechanism that excludes passage through any other minimum energy conformers of different planar chirality. Therefore, the inversion of the macro-ring could be promoted by a domino effect, as already hypostasized by Ogoshi for pillarene molecules.[14]Analogously to the **PrS[6]^{nPr}**, the ^{1}H NMR spectrum of **PrS[6]^{Et}** (see **Figure 46**, paragraph **3.6.2**) at 243 K is again in agreement with a pseudo D_2 point symmetry. In this case, with respect to the propoxy derivative, a lower coalescence temperature of 343 K was found for the diastereotopic OCH_2 signals of **PrS[6]^{Et}**, corresponding to a $\Delta G^{\ddagger}$ value of 16.6 kcal/mol for the interconversion process between all-*p*S/all-*pR*.

Similarly, the presence of OCH_2 diastereotopic resonances in the ^{1}H NMR spectra of **PrS[5]^{R}** (R = Et, *n*-Pr, see **Figure 42** and **Figure 44**, respectively, paragraph **3.6.2**) confirms their planar chirality (all *p*S or all *pR*). On heating, the diastereotopic OCH_2 signals coalesced at 383 and 403 K for the **PrS[5]^{Et}** and **PrS[5]^{nPr}**, respectively. The corresponding energy barriers were calculated at 18.3 for **PrS[5]^{Et}** (see **Figure 50**, paragraph **3.6.3**) and 20.1 kcal/mol for **PrS[5]^{nPr}** (see **Figure 51**, paragraph **3.6.3**). The DFT calculations show that, the energies of all the other conformations (II–IV in **Figure 38**) of **PrS[5]^{nPr}** are higher (8.0-15 kcal/mol) than the two I conformations (see **Table 7** paragraph **3.6.5**), all-*p*S and all-*p*R. Thus, differently by the hexamer **PrS[6]^{nPr}**, the comparison of these values with the $\Delta G^{\ddagger}$ value of 20.1 kcal/mol calculated from the coalescence temperature indicates that the interconversion between all-*p*S/all-*p*R should take place by a mechanism that involves the passage through other minimum energy conformers of different planar chirality.

3.4 Molecular Recognition Properties of Ethoxy and Propoxy Prism[6]arenes [47,66]

At this point, it was interesting to study the recognition abilities of **PrS[6]^{nPr}** and **PrS[6]^{Et}** hosts toward cationic ammonium guests (**Scheme 4**), as done for **PrS[n]^{Me}** [45] (See paragraph **2.2**).

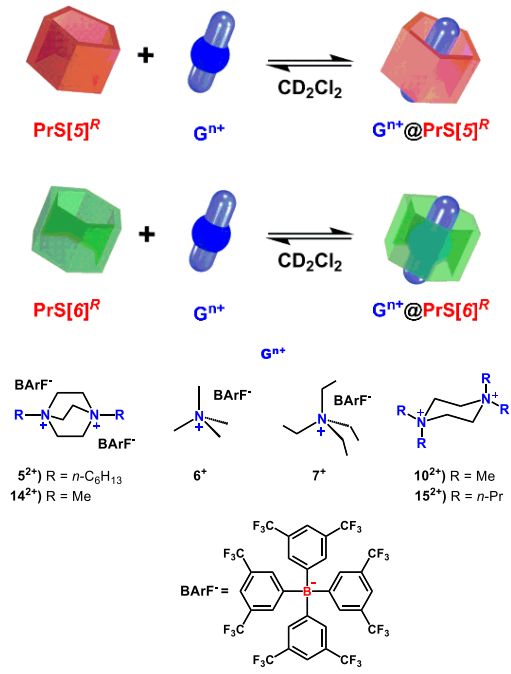

Scheme 4. Schematic complexation equilibrium of **PrS[*n*]^{R}** with ammonium guests **5^{2+}–7^{+}**, **10^{2+}**, **14^{2+}** and **15^{2+}**, as barfate salts.[47]

[66] For all 1D and 2D NMR spectra of prismarenes complexes and for the details on stability constant determination see: Della Sala, P.; Del Regno, R.; Di Marino, L.; Calabrese, C.; Palo, C.; Talotta, C.; Geremia, S.; Hickey, N.; Capobianco, A.; Neri, P.; Gaeta, C. *Chem. Sci.* **2021**, *12*, 9952-9961.

In particular, the complexation of *N,N,N′,N′*-tetramethylpiperazonium $\mathbf{10^{2+}}$ cation (**Scheme 4**) is found to be very interesting. In fact, when 1 equiv of $\mathbf{10^{2+}}$ $\mathbf{BArF^-}$ was added to a solution of $\mathbf{PrS[6]^{nPr}}$ in CD_2Cl_2, its ^{1}H NMR spectrum shows significant changes.[47]

In detail, the ^{1}H NMR spectrum of the complex $\mathbf{10^{2+}@PrS[6]^{nPr}}$ (**Figure 40b**) shows a D_6 symmetry. In addition, ^{1}H NMR signals of the guest was observed at negative value of chemical shifts between −0.80 ppm and −1.02 ppm (J = 11.4 Hz), indicative of the formation of the complex- **Figure 40b**.[47]

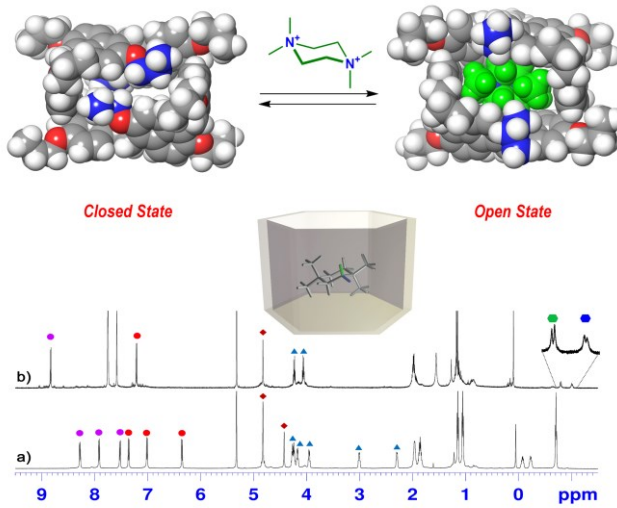

Figure 40. ^{1}H NMR spectra of (a) $\mathbf{PrS[6]^{nPr}}$ in CD_2Cl_2 at 243 K (600 MHz) and (b) a 1:1 mixture of $\mathbf{PrS[6]^{nPr}}$ and $\mathbf{10^{2+}}\cdot(BArF)_2$ (3 mM) in CD_2Cl_2 at 298 K (600 MHz). The correspondence between the marked signals indicates the conformation change from closed state to open state upon complexation with $\mathbf{10^{2+}}$. The blue and green hexagons indicate the diastereotopic methylene H-atoms of $\mathbf{10^{2+}}$ shielded inside the macrocycle. (Top) DFT optimized structure of $\mathbf{PrS[6]^{nPr}}$ in closed state and of its complex with $\mathbf{10^{2+}}$.[47]

The presence of the guest into the macrocycle cavity forces the cuboid scaffold to open. In fact, the DFT-optimized structure (**Figure 41**) of the complex **10^{2+}@PrS[6]^{nPr}** shows an opening of the macrocycle, with the guest **10^{2+}** in the central cavity to establish ion-dipole (N+···OR), cation···π, C-H···π, and van der Waals interactions.[47]

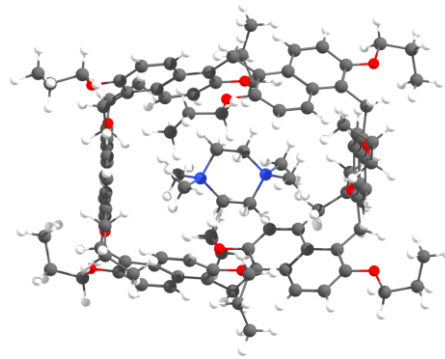

Figure 41. DFT-optimized structure (B97D3/SVP/SVPFIT) of the **10^{2+}@ PrS[6]^{nPr}** complex.[47]

	5^{2+}	7^{+}	10^{2+}	14^{2+}	15^{2+}
PrS[5]^{Me}	3.9×10^{7}	90	1.8×10^{7}	6.6×10^{6}	5.8×10^{3}
PrS[5]^{Et}	1.4×10^{8}	50	2.8×10^{8}	2.9×10^{6}	1.0×10^{5}
PrS[5]^{nPr}	1.7×10^{8}	100	1.4×10^{9}	6.3×10^{7}	4.8×10^{5}
PrS[6]^{Me}	50	2700	[a]	4200	3700
PrS[6]^{Et}	790	2745	1.0×10^{8}	420	[a]
PrS[6]^{nPr}	400	340	1.2×10^{8}	370	[a]

[a] An intricate mixture of complexes was present at the equilibrium due to the presence of macrocyclic hosts in different conformations.

Table 4. Binding constant values of prism[*n*]arene host-guest complexes determined by ^{1}H NMR experiments in CD_2Cl_2 (600 MHz). Errors < 15 % calculated as mean values of three measures. [66]

Finally, an association constant value of 1.2×10^{8} M^{-1} (**Table 4**)[66], was calculated for the formation of the **10^{2+}@PrS[6]^{nPr}** complex, by competition experiments.[46] An analogous behaviour was observed also for the **PrS[6]^{Et}** host after the complexation with **10^{2+}** (**Table 4**).[47,66]

3.5 Conclusions[47]

In conclusion, **PrS[6]^{Et}** and **PrS[6]^{nPr}** are obtained in high yields and in short reaction times, independently of the nature and size of the solvent. Under the reversible macrocyclization conditions here reported **PrS[6]^{Et}** and **PrS[6]^{nPr}** macrocycles are thermodynamic products. The data were collected, show that the synthesis of prismarene hexamers is thermodynamically driven by intramolecular self-templating effect of the Et or *n*Pr alkyl chains. Clarification of this effect were obtained by X-ray studies, 1D and 2D NMR and DFT calculations, which showed that **PrS[6]^{Et}** and **PrS[6]^{nPr}** are folded into a square cuboid-shape conformation with D_2 symmetry, where four alkyl chains are inward-cavity oriented, stabilizing their conformation. Differently, in the presence of shorter methyl groups, an external ammonium template is necessary to drive the macrocyclization toward the pentamer or hexamer.[46] Finally, molecular recognition studies, show that the inclusion of guests inside the internal cavity of the hexamers forces the cuboid structure of **PrS[6]^{Et}** and **PrS[6]^{nPr}** to open.

3.6 Experimental Section

3.6.1 General Section

See **Paragraph 2.4.1**

3.6.2 General Procedure for the synthesis of Prism[n]arenes PrS[n]^{R} and Copies of NMR Spectra [47, 67]

A solution of 2,6-dialkoxynaphthalene **4b-e**, paraformaldehyde (1.2 equiv) in appropriate solvent (**Table 3**, 5.0 mM) was heated at 70 °C, then trifluoroacetic acid (15 equiv) was added and the solution was stirred at 70 °C for the time indicated in **Table 3**. Then, an aqueous saturated solution of $NaHCO_3$ (100 mL) was added in the reaction mixture and the organic layer was extracted. Finally, the organic phase was dried on Na_2SO_4 and concentrated to give a light brown solid.

- Starting by 2,6-diethoxynaphthalene **4b** (250 mg, 1.2 mmol): The crude was purified through chromatographic column on silica gel (only dichloromethane) to give the macrocycle **PrS[6]^{Et}** as white solid (see **Table 3**).

[67] For all detailed synthetic procedures and 1D and 2D NMR spectra of prismarenes see: Della Sala, P.; Del Regno, R.; Di Marino, L.; Calabrese, C.; Palo, C.; Talotta, C.; Geremia, S.; Hickey, N.; Capobianco, A.; Neri, P.; Gaeta, C. *Chem. Sci.* **2021**, *12*, 9952-9961.

- Starting by 2,6-dipropoxynaphthalene **4c** (250 mg, 1.0 mmol): The crude was purified through chromatographic column on silica gel (*n*-hexane/dichloromethane = 1/1) to give the macrocycle **PrS[6]^{nPr}** as white solid (see **Table 3**).

Quaternary ammonium-templated synthesis.
Templated synthesis in presence of $7^{+}\cdot I^{-}$ salt:

In a solution of 2,6-dialkoxynaphthalene **4b-c** in 1,2-dichloroethane (5 mM) was added paraformaldehyde (1.2 equiv) and the templating agent **$7^{+}\cdot I^{-}$** (1.0 equiv). The mixture was heated at 70° C and then trifluoroacetic acid (15 equiv) was added. The solution was stirred for 22 h at 70 °C and subsequently the solvent was evaporated under reduced pressure. The residue was dissolved in CH_2Cl_2 (30 mL) and the mixture was washed with an aqueous saturated solution of $NaHCO_3$ (30 mL). Finally, the organic layer was washed with a 10 % aqueous solution of sodium thiosulfate (100 mL), and the organic phase was dried on Na_2SO_4 and concentrated to give a light brown solid.

- Starting by 2,6-diethoxynaphthalene **4b** (250 mg, 1.2 mmol): The crude was purified through chromatographic column on silica gel (only dichloromethane) to give the macrocycle **PrS[6]^{Et}** as white solid (162 mg, 60 %).
- Starting by 2,6-dipropoxynaphthalene **4c** (250 mg, 1.0 mmol): The crude was purified through chromatographic column on silica gel (*n*-hexane/dichloromethane = 1/1) to give the macrocycle **PrS[6]^{nPr}** as white solid (150 mg, 55 %).

Templated synthesis in presence of $5^{2+}\cdot 2I^-$ salt:

In a solution of 2,6-dialkoxynaphthalene **4b-c** in 1,2-dichloroethane (5 mM) was added paraformaldehyde (1.2 equiv) and templating agent $\mathbf{5^{2+}\cdot I^-}$ (1.0 equiv). The mixture was heated at 70 °C and then trifluoroacetic acid (15 equiv) was added. The solution was stirred at 70 °C for 22 h. After, 250 mL of an aqueous saturated solution of $NaHCO_3$ was added and the organic layer was washed with a 10 % aqueous solution of sodium thiosulfate (200 mL). Finally, the organic layer was dried on Na_2SO_4 and evaporated in vacuum to give a light brown solid.

- Starting by 2,6-diethoxynaphthalene **4b** (1.00 g, 4.6 mmol): The crude product was purified through chromatographic column on silica gel (*n*-hexane/toluene/dichloromethane = 1/2/7) to give the macrocycles **PrS[5]*Et*** (110 mg, 10 %) and **PrS[6]*Et*** (370 mg, 35 %) as white solids.
- Starting by 2,6-dipropoxynaphthalene **4c** (1.00 g, 4.1 mmol): The crude product was purified through chromatographic column on silica gel (*n*-hexane/toluene/dichloromethane = 2.5/2.5/5) to give the macrocycles **PrS[5]*nPr*** (270 mg, 25 %) and **PrS[6]*nPr*** (260 mg, 25 %) as white solids.

Derivative PrS[5]*Et*:
M.p.: > 372 °C dec. **^{1}H NMR** (CD_2Cl_2, 400 MHz, 298 K): *δ* 7.85 (*d*, 10H, Ar-*H, J* = 9.2 Hz), 6.81 (*d*, 10H, Ar-*H, J* = 9.2 Hz), 4.70 (*s*, 10H, ArC*H*$_2$Ar), 3.86 (*m*, 10H, O*CH*$_2$), 3.66 (*m*, 10H, O*CH*$_2$), 0.94 (*m*, 30H, *CH*$_3$). **^{13}C NMR** {^{1}H} (CD_2Cl_2, 100 MHz, 298 K): *δ* 152.0, 129.8, 125.1, 124.1,

114.5, 65.5, 22.2, 15.2. **HR MS** (MALDI**)** m/z $[M]^+$ calcd for $C_{75}H_{80}O_{10}$: 1140.5751; found: 1140.5796.

Derivative PrS[5]^{nPr}:
M.p.: > 333 °C dec. **^{1}H NMR** (CD_2Cl_2, 400 MHz, 298 K): *δ* 8.06 (*d*, 10H, Ar-*H, J* = 9.6 Hz), 6.88 (*d*, 10H, Ar-*H, J* = 9.6 Hz), 4.71 (*s*, 10H, ArC*H*$_2$Ar), 3.88 (*m*, 10H, O*CH*$_2$), 3.76 (*m*, 10H, O*CH*$_2$), 1.63 (*m*, 20H, OCH$_2$*CH*$_2$), 0.92 (*t*, 30H, *CH*$_3$, *J* = 8.0 Hz). **^{13}C NMR** {^{1}H} (CD_2Cl_2, 100 MHz, 298 K): *δ* 152.0, 129.9, 125.2, 123.7, 114.4, 71.5, 23.4, 21.7, 11.0. **HR MS** (MALDI) *m*/*z* $[M]^+$ calcd for $C_{85}H_{100}O_{10}$: 1280.7316; found: 1280.7388.

Derivative PrS[6]^{Et}:
M.p.: > 340 °C dec. **^{1}H NMR** (CD_2Cl_2, 600 MHz, 243 K): *δ* 8.19 (*d*, 4H, Ar-*H, J* = 9.6 Hz), 7.73 (*d*, 4H, Ar-*H, J* = 9.6 Hz), 7.40 (*d*, 4H, Ar-*H, J* = 9.6 Hz), 7.37 (*d*, 4H, Ar-*H, J* = 9.6 Hz), 6.91 (*d*, 4H, Ar-*H, J* = 9.6 Hz), 6.27 (*d*, 4H, Ar-*H, J* = 9.6 Hz), 4.82 (*s*, 8H, ArC*H*$_2$Ar), 4.47 (*s*, 4H, ArC*H*$_2$Ar), 4.39 (*m*, 4H, O*CH*$_2$), 4.33 (*m*, 4H, O*CH*$_2$), 4.20 (*m*, 4H, O*CH*$_2$), 4.06 (*m*, 4H, O*CH*$_2$), 3.04 (*m*, 4H, O*CH*$_2$), 1.54 (*overlapped*, 16H, O*CH*$_2$ and *CH*$_3$), 1.42 (*t*, 12H, *CH*$_3$, *J* = 6.6 Hz), -0.94 (*t*, 12H, *CH*$_3$, *J* = 6.6 Hz). **^{13}C NMR** {^{1}H} (TCE-*d*$_2$, 150 MHz, 298 K): *δ* 152.0, 151.6, 150.9, 129.6, 126.4, 124.9, 123.9, 123.5, 116.2, 114.8, 114.0, 66.0, 65.4, 65.1, 23.5, 21.2, 15.5, 13.5. **HR MS** (MALDI) m/z $[M]^+$ calcd for $C_{90}H_{96}O_{12}$: 1368.6902; found: 1368.6941.

Derivative PrS[6]^{nPr}:
M.p.: > 306°C dec. **^{1}H NMR** (CD_2Cl_2, 600 MHz, 243 K, **Figure 36**): *δ* 8.28 (*d*, 4H, Ar-*H, J* = 9.6 Hz), 7.91 (*d*, 4H, Ar-*H, J* = 9.6 Hz), 7.52 (*d*, 4H, Ar-*H, J* = 9.6 Hz), 7.35 (*d*, 4H, Ar-*H, J* = 9.6 Hz), 7.01 (*d*, 4H, Ar-*H, J* = 9.6 Hz), 6.35

(*d*, 4H, Ar-*H,* J = 9.6 Hz), 4.82 (*s*, 8H, ArCH_2Ar), 4.42 (*s*, 4H, ArCH_2Ar), 4.25 (*overlapped*, 8H, OCH_2), 4.17 (*m*, 4H, OCH_2), 3.95 (*m*, 4H, OCH_2), 3.00 (*m*, 4H, OCH_2), 2.29 (*m*, 4H, OCH_2), 1.95 (*m*, 8H, OCH$_2$CH_2), 1.85 (*m*, 8H, OCH$_2$CH_2), 1.14 (*t*, 12H, CH_3, J = 7.2 Hz), 1.05 (*m*, 12H, CH_3, J = 7.2 Hz), -0.08 (*m*, 4H, OCH$_2$CH_2), -0.24 (*m*, 4H, OCH$_2$CH_2), -0.71 (*m*, 12H, CH_3, J = 7.2 Hz). **^{13}C NMR** {^{1}H} (CD_2Cl_2, 150 MHz, 298 K): δ 153.3, 151.7, 130.2, 125.1, 124.9, 124.3, 115.8, 114.8, 114.3, 71.9, 71.7, 71.4, 23.7, 22.1, 21.6, 11.2, 10.4. **HR MS** (MALDI) m/z [M]$^+$ calcd for $C_{102}H_{120}O_{12}$: 1536.8780; found: 1536.8790.

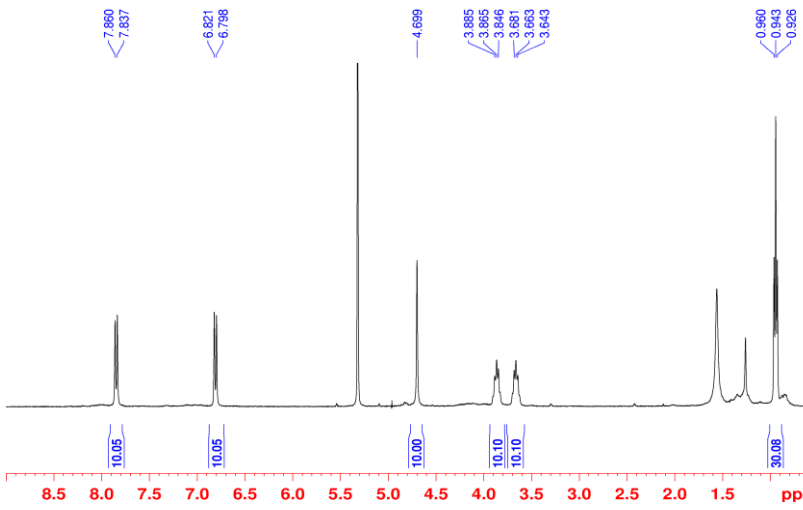

Figure 42. ^{1}H NMR spectrum of **PrS[5]^{Et}** (CD_2Cl_2, 400 MHz, 298 K).

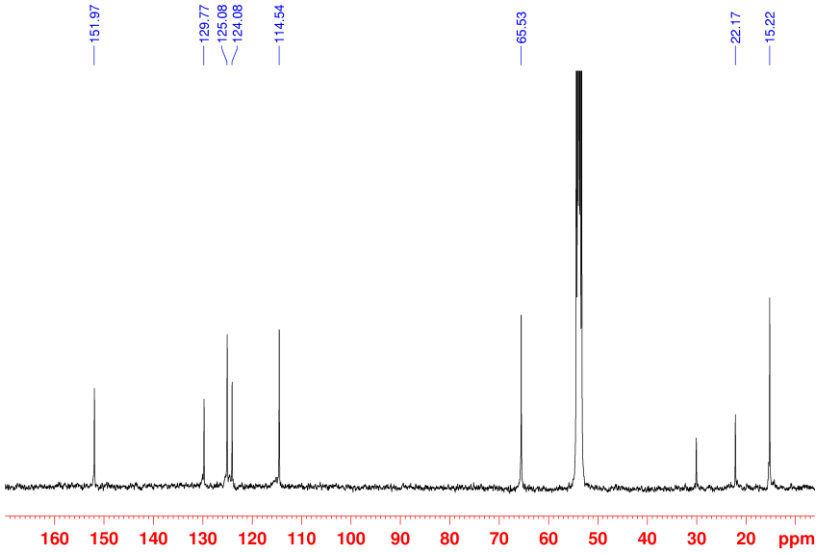

Figure 43. ^{13}C NMR spectrum of **PrS[5]*Et*** (CD_2Cl_2, 100 MHz, 298 K).

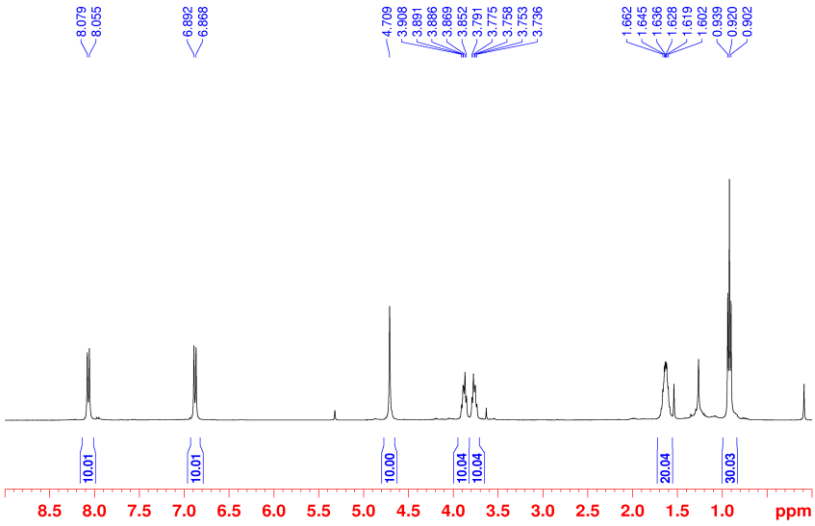

Figure 44. ^{1}H NMR spectrum of **PrS[5]*nPr*** (CD_2Cl_2, 400 MHz, 298 K).

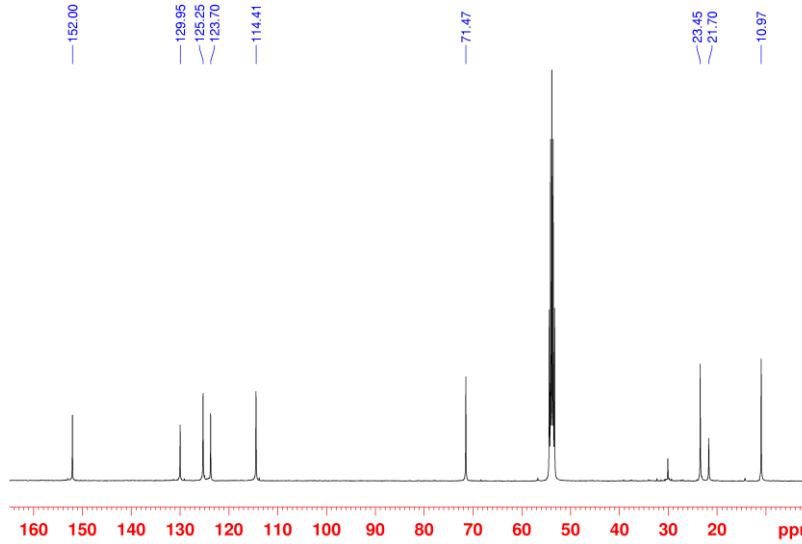

Figure 45. ^{13}C NMR spectra of **PrS[5]**^{nPr} (CD_2Cl_2, 100 MHz, 298 K).

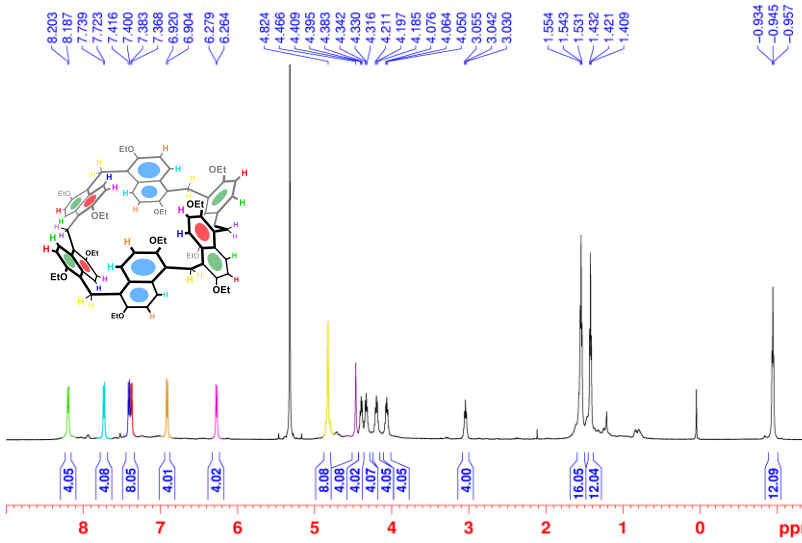

Figure 46. ^{1}H NMR spectrum of **PrS[6]**^{Et} (CD_2Cl_2, 600 MHz, 243 K).

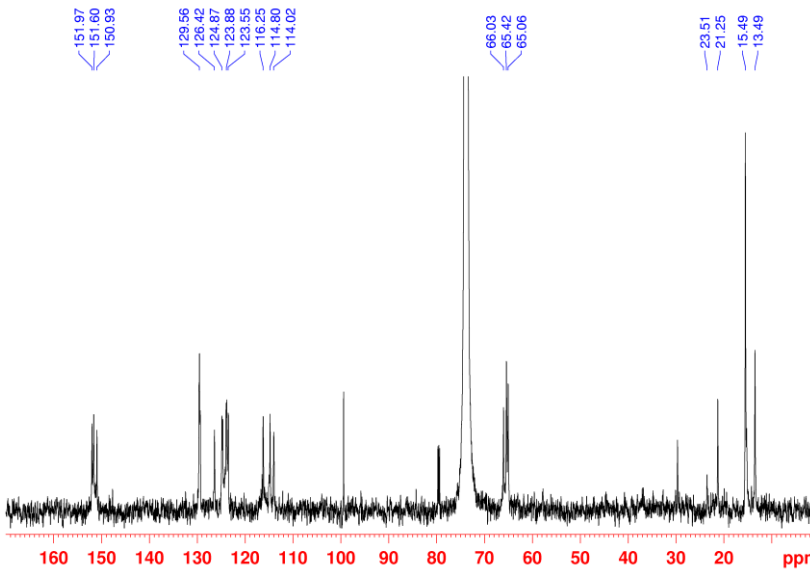

Figure 47. ^{13}C NMR spectra of **PrS[6]**^{Et} (TCE-d_2, 150 MHz, 298 K).

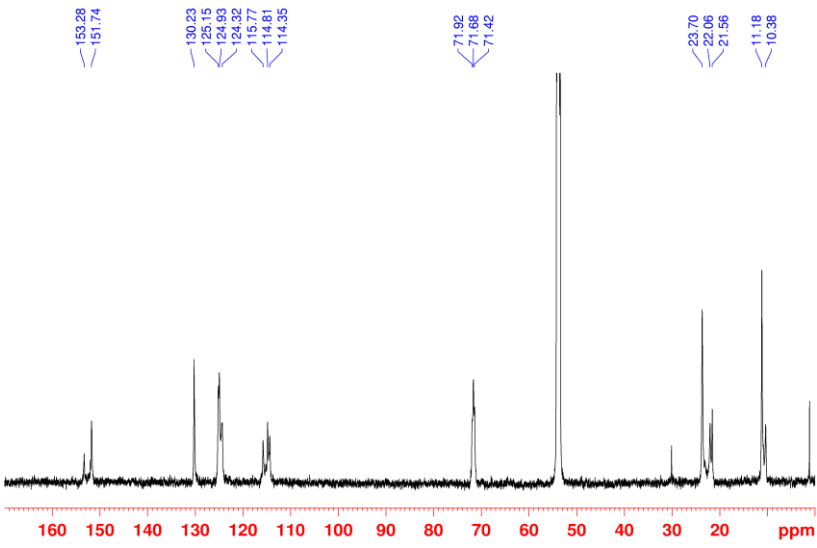

Figure 48. ^{13}C NMR spectra of **PrS[6]**^{nPr} (TCE-d_2, 150 MHz, 298 K).

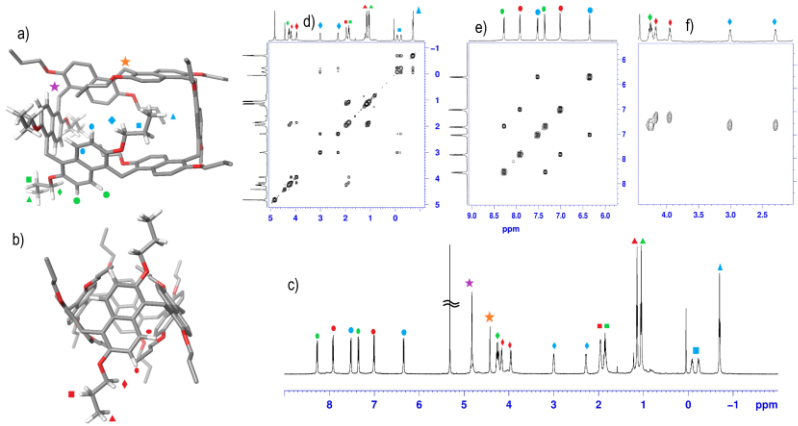

Figure 49. (a and b) Different views of the DFT-optimized structure of **PrS[6]^{nPr}** at the B97D3/SVP/SVPFIT level of theory. (c) ^{1}H NMR spectrum of **PrS[6]^{nPr}** in CD_2Cl_2 at 243 K (600 MHz). (d,e) Significant portions of the 2D COSY spectrum of **PrS[6]^{nPr}** (600 MHz, CD_2Cl_2, 243 K). (f) Significant portions of the 2D HSQC spectrum of **PrS[6]^{nPr}** in which the resonances of distereotopic OCH_2 groups are reported. The assignment of ^{1}H NMR signals is indicated by the colored symbols of (a and b).

3.6.3 HT NMR Studies of PrS[n]^{R}

Energy barrier calculation of **PrS[5]^{nPr}** by VT NMR studies

$$\Delta G_c^{\neq} = aT_c\left[9.972 + \log\left(\frac{T_c}{\Delta\nu}\right)\right]$$

Kurland, R. J.; Rubin, M. B.; Wise, M. B. *J. Chem. Phys.* **1964**, *40*, 2426-2431.

T_C = 383 K; $\Delta\nu$ = 80 Hz for OCH_2 signals in **Figure 42**;
$a = 4.575 \cdot 10^{-3}$ ($\Delta G^{\neq}_c$ in Kcal/mol)

$\Delta G^{\neq}_c$ = 18.3 Kcal/mol

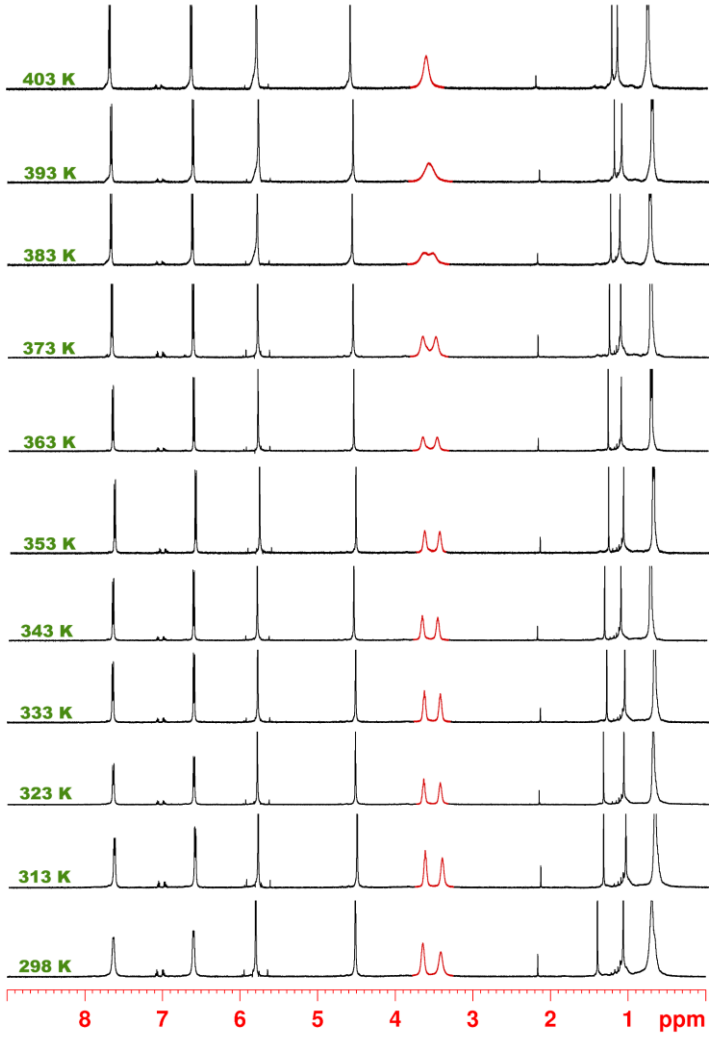

Figure 50. ^{1}H NMR spectra of **PrS[5]**^{Et} (600 MHz, TCE-d_2) at (from bottom to top): 298, 313, 323, 333, 343, 353, 363, 373, **383** (*Tc*), 393 and 403 K.

Energy barrier calculation of **PrS[5]**^{nPr} by VT NMR studies

T_C = 403 K; Δv = 36 Hz calculated for OCH_2 signals in **Figure 44**;

$$\Delta G^{\neq}_{c} = 20.1 \text{ Kcal/mol}$$

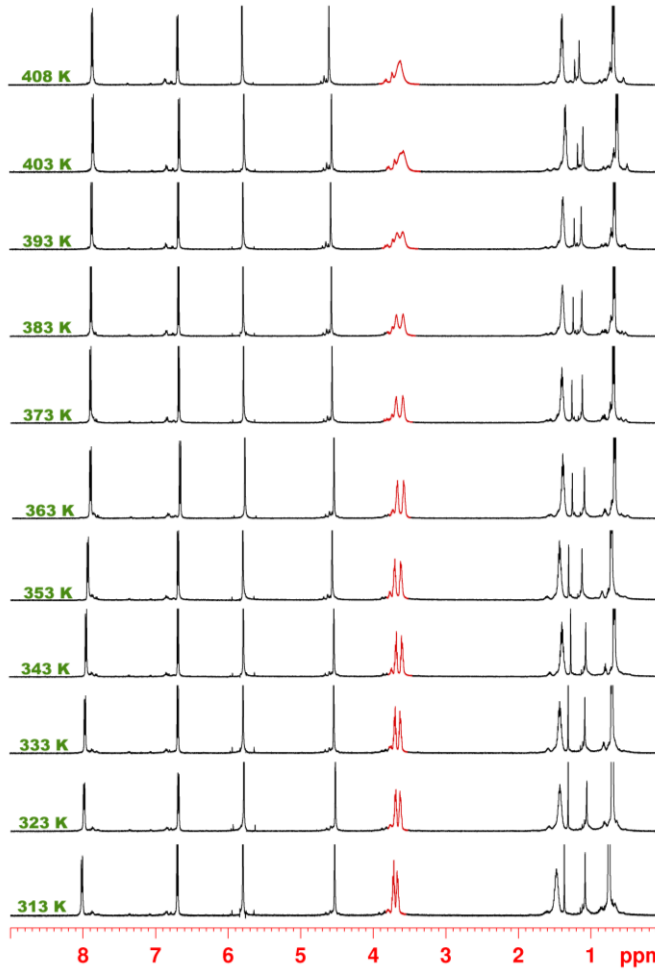

Figure 51. ^{1}H NMR spectra of **PrS[5]**^{nPr} (300 MHz, TCE-d_2) at (from bottom to top): 313, 323, 333, 343, 353, 363, 373, 383, 393, **403** (*Tc*) and 408 K.

Energy barrier calculation of **PrS[6]^{Et}** by VT NMR studies

T_C = 343 K; Δv = 84 Hz calculated for OCH_2 signals at 4.21 and 4.07 ppm, in **Figure 46**;

$\Delta G^{\neq}_c$ = 16.6 Kcal/mol

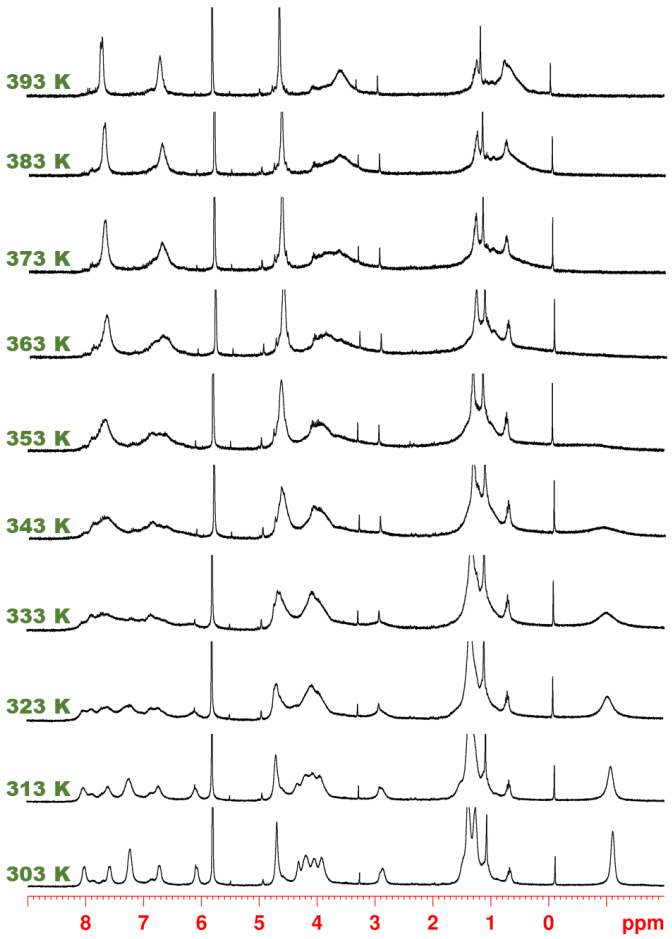

Figure 52. ^{1}H NMR spectra of **PrS[6]^{Et}** (300 MHz, TCE-d_2) at (from bottom to top): 303, 313, 323, 333, **343** (*Tc*), 353, 363, 373, 383 and 393 K.

Energy barrier calculation of **PrS[6]^{nPr}** by VT NMR studies

T_C = 363 K; $\Delta\nu$ = 126 Hz calculated for OCH_2 signals at 4.16 and 3.95 ppm, **in Figure 36**;

$\Delta G^{\neq}_c$ = 17.3 Kcal/mol

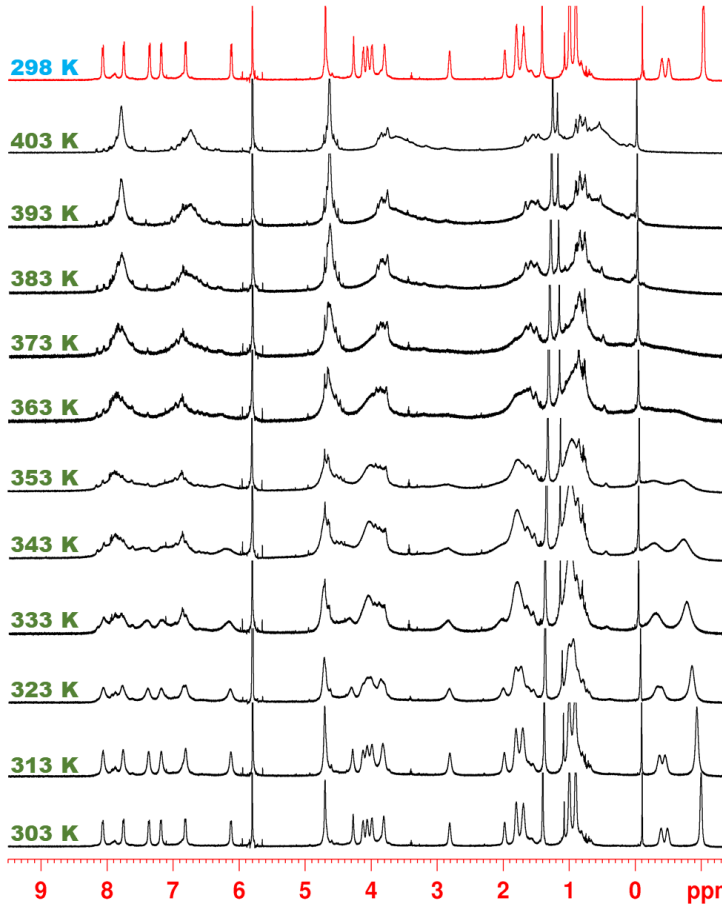

Figure 53. ^{1}H NMR spectra of **PrS[6]^{nPr}** (600 MHz, TCE-d_2) at (from bottom to top): 303, 313, 323, 333, 343, 353, **363** (*T*c), 373, 383, 393 and 403 K; in red the spectrum at 298 K after high temperature acquisition.

3.6.4 ^{1}H NMR determination of K_{ass} values[47, 68]

The association constant values for the formation of the complexes were calculated by means of three methods (see **paragraph 2.4.4**).

	PrS[5]^{Me}	PrS[6]^{Me}	PrS[5]^{Et}	PrS[6]^{Et}	PrS[5]^{nPr}	PrS[6] ^{nPr}
5^{2+}	$3.9\cdot10^7$ M^{-1} [a]	50 M^{-1} [a]	$1.4\cdot10^8$ M^{-1} [b]	790 M^{-1} [e]	$1.7\cdot10^8$ M^{-1} [c]	400 M^{-1} [d]
7^{+}	90 M^{-1} [a]	$2.7\cdot10^3$ M^{-1} [a]	50 M^{-1} [f]	2745 M^{-1} [g]	100 M^{-1} [h]	340 M^{-1} [i]
10^{2+}	$1.8\cdot10^7$ M^{-1} [a]	----	$2.8\cdot10^8$ M^{-1} [j]	$1.0\cdot10^8$ M^{-1} [k]	$1.4\cdot10^9$ M^{-1} [l]	$1.2\cdot10^8$ M^{-1} [m]
14^{2+}	$6.6\cdot10^6$ M^{-1} [n]	$4.2\cdot10^3$ M^{-1} [s]	$2.9\cdot10^6$ M^{-1} [o]	420 M^{-1} [u]	$6.3\cdot10^7$ M^{-1} [w]	370 M^{-1} [v]
15^{2+}	5780 M^{-1} [p]	$3.7\cdot10^3$ M^{-1} [r]	$1.0\cdot10^5$ M^{-1} [q]	----	$4.8\cdot10^5$ M^{-1} [t]	----

Table 5. Association constant (K_{ass}, M^{-1}) values for the formation of the complexes between the ammonium **5^{2+}**, **7^{2+}**, **10^{2+}**, **14^{2+}** and **15^{2+}** cations as **BArF$^-$** salts and the prism[n]arenes. Determined by ^{1}H NMR experiments in CD_2Cl_2. Errors < 15% calculated as mean values of three measures.

[a] Reported in reference 46. **[b]** Calculated by competition experiment at 298 K with **PrS[5]^{Me}** . **[c]** Calculated by competition experiment at 298 K with **PrS[5]^{Me}**. [d]Calculated by integration at 298 K of ^{1}H NMR signals of free and complexed species.[e] Calculated by integration at 298 K of ^{1}H NMR signals of free and complexed species. [f]Calculated by quantitative ^{1}H NMR spectroscopy using TCE as internal standard. [g] Calculated by integration at 183 K of ^{1}H NMR signals of free and complexed species. [h]Calculated by quantitative ^{1}H NMR spectroscopy at 183 K. [i]Calculated by integration at 183 K of ^{1}H NMR signals of free and complexed species. [j] Calculated by competition experiment at 298 K with **PrS[5]^{Me}**. [k] Calculated by competition experiment at 298 K with **PrS[5]^{Me}**. [l] Calculated by competition

[68] For all 1D NMR spectra of the experiments for the calculation of K_{ass} values see: Della Sala, P.; Del Regno, R.; Di Marino, L.; Calabrese, C.; Palo, C.; Talotta, C.; Geremia, S.; Hickey, N.; Capobianco, A.; Neri, P.; Gaeta, C. *Chem. Sci.* **2021**, *12*, 9952-9961.

experiment at 298 K with **PrS[5]^{Me}**.[m] Calculated by competition experiment at 298 K with **PrS[6]^{Et}**.[n] Calculated by competition experiment at 298 K with **5^{2+}**. [o]Calculated by competition experiment at 298 K with **PrS[5]^{Me}**.[p] Calculated by integration at 298 K of ^{1}H NMR signals of free and complexed species.[q] Calculated by competition experiment at 298 K with **PrS[5]^{Me}**.[r] Calculated by competition experiment at 298 K with **PrS[5]^{Et}**.[s] Calculated by competition experiment at 298 K with **15^{2+}**.[t] Calculated by competition experiment at 298 K with **PrS[5]^{Me}**.[u] Calculated by competition experiment at 298 K with **PrS[6]^{Me}**.[v] Calculated by competition experiment at 298 K with **PrS[6]^{Me}**.[w] Calculated by competition experiment at 298 K with **PrS[5]^{Me}**.[68]

3.6.5 Conformational Studies by DFT Calculations

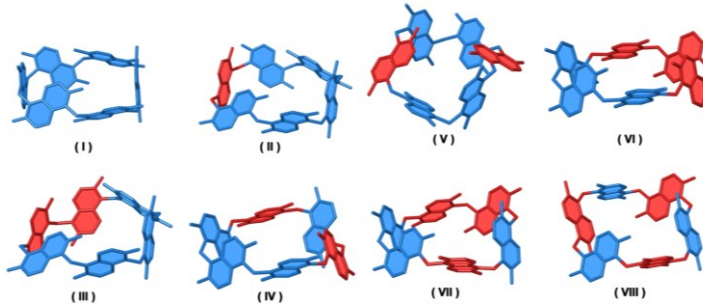

Figure 54. Eight possible conformations for the **PrS[6]^{nPr}**.

	B97D3/SVP/SVPFIT Single point energy (Hartree)	ΔE in kcal/mol
I	-4855.487818	0
II	-4855.439775	30.0
III	-4855.421385	41.7
IV	-4855.419716	42.7
V	-4855.426402	38.5
VI	-4855.433125	34.3
VII	-4855.416025	45.0
VIII	-4855.416056	45.0

Table 6. Single point energies of the eight conformations of **PrS[6]^{nPr}**.

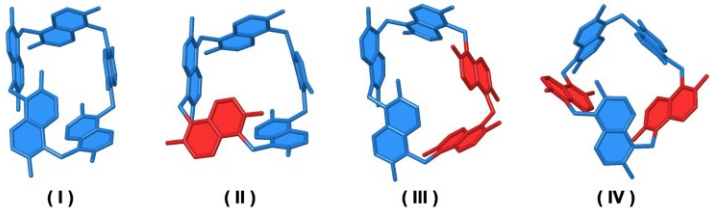

Figure 55. Four possible conformations for the **PrS[5]^{nPr}**.

	B97D3/SVP/SVPFIT Single point energy (Hartree)	ΔE in kcal/mol
I	-4046.234598	0
II	-4046.215840	11.77
III	-4046.211091	14.75
IV	-4046.221658	8.12

Table 7. Single point energies of the four conformations of **PrS[5]^{nPr}**.

3.6.6 DFT Calculations[47,69]

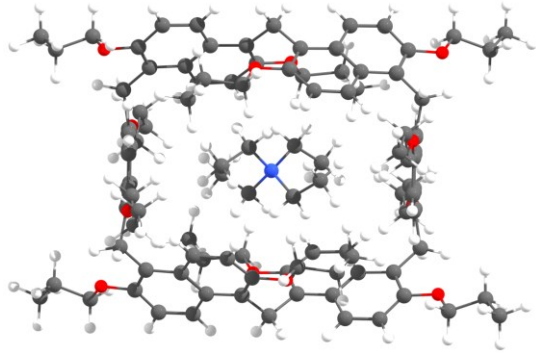

Figure 56. DFT-optimized structure (B97D3/SVP/SVPFIT) of the **7^{+}@PrS[6]^{nPr}** complex.

[69] For all DFT calculation details and figures see: Della Sala, P.; Del Regno, R.; Di Marino, L.; Calabrese, C.; Palo, C.; Talotta, C.; Geremia, S.; Hickey, N.; Capobianco, A.; Neri, P.; Gaeta, C. *Chem. Sci.* **2021**, *12*, 9952-9961.

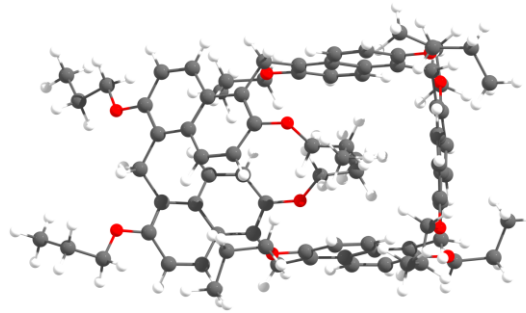

Figure 57. DFT-optimized structure (B97D3/SVP/SVPFIT) of the **PrS[5]**^{nPr}.

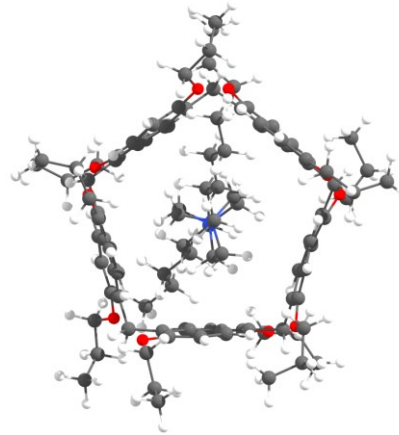

Figure 58. DFT-optimized structure (B97D3/SVP/SVPFIT) of the **5**$^{2+}$**@PrS[5]**^{nPr} complex.

4.0 Solid-State Structures of Prism[n]arenes and Their Complexes

4.1 Determination of the Crystallographic Structures of Prism[n]arenes[46,47]

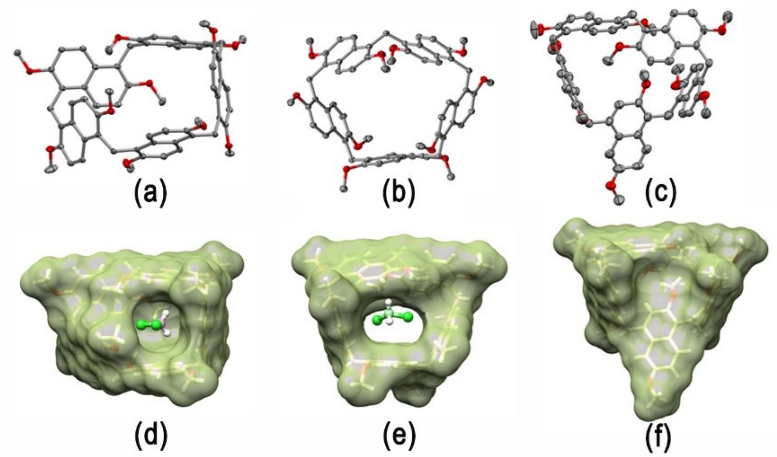

Figure 59. Ellipsoid representation (50% probability) of the a) α and b) γ forms of prism[5]arene **1** and of c) isomer A of the β form of 1,4-*confused*- prism[5]arene **2**. Solvent molecules, disordered atoms with low occupancy factors and hydrogen atoms are not included for clarity. For each molecule the α and β forms have similar conformations. The solvent excluded molecular surfaces (1.4 Å probe) of the: d) α and e) γ forms of prism[5]arene and of f) isomer A of the β form of 1,4-*confused*- prism[5]arene. The encapsulated CH_2Cl_2 solvent molecules are represented as ball and stick model.[46]

These studies were performed in collaboration with prof. Silvano Geremia and Dr. Neal Hickey from the *Università di Trieste*. All single crystals suitable for X-ray investigation were obtained by slow evaporation of

solutions containing **PrS[5]^{Me} 1** or **1,4-*c*-PrS[5]^{Me} 2**. The single crystals of three pseudopolymorphic forms of **1** and two pseudopolymorphic forms **2**, were analysed using synchrotron radiation and cryo-cooling techniques.[46]

The three prism[5]arenes pseudo-polymorphs were obtained by CH_2Cl_2 / hexane, for the α form, and CH_2Cl_2 / ethyl acetate, for the β and γ forms, as solvents. The three pseudo-polymorphs are distinguished by a different amount of co-crystallized CH_2Cl_2 solvent molecules located between the packed molecules of **1** outside the prismarenes rings **- Figures 59a** and **59b**. In the case of the α form, the asymmetric unit contains two additional external CH_2Cl_2 molecules; while in the β form there is just one external site partially occupied by a disordered CH_2Cl_2 **- Figures 59d**. Finally, γ form contains the encapsulated CH_2Cl_2 molecule only- **Figures 59e.** In addition, the α and β forms feature a molecular cavity sealed on one site by a methoxy group (**Figure 59d**); while the more symmetric γ form present a central hole - **Figure 59e**.[46]

	1		
	α form	β form	γ form
Empirical formula	($C_{65}H_{60}O_{10}$), 3 (CH_2Cl_2)	($C_{65}H_{60}O_{10}$), 1.9 (CH_2Cl_2)	($C_{65}H_{60}O_{10}$), (CH_2Cl_2)
Formula weight	1255.91	1162.49	1086.06
Temperature (K)	100(2)	100(2)	100(2)
Wavelength (Å)	0.7	0.7	0.7
Crystal system	Triclinic	Triclinic	Monoclinic
Space group	P -1	P -1	C 2/c
Unit cell dimensions (Å, °)	*a* = 13.171(3) *α* = 76.093 (7) *b* = 13.404(13) *β* = 80.772(6) *c* = 17.673(11) *γ* = 88.492(4)	*a* = 10.323(15) *α* = 107.381(3) *b* = 13.772(8) *β* = 86.09(1) *c* = 21.117(6) *γ* = 99.769(10)	*a* = 26.397(2) *α* = 90 *b* = 12.179(3) *β* = 96.210(1) *c* = 16.2740(6), *γ* = 90
Volume (Å^3)	2989.2(7)	2823.5(5)	5201.2(9)
Z	2	2	4
ρ_{calcd} (g/cm^3)	1.395	1.367	1.387
μ (mm^{-1})	0.330	0.249	0.188

F(000)	1312	1220	2288
Reflections collected	47654	53515	49253
Independent reflections	23371 [R(int) = 0.0169]	15564 [R(int) = 0.0184]	7601 [R(int) = 0.0468]
Data / restraints / parameters	13771 / 0 / 768	15564 / 0 / 765	7601 / 0 / 372
GooF	1.052	1.023	1.026
R_1 / wR_2 [I>2σ(I)]	0.0436 / 0.1143	0.044 / 0.1164	0.0528 / 0.1324
R_1 / wR_2 all data	0.0468 / 0.1149	0.0492 / 0.1209	0.0729 / 0.1477
Largest. Diff. peak/hole (e Å^{-3})	0.872 / -0.962	0.674 / -0.607	0.849 / -0.543
CCDC code	1950823	1950824	1950825

Table 8. Crystal data for the three crystalline forms of **prism[5]arene 1**.[46]

The two pseudo-polymorphic forms of 1,4-*c*-prism[5]arene were obtained by CH_2Cl_2 / decaline, for the α form, and CH_2Cl_2 / pyridine for the β form, as solvents – **Figure 59c**.[46]

The asymmetric unit of the monoclinic α form is composed of two molecules of **2**. Both forms show a similar disorder in the position of the methoxy groups of the 1,4-naphthalene ring, corresponding to an overlap of two positions of the molecule related by a pseudo-twofold axis passing through the 1,4-naphthalene ring and the opposite methylene bridge, and which differ in the positions of the two methoxy groups of the 1,4-naphthalene ring. In addition, the 1,4-naphthalene ring adopts a conformation that takes up the cavity of the prismarene - **Figure 59f**.[46]

	2	
	α form	β form
Empirical formula	C_{65} H_{60} O_{10}	C_{65} H_{60} O_{10}[a]
Formula weight	1001.13	1001.13
Temperature (K)	100(2)	100(2)

Wavelength (Å)	0.7	0.7
Crystal system	Monoclinic	Triclinic
Space group	P 2_1/c	P -1
Unit cell dimensions (Å, °)	*a* = 16.777 (8), *α* = 90, *b* = 32.962 (13), *β* = 91.3 (2), *c* = 19.166 (7), *γ* = 90	*a* = 8.593 (3), *α* = 62.663 (10), *b* = 18.778 (6), *β* = 84.421 (11), *c* = 19.167 (5), *γ* = 85.31 (3)
Volume (Å^3)	10596 (7)	2732.0 (15)
Z	8	2
ρ_{calcd} (g/cm^3)	1.255	1.217
μ (mm^{-1})	0.080	0.078
F(000)	4240	1060
Reflections collected	106357	25651
Independent reflections	106357	25651
Data / restraints / parameters	106357 / 0 / 1406	25651 / 0 / 709
GooF	1.020	1.021
R_1 / wR_2 [I>2σ(I)]	0.0890 / 0.2247	0.1213 / 0.3136
R_1 / wR_2 all data	0.1535 / 0.2667	0.1935 / 0.3725
Largest. Diff. peak/hole (e Å^{-3})	0.519 / -0.362	0.761 / -0.472
CCDC code	1901808	1919471

[a] The cell also contained ca. 1.2 severely disordered dichloromethane solvent molecules with partial occupation, which were accounted for using the Platon squeeze tool.

Table 9. Crystal data for the two crystalline forms of **1,4-*confused*-prism[5]arene 2**.[46]

	PrS[5]^{Et}	**PrS[5]^{nPr}**	**PrS[6]^{Et}**	**PrS[6]^{nPr}**
Empirical formula	$C_{75}H_{80}O_{10}$, $C_4H_8O_2$	$C_{85}H_{100}O_{10}$	$C_{90}H_{96}O_{12}$, 1.775 (CH_2Cl_2)	$C_{102}H_{120}O_{12}$, C_7H_8
Formula weight	1229.49	1281.64	1520.41	1630.11
Temperature (K)	100(2)	100(2)	100(2)	100(2)
Wavelength (Å)	0.7	0.7	0.7	0.7
Crystal system	Triclinic	Monoclinic	Triclinic	Monoclinic
Space group	*P* -1	*P* 2_1/c	*P* -1	*C* 2/c
Unit cell dimensions (Å, °)	*a* = 16.42(8) *b* = 20.342(12) *c* = 21.545(17) *α* = 83.045(14) *β* = 80.54(8) *γ* = 67.32(11)	*a* = 10.909(5) *b* = 34.548(3) *c* = 18.627(1) *β* = 91.334(6)	*a* = 19.356(8) *b* = 19.428(5) *c* = 21.732(4) *α* = 96.664(4) *β* = 90.158(18) *γ* = 95.38(2)	*a* = 13.308(9) *b* = 30.108(18) *c* = 23.23(3) *β* = 104.36(16)
Volume (Å^3)	6540(30)	7018(3)	8081(4)	9017(14)
Z	4	4	4	4

ρ_{calcd} (g/cm^3)	1.249	1.213	1.25	1.201
μ (mm^{-1})	0.079	0.075	0.191	0.076
F(000)	2632	2760	3226	3512
Reflections collected	96777	121074	88777	20991
Indep. Reflections	31258	20580	25663	6384
restraints/parameters	0/1705	0/867	0/1861	84/569
GooF	1.017	1.093	1.027	1.036
Final *R* indices [I>2σ(I)]	R_1 = 0.0962 wR_2 = 0.2623	R_1 = 0.0762 wR_2 = 0.1869	R_1 = 0.0684 wR_2 = 0.1895	R_1 = 0.0912 wR_2 = 0.2549
R indices (all data)	R_1 = 0.145 wR_2 = 0.3057	R_1 = 0.0999 wR_2 = 0.2038	R_1 = 0.0987 wR_2 = 0.2133	R_1 = 0.1362 wR_2 = 0.2983
CCDC code	2025594	2025589	2025583	2025585

Table 10. Crystal data and structure refinement for prismarenes: **PrS[5]^{Et}**, **PrS[5]^{nPr}**, **PrS[6]^{Et}** and **PrS[6]^{nPr}**.[47]

4.2 Determination of the Crystallographic Structures of Prism[n]arenes Host-Guest Complexes: **7@PrS[5]^{Me}**·(BArF)$_2$, **10@PrS[5]^{Me}**·BArF and **6@PrS[6]^{Me}**·BArF [47]

Single crystals suitable for an X-ray investigation were obtained by slow evaporation of solutions containing the complexes, using hexane/dichloromethane, as solvents, for the host-guest complexes **10@PrS[5]^{Me}·(BArF)$_2$**, **6@PrS[5]^{Me}·BArF** and **7@PrS[6]^{Me}·BArF**- **Figure 60**.[47]

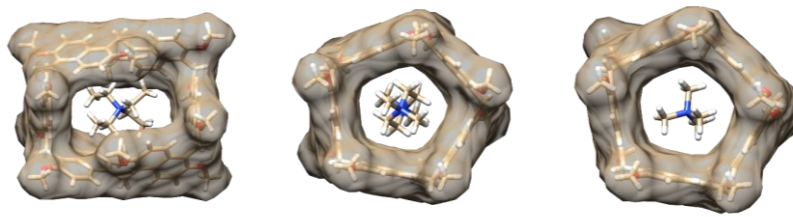

Figure 60. X-ray structural models of the host-guest complexes **7$^+$@PrS[6]^{Me}**, **10^{2+}@PrS[5]^{Me}** and **6$^+$@PrS[5]^{Me}**. The transparent van der Waals surface of the host is shown to illustrate the effective cavities of the prismarens. The counter-ions, solvent and disordered guest atoms are omitted for clarity.[47]

The host-guest complex **10^{2+}@PrS[5]^{Me}·(BArF)$_2$** lies on a crystallographic two-fold axis that passes through a methylene bridging atom and the center of the opposite naphthalene ring of the **PrS[5]^{Me}** host – **Figure 60b**. Finally, the X-ray structure of **10^{2+}@PrS[5]Me** complex reveals C–H···π interactions for the host-guest

complexation- **Figure 60b** and **Figure 61**. In detail, C–H···π interactions are present with a C–H···π centroid average distance of about 2.9 °A. [47]

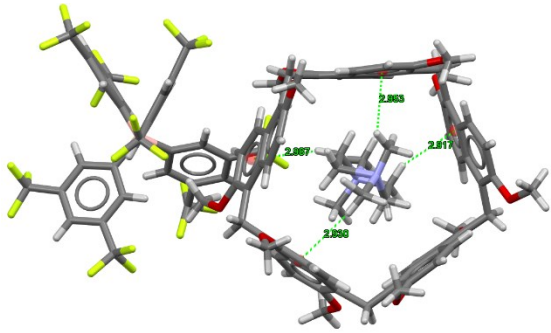

Figure 61. X-ray structural models of the host-guest complex **10^{2+}@PrS[5]*Me***.[47]

The crystal structure of **6^{+}@PrS[5]*Me*·BArF** (**Figure 60c**) also evidences an opening of the prismatic host. The macrocycle adopts an almost regular pentagon prism with canting angles[70] of 90.0°±3.3° and interior dihedral angles ranging from 102.1° to 113.7°, with an average angle of 108°, equal to the ideal angle. The tetramethylammonium guests are well-centered in the **PrS[5]*Me*** cavity to give the cationic C-H···π interactions, with a C–H···π centroid distance of about 2.5 and 2.9 °A - **Figure 62**.[47]

[70] The canting angle is defined as the dihedral angle between the naphthalene plane and the mean plane of the bridging methylene carbon atoms of the prism[n]arene molecule.

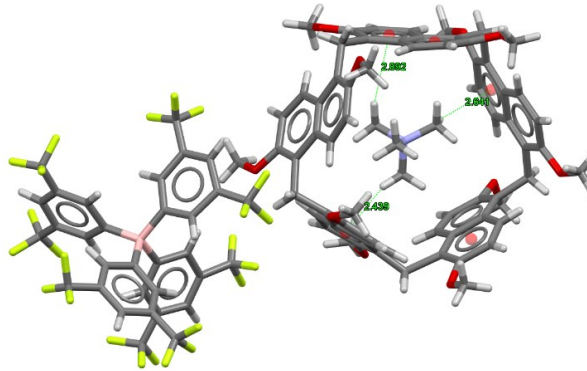

Figure 62. X-ray structural models of the host-guest complex **6⁺@PrS[5]*Me***.[47]

Finally, the host-guest complex **7⁺@PrS[6]*Me*·BArF** (**Figure 60a**) lies on a crystallographic two-fold axis. This symmetry axis passes through the centers of two opposite naphthalene rings of the **PrS[6]*Me*** host. Even in this case, the solid-state structure of complex reveals the important role of cationic C–H···π interactions for the host-guest complexation, with a C–H···π ^{centroid} distance of about 2.8 °A - **Figure 63**.[47]

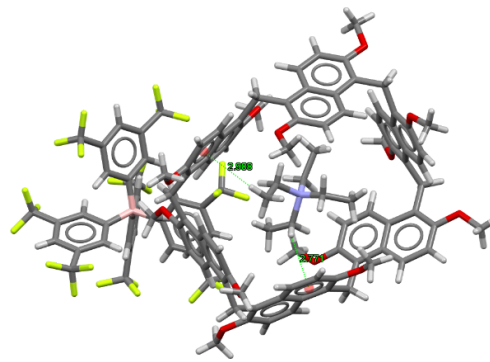

Figure 63. X-ray structural models of the host-guest complex **7⁺@PrS[6]*Me***.[47]

	10@PrS[5]^{Me}·(BArF)$_2$	**6@PrS[5]^{Me}·BArF**	**7@PrS[6]^{Me}·BArF**
Empirical formula	$C_{65}H_{60}O_{10}$, $C_8H_{20}N_2$, 2($C_{32}H_{12}BF_{24}$), 0.7(CH_2Cl_2)	$C_{65}H_{60}O_{10}$, C_4 $H_{12}N$, $C_{32}H_{12}BF_{24}$, 1.1(CH_2Cl_2)	$C_{78}H_{72}O_{12}$, $C_8H_{20}N$, $C_{32}H_{12}BF_{24}$, 3.575(CH_2Cl_2)
Formula weight	2931.28	20131.92	2498.44
Temperature (K)	100(2)	100(2)	100(2)
Wavelength (Å)	0.7	0.7	0.7
Crystal system	Monoclinic	Triclinic	orthorhombic
Space group	*C* 2/*c*	*P* -1	*C* m c a
Unit cell dimensions (Å, °)	a = 38.56(3) b = 17.306(2) c = 22.875(7) β = 120.862(15)	a = 21.686(11) b = 22.528(10) c = 22.906(7) α = 81.367(6) β = 80.862(14) γ = 68.83(3)	a = 34.824(14) b = 30.10(3) c = 26.489(7)
Volume (Å3)	13105(11)	10251(8)	27770(30)
Z	4	4	8
ρ calcd (g/cm3)	1.486	1.317	1.195
μ (mm–1)	0.158	0.163	0.225
F(000)	5966	4177	10289
Reflections collected	121183	82571	79718
Indep. Reflections	19594	23532	6110
restraints/parameters	0/ 998	3486/2470	804/644
GooF	1.029	1.197	1.607
Final R indices [I>2σ(I)]	R_1 = 0.0646 wR_2 = 0.1691	R_1 = 0.1565 wR_2 = 0.3939	R_1 = 0.1760 wR_2 = 0.4399
R indices (all data)	R_1 = 0.0959 wR_2 = 0.202	R_1 = 0.2416 wR_2 = 0.4607	R_1 = 0.1959 wR_2 = 0.4581
CCDC code	2050614	2050617	2050618

Table 11. Crystal data and structure refinement for the prismarene host-guest complexes **10^{2+}@PrS[5]^{Me}·(BArF)$_2$**, **6^{+}@PrS[5]^{Me}·BArF**, and **7^{+}@PrS[6]^{Me}·BArF**.[47]

4.3 Potential Void Volumes of Prismatic Macrocycles[47]

In order to compare the potential cavity of the hosts for complex formation, the surface and volume of the ideal prismatic solids enclosed by the aromatic walls of some strictly related cyclophanes: pillar[5]arene, pillar[6]arene, prism[5]arene, prism[6]arene, and pagoda[4]rene were evaluated - **Figure 64**.

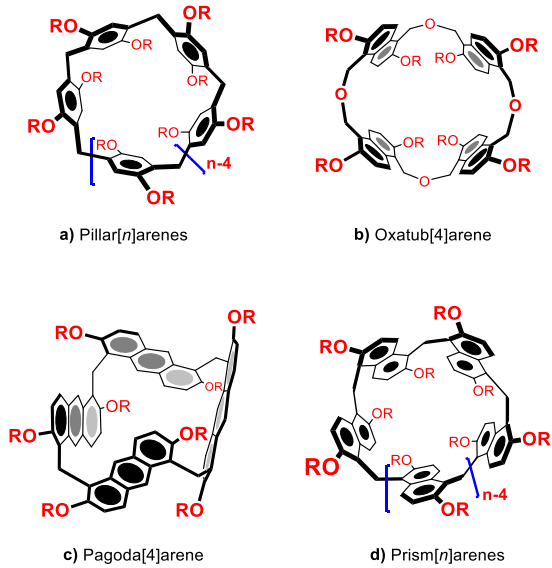

Figure 64. Chemical drawing of a) Pillar[n]arenes, b) Oxatub[4]arene, c) Pagoda[4]arene and d) Prism[n]arenes.

The geometrical parameters used for these calculations were obtained from the CCDC database as mean values of distances and angles observed in the X-ray structures (**Figure 65**). From the areas of the polyhedron bases (**B**) and the geometric heights (**h**), the volumes of the ideal prismatic solids contained by the macrocycles (**V**) were calculated. The entire area of the rectangular prism faces was used to compute the potential contact surface areas (**A**). The area of the polyhedron base, **B**, was used to calculate the opening of the cavity of these macrocycles (**Figure 64**), which was pentagon for the prism[5]arene and pillar[5]arene, square for the pagod[4]arene, and hexagon for the prism[6]arene and pillar[6]arene.
Thus, the prism[6]arene (52.4 $Å^2$) shows a wider cavity than the pillar[6]arene (39.1 $Å^2$) and the prism[5]arene

shows a wider cavity than pillar[5]arene (27.3 vs 19.6 Å^2) and pagod[4]arene (19.1 Å^2). The depth of the cavity, evaluated by the geometric height of the prism, is related to the number of fused-rings in the aromatic walls **(Figure 65)**.

Thus the order is pagodarene (10.78 Å), prismarene (9.35 Å), and pillararene (7.76 Å). As a result, the volumes of the cavities of these macrocycles clearly indicate that primarenes have bigger cavities than the corresponding pillararenes: prism[6]arene (490 Å^3) vs. pillar[6]arene (303 Å^3); prism[5]arene (255 Å^3) vs. pillar[5]arene (152 Å^3).

The tetrameric pagoda[4]arene (206 Å^3) lie between the two pentamers, prism[5]arene and pillar[5]arene. Another important geometric feature is the potential contact surface areas (**A**). The prism[6]arene (252 Å^2) shows the highest surface area, while the prism[5]arene (186 Å^2), pagod[4]arene (188 Å^2) and pillar[6]arene (181 Å^2) have comparable values. Finally, the pillar[5]arene (131 Å^2) exhibits the smallest potential contact area.[47]

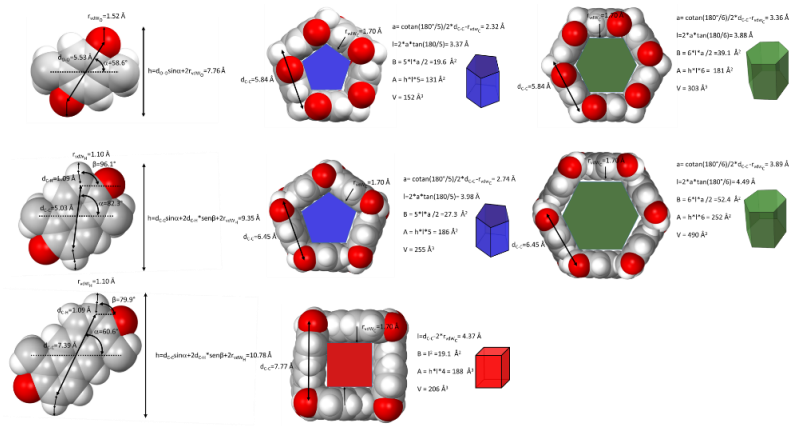

Figure 65. Comparison of the potential void volume in prismatic macrocycles: Pillarenes, prismarenes and pagodarenes.[47]

5.0 Supramolecularly Assisted Synthesis of *per*-Hydroxylated Prismarenes[71]

5.1 Synthesis of *per*-Hydroxylated Prism[n]arenes: Dealkylation of PrS[5]*Me* [71]

In recent years, pillararenes macrocyles,[14] have been widely investigated for their potential applications in the field of supramolecular chemistry due to their easy functionalization. The synthetic versatility of these macrocycles is mainly due to the easy dealkylation reaction of alkoxy-substituted aromatic units.[31] In fact, *per*-hydroxylated macrocycles are key synthetic precursors to realize new hosts with different supramolecular properties compared to the parent macrocycles.[31, 72]

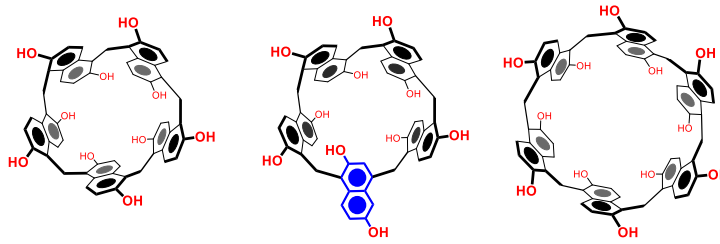

Figure 66. Chemical drawing of *per*-Hydroxylated Prism[n]arenes.[71]

[71] Del Regno, R.; Della Sala, P.; Picariello, D.; Talotta, C.; Spinella, A.; Neri, P.; Gaeta, C. *Org. Lett.* **2021**, *23*, 8143–8146.
[72] Ma, Y.; Chi, X.; Yan, X.; Liu, J.; Yao, Y.; Chen, W.; Huang, F.; Hou, J.-L. *Org. Lett*. **2012**, *14*, 1532–1535.

Prompted by these considerations, during the second year of this PhD project, the synthesis of *per*-hydroxylated prism[n]arenes **PrS[n]^{OH}** has been studied - **Figure 66**.[71] We studied the dealkylation of **PrS[5]^{Me}** under the conditions reported for the synthesis of *per*-hydroxylated pillar[5]arene[31], thus **PrS[5]^{Me}** was reacted with BBr_3 in dry CH_2Cl_2 at 25 °C for 12 h. But, unexpectedly, we detected the presence of a mixture of *per*-hydroxylated **PrS[5]^{OH}** and **PrS[6]^{OH}** in 55% and 40 % respectively. Thus we decide to lower the reaction temperature to prevent the formation of **PrS[6]^{OH}** (**Scheme 5**), but, similarly, we obtained a mixture of *per*-hydroxylated **PrS[5]^{OH}** and **PrS[6]^{OH}** derivatives.[71]

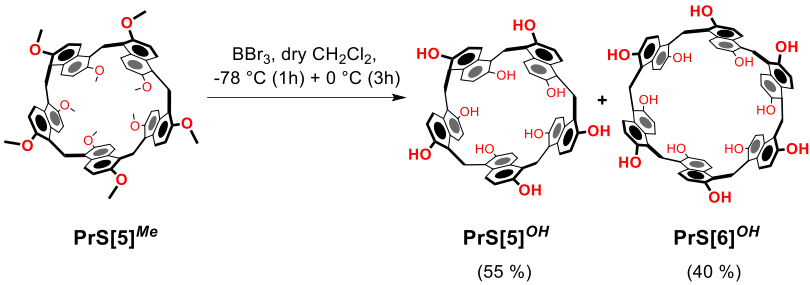

Scheme 5. Dealkylation of **PrS[5]^{Me}**.[71]

At this point, we decided to monitor the reaction of dealkylation of **PrS[5]^{Me}** in **Scheme 5**, by chromatographic analysis and HR FT ICR mass spectrometry.[71]
In particular we have found that, during the dealkylation of **PrS[5]^{Me}** under these conditions (**Scheme 5**), the pentamer was first converted into linear oligomers and after the hexamer appeared in the reaction mixture. In fact, **PrS[6]^{Me}** appears after 15 min (**Figure 67**), and finally, the mixture of **PrS[5]^{Me}** and **PrS[6]^{Me}** was dealkylated.[71]

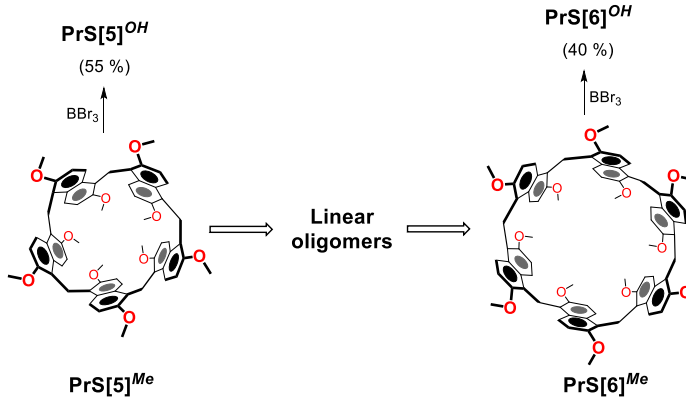

Figure 67. Proposed mechanism for the conversion of **PrS[5]*Me*** to **PrS[6]*Me*** and their demethylation. Reaction conditions in **Scheme 5**: BBr_3, dry CH_2Cl_2, 1 h, at –78 °C and 3 h at 0 °C.[71]

Previously[46,47] we observed a similar behaviour; in fact, when **PrS[5]*Et*** is treated with trifluoracetic acid at 70 °C in 1,2-dichloroethane as solvent,[47] a conversion to **PrS[6]*Et*** was observed after 22 h, due to an acid-catalyzed ring opening.[47]

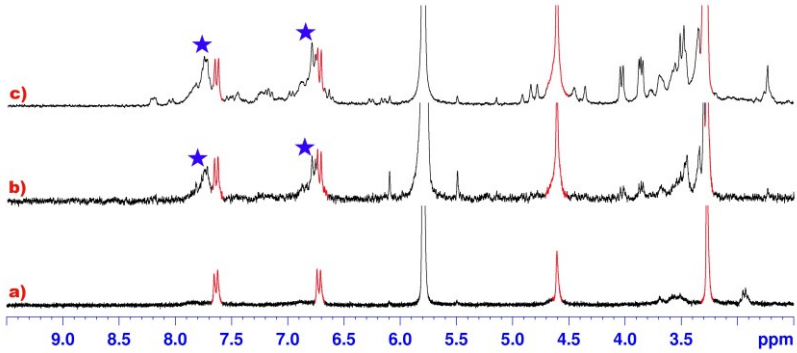

Figure 68. ^{1}H NMR spectra (393 K, 300 MHz, TCE-d_2) of: a) **PrS[6]*Me***; b) crude product of the reaction after 2 h at 273 K ; c) crude product of the reaction after 3 h at 273 K. In red, ^{1}H NMR signals of **PrS[6]*Me***, marked with blue star the ^{1}H NMR signals of **PrS[5]*Me***.[71]

Thus, we decided to study the reactions of conversion under the conditions reported in **Scheme 5**, but in the presence of TFA, as acid, instead of the boron tribromide (BBr_3).[71] In detail, ^1H NMR spectrum of the crude product, highlighted the presence of a mixture of **PrS[6]*Me*** and **PrS[5]*Me*** in a 1:1 ratio after 3 h - **Figure 68**.[71] Probably, under these reaction conditions (**Scheme 5**), the conversion of **PrS[5]*Me*** to **PrS[6]*Me*** occurs with a higher rate constant than that of dealkylation ($k_{conversion} > k_{dealkylation}$).[71] Thus, we can deduce that **PrS[5]*Me*** was first converted to **PrS[6]*Me*** in the presence of BBr_3 (**Figure 67**) and subsequently, the mixture of **PrS[5]*Me*** and **PrS[6]*Me*** was dealkylated, while no conversion occurred starting by **PrS[5]*OH***. To confirm this hypothesis, we treated the *per*-hydroxylated of the prism[5]arene **PrS[5]*OH*** in the presence of TFA in 1,2-DCE as solvent at 70 °C, and, under these conditions, this derivative was stable up to 24 h; in contrast, treating **PrS[5]*OH*** with BBr_3 in dichloromethane (1 h at −78 °C and 3 h at 0 °C), we obtained a polymeric insoluble product, but no hint of hexamer **PrS[6]*OH*** was detected in both reaction mixtures.

5.2 Supramolecularly Assisted Dealkylation of PrS[5]*Me*: The Role of Ammonium Guests [71]

As previously described in the **Chapter 2**,[46] the **PrS[5]*Me*** and **PrS[6]*Me*** can be selectively caught from the equilibrium mixture by using the appropriate ammonium templating agent, through a templated approach of a thermodynamically controlled synthesis.[46] Based on these considerations, we aimed to inquire if an appropriate

ammonium salt, such as tetramethylammonium iodide $\mathbf{6}^{+}$, could also affect the dealkylation reaction and, therefore, the ratio between **PrS[5]**^{Me} and **PrS[6]**^{Me}, by the formation of the $\mathbf{6}^{+}$**@PrS[5]**^{Me} complex.[46]

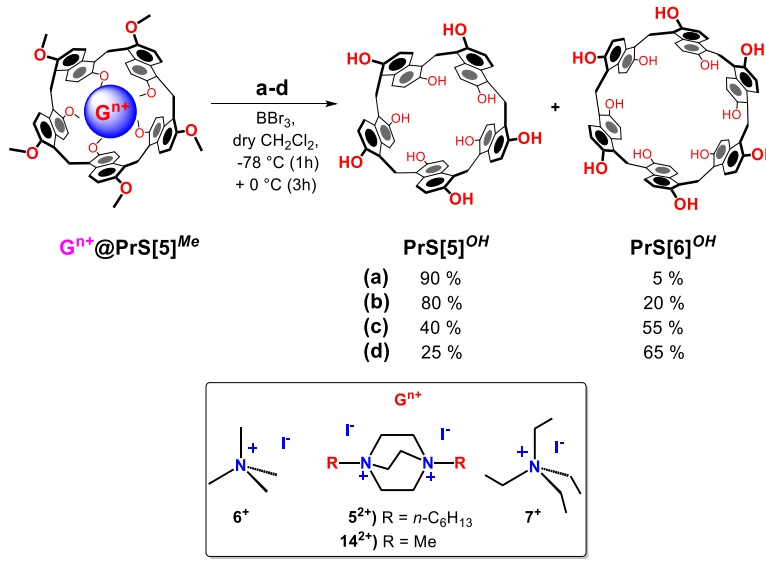

Scheme 6. Supramolecularly assisted dealkylation of **PrS[5]**^{Me} in the presence of template agent $\mathbf{5}^{2+}$–$\mathbf{7}^{+}$ and $\mathbf{14}^{2+}$ as iodide salts. Reaction conditions: BBr_3, dry CH_2Cl_2, 1 h at –78 °C and 3 h at 0 °C: a) $\mathbf{6}^{+}$; b) $\mathbf{14}^{2+}$; c) $\mathbf{5}^{2+}$; d) $\mathbf{7}^{+}$.[71]

In fact, treating **PrS[5]**^{Me} with BBr_3 in dry CH_2Cl_2 for 1 h at –78 °C and 3 h at 0 °C (**Scheme 6**), in the presence of tetramethylammonium iodide, surprisingly we obtained **PrS[5]**^{OH} in 90 % yield.[71] Thus, in the presence of $\mathbf{6}^{+}$ the selectivity of dealkylation reaction of **PrS[5]**^{Me} significantly improves.

In other words, the reaction of dealkylation is supramolecularly driven by the tetramethylammonium guest, because, probably, the formation of $\mathbf{6}^{+}$**@PrS[5]**^{Me}

complex favors kinetically the demethylation of **PrS[5]^{Me}** with respect to its conversion to hexamer, with $k_{conversion} < k_{dealkylation}$ for **6^{+}@ PrS[5]^{Me}**.[71]
In fact, as reported by us[47], in the complex **6^{+}@PrS[5]^{Me}**, the macrocycle adopts an open conformation, with the methoxy groups more accessible with respect to the closed conformation present in absence of ammonium guest - **Figure 69**.[47,71]

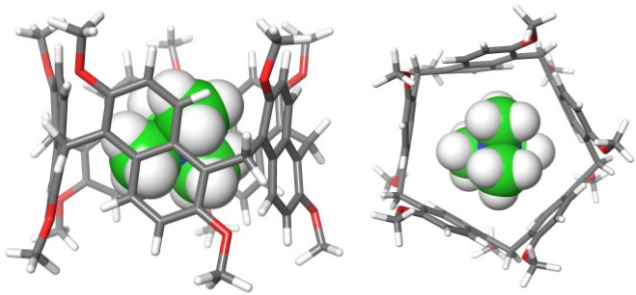

Figure 69. DFT-Optimized structure (GFN2-xTB) of **6^{+}@PrS[5]^{Me}** complex.[71]

At this point, we performed the demethylation reaction in the presence of 1,4-dihexyl-DABCO **5^{2+}**, because, as previously reported,[46] the **5^{2+}@PrS[5]^{Me}** complex shows an association constant value more higher than that for **6^{+}@PrS[5]^{Me}** (3.9×10^{7} M^{-1} *vs* 6.4×10^{4} M^{-1})[46]. Surprisingly, in the presence of **5^{2+}** as iodide salt, **PrS[6]^{OH}** was isolated in 55% yield and **PrS[5]^{OH}** in 40% yield (**Scheme 6**). Probably, in the presence of **5^{2+}@PrS[5]^{Me}** complex, the dealkylation reaction is kinetically unfavoured due to steric reasons, as it the methoxy groups are impeded by the presence of the hexyl chains (**Figure 70**), therefore favouring the conversion of **PrS[5]^{Me}** to **PrS[6]^{Me}** respect to the demethylation reaction.[71]

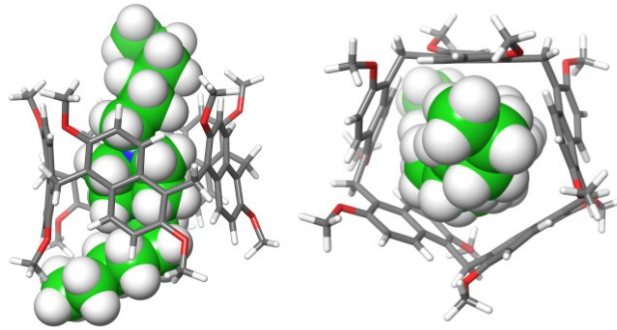

Figure 70. DFT-Optimized structure (GFN2-xTB) of $\mathbf{5^{2+}@PrS[5]^{Me}}$ complex.[71]

In addition, in the presence of $\mathbf{14^{2+}}$ cation, $\mathbf{PrS[5]^{OH}}$ was again the favoured product (**Scheme 6**), confirming this assumption.[71]

Finally, we studied the demethylation of $\mathbf{PrS[5]^{Me}}$ in the presence of tetraethylammonium $\mathbf{7^{+}}$. In this conditions (**Scheme 6**), we obtained $\mathbf{PrS[6]^{OH}}$ in 65% yield and $\mathbf{PrS[5]^{OH}}$ in 25% yield. This is not a surprising result for us, because, as previously reported[45], the tetraethylammonium $\mathbf{7^{+}}$ shows higher affinity for $\mathbf{PrS[6]^{Me}}$ compared to $\mathbf{PrS[5]^{Me}}$ [46]. [71]

5.3 Synthesis of per-Hydroxylated Prism[n]arenes: Dealkylation of 1,4-*c*-PrS[5]^{Me}, PrS[6]^{R} and PrS[5]^{R} (R = Et, *n*Pr) [71]

At this point our attention focused on the dealkylation reactions of $\mathbf{PrS[6]^{R}}$, to investigate if even the dealkylation of hexamers leads to the formation of a mixture of $\mathbf{PrS[6]^{OH}}$ and $\mathbf{PrS[5]^{OH}}$.[71]

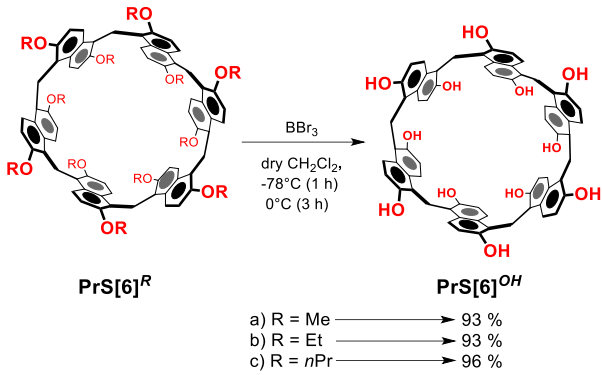

Scheme 7. Dealkylation of **PrS[6]^{R}**. [71]

Starting by **PrS[6]^{Me}**, in a presence of BBr_3 in dry CH_2Cl_2, **PrS[6]^{OH}** was the only product (93 %, **Scheme 7**) and no hint of **PrS[5]^{OH}** was detected in the reaction mixture, because, probably, no conversion of **PrS[6]^{Me}** to **PrS[5]^{Me}** occurs. [71]

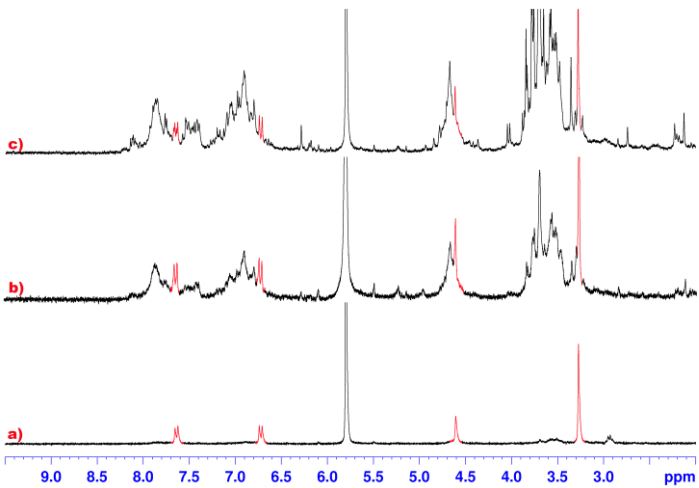

Figure 71. ^{1}H NMR spectra (393 K, 300 MHz, TCE-d_2) of: a) **PrS[6]^{Me}**; b) crude product of the reaction after 2 h at 273 K ; c) crude product of the reaction after 3 h at 273 K. In red, ^{1}H NMR signals of **PrS[6]^{Me}**.[71]

To understand this aspect, **PrS[6]^{Me}** was reacted in a presence of TFA and in dry CH_2Cl_2 (1 h at –78 °C and 3 h at 0 °C). By ^{1}H NMR spectrum (**Figure 71**) the absence of **PrS[5]^{Me}** is evident during the reaction, while **1,4-*c*-PrS[5]^{Me}** appears after 3 h.[71] In fact, as previously reported by us[46], **1,4-*c*-PrS[5]^{Me}** is the thermodynamic product because when the **PrS[6]^{Me}** is reacted in CH_2Cl_2 at reflux in the presence of TFA, the hexamer is completely converted to confused ***c*-PrS[5]^{Me}**.[46,71]

Finally, also the **1,4-*c*-PrS[5]^{Me}** was demethylated in the same conditions (**Scheme 7**), and its analogues *per*-hydroxylated prism[n]arenes was isolated in 93 % yield; no hint of other prismarenes was observed during the reaction.[71]

These studies agree with the data previously reported[46], clearly indicating that **PrS[5]^{Me}** and **PrS[6]^{Me}** are kinetic adducts and **1,4-*c*-PrS[5]^{Me}** is the thermodynamic macrocycle.[46,71]

Analogously, we decided to investigate the synthesis of per-hydroxylated prismarenes starting by **PrS[n]^{Et}** and propoxy **PrS[n]^{nPr}** derivatives, especially as **PrS[6]^{Et}** and **PrS[6]^{nPr}** are obtained in high yields.[47] When **PrS[6]^{Et}** and **PrS[6]^{nPr}** were treated in the presence of BBr_3 in CH_2Cl_2 (**Scheme 7**), **PrS[6]^{OH}** was isolated in 93 % and 96 % yield, respectively.[71] These results are in agreement with previously reported by us[47], because the stability of ethoxy- and propoxy-prismarenes under acid conditions is determined by the self-filling of the cavity by their alkyl chains.[47] This is why **PrS[6]^{Et}** and **PrS[6]^{nPr}** were easily dealkylated without any conversion to other macrocycles.[71]

In addition, when **PrS[5]^{Et}** and **PrS[5]^{nPr}** were dealkylated in the same conditions, the hexamer **PrS[6]^{OH}** was

obtained in 90 % yield, while **PrS[5]^{OH}** was isolated in traces; these results confirmed under acid conditions the conversion of pentamers **PrS[5]^{Et}** and **PrS[5]^{nPr}** to their respective hexamers is kinetically favored with respect to dealkylation of ethyl and propyl chains.[71]

5.4 Conclusions[71]

In conclusion, **PrS[5]^{Me}** can be efficiently demethylated by a supramolecularly assisted reaction. In detail, when the complex **6^{+}@PrS[5]^{Me}** is formed, the reaction of demethylation is kinetically favored with respect to the conversion to hexamer. In addition, the dealkylation of prismarenes, such as **PrS[6]^{R}** (R = Et, *n*Pr), can be obtained in high yields in the presence of BBr_3.

5.5 Experimental Section

5.5.1 General Section

See **Paragraph 2.4.1**

5.5.2 General Procedures for the Synthesis of *per*-hydroxylated Prism[n]arenes (PrS[n]^{OH}) and Copies of NMR Spectra[71]

Procedure A: To a solution of **PrS[n]^{R}** in dry CH_2Cl_2 (5.0 mM) was added BBr_3 under nitrogen atmosphere at –78 °C. The mixture was stirred at this temperature for 1 h, and at 0 °C for three hours.

- Starting by ***c*-PrS[5]^{Me}** (200 mg, 0.20 mmol) and BBr_3 (1.9 mL, 20.00 mmol): The reaction was stopped by adding slowly an aqueous solution of $NaHCO_3$ (5.0 g of $NaHCO_3$ dissolved in 50 mL of cold water) and, then, the precipitate was filtered. The solid was washed with a 10 % aqueous solution of sodium sulfite (50 mL), and two times with water (2 x 50 mL). The precipitate consisted of ***c*-PrS[5]^{OH}** in 93 % yield (160 mg), as a white solid.
- Starting by **PrS[5]^{Me}** (50 mg, 50.00 µmol) and BBr_3 (0.5 mL, 5.00 mmol): The reaction was stopped by adding slowly an aqueous solution of $NaHCO_3$ (1.3 g of $NaHCO_3$ dissolved in 15 mL of cold water) and, then, the precipitate was filtered. The solid was washed with a 10 % aqueous solution of sodium sulfite (25 mL), and two times with water (2 x 50 mL). ^{1}H NMR analysis and HR FT ICR MALDI mass spectrum of the crude product indicated that the precipitate was constituted by a mixture of **PrS[5]^{OH}** and **PrS[6]^{OH}**. Ethyl acetate was added (25 mL) and the suspension was stirred at room temperature for 10 min. The precipitate was filtered off to give **PrS[6]^{OH}** in 40 % yield (17 mg), while the filtrated contained **PrS[5]^{OH}** that was recovered in 55 % yield (24 mg) after evaporation of the solvent under reduced pressure.
- Starting by **PrS[5]^{Et}** (50 mg, 43.80 µmol) and BBr_3 (0.4 mL, 4.00 mmol): The reaction was stopped by adding slowly an aqueous solution of $NaHCO_3$ (1.1 g of $NaHCO_3$ dissolved in 15 ml of cold water) and, then, the precipitate was filtered. The solid was washed with a 10 % aqueous solution of sodium sulfite (25 mL), and

two times with water (2 x 25 mL). The precipitate consisted of **PrS[6]^{OH}** in 90 % yield (34 mg), as a white solid.

- Starting by **PrS[5]^{nPr}** (50 mg, 39.00 µmol) and BBr_3 (0.4 mL, 4.00 mmol): The reaction was stopped by adding slowly an aqueous solution of $NaHCO_3$ (1.1 g of $NaHCO_3$ dissolved in 15 mL of cold water) and, then, the precipitate was filtered. The solid was washed with a 10% aqueous solution of sodium sulfite (25 mL), and, later, two times with water (2 x 25 mL). The precipitate consisted of **PrS[6]^{OH}** in 90 % yield (30 mg), as a white solid.
- Starting by **PrS[6]^{Me}** (100 mg, 83.30 µmol) and BBr_3 (1.0 mL, 9.60 mmol): The reaction was stopped by adding slowly an aqueous solution of $NaHCO_3$ (2.6 g of $NaHCO_3$ dissolved in 50 ml of cold water) and, then, the precipitate was filtered. The solid was washed with a 10% aqueous solution of sodium sulfite (50 mL), and, later, two times with water (2 x 50 mL). The precipitate consisted of **PrS[6]^{OH}** in 93 % yield (80 mg), as a white solid.
- Starting by **PrS[6]^{Et}** (200 mg, 146.01 µmol) and BBr_3 (1.7 mL, 18.00 mmol): The reaction was stopped by adding slowly an aqueous solution of $NaHCO_3$ (4.4 g of $NaHCO_3$ dissolved in 50 ml of cold water) and, then, the precipitate was filtered. The solid was washed with a 10% aqueous solution of sodium sulfite (50 mL), and, later, two times with water (2 x 50 mL). The precipitate consisted of **PrS[6]^{OH}** in 93 % yield (140 mg), as a white solid.

- Starting by **PrS[6]^{nPr}** (200 mg, 0.13 mmol) and BBr_3 (1.5 mL, 15.60 mmol): The reaction was stopped by adding slowly an aqueous solution of $NaHCO_3$ (4.6 g of $NaHCO_3$ dissolved in 50 ml of cold water) and, then, the precipitate was filtered. The solid was washed with a 10% aqueous solution of sodium sulfite (50 mL), and, later, two times with water (2 x 50 mL). The precipitate consisted of **PrS[6]^{OH}** in 96 % yield (130 mg), as a white solid.

Procedure B: To a solution of **PrS[n]^{R}** and templating agent **$6^+ \cdot I^-$** or **$7^+ \cdot I^-$** (1 equiv) in dry CH_2Cl_2 (5.0 mM) was added BBr_3 under nitrogen atmosphere at –78 °C. The mixture was stirred at this temperature for 1 h and at 0 °C for three hours.

- Starting by **PrS[5]^{Me}** (50 mg, 50.00 μmol), the templating agent **$6^+ \cdot I^-$** (10 mg, 50.00 μmol) and BBr_3 (0.5 mL, 5.00 mmol): The reaction was stopped by adding slowly an aqueous solution of $NaHCO_3$ (1.3 g of $NaHCO_3$ dissolved in 15 mL of cold water). Then, 30 mL of ethyl acetate were added to the reaction mixture. The aqueous layer was washed with ethyl acetate (3 x 20 mL). Later, the organic layer was washed with a 10 % aqueous solution of sodium sulfite (25 mL), and it was dried with Na_2SO_4 and concentrated to give, as a white solid, the macrocycle **PrS[5]^{OH}** in 90 % yield (38 mg).
- Starting by **PrS[5]^{Et}** (50 mg, 43.80 μmol), the templating agent **$6^+ \cdot I^-$** (8.0 mg, 43.80 μmol) and BBr_3 (0.4 mL, 4.00 mmol): The reaction was stopped by

adding slowly an aqueous solution of $NaHCO_3$ (1.1 g of $NaHCO_3$ dissolved in 15 mL of cold water) and, then, the precipitate was filtered. The solid was washed with a 10 % aqueous solution of sodium sulfite (25 mL), and, later, two times with water (2 x 25 mL). The precipitate was filtered. Ethyl acetate was added (25 mL) and the suspension was stirred at room temperature for 10 min. The precipitate was filtered off to give and **PrS[6]**^{OH} in 69 % yield (26 mg), while the filtrated contained **PrS[5]**^{OH} that was recovered in 24 % yield (9 mg) after evaporation of the solvent under reduced pressure.

- Starting by **PrS[5]**^{nPr} (50 mg, 39.00 μmol), the templating agent $\mathbf{6^+ \cdot I^-}$ (8 mg, 39.00 μmol) and boron bromide (0.4 mL, 4.00 mmol): The reaction was stopped slowly adding an aqueous solution of $NaHCO_3$ (1.1 g of $NaHCO_3$ dissolved in 15 ml of cold water) and, then, the precipitate was filtrated. The solid was washed with a 10% aqueous solution of sodium sulfite (25 mL), and, later, two times with water (2 x 25 mL). The precipitate was recovered. Ethyl acetate was added (25 mL) and the suspension was stirred at room temperature for 10 min. The precipitate was filtered off to give and **PrS[6]**^{OH} in 84 % yield (28 mg), while the filtrated contained **PrS[5]**^{OH} that was recovered in 9 % yield (3 mg) after evaporation of the solvent under reduced pressure.
- Starting by **PrS[5]**^{Me} (50 mg, 50.00 μmol), the templating agent $\mathbf{7^+ \cdot I^-}$ (13 mg, 50.00 μmol) and BBr_3 (0.5 mL, 5.00 mmol): The reaction was stopped by adding slowly an aqueous solution of $NaHCO_3$ (1.3 g

of $NaHCO_3$ dissolved in 15 mL of cold water) and, then, the precipitate was filtered. The solid was washed with a 10% aqueous solution of sodium sulfite (25 mL), and, later, two times with water (2 x 25 mL). The precipitate was recovered. Ethyl acetate was added (25 mL) and the suspension was stirred at room temperature for 10 min. The precipitate was filtered off to give **PrS[6]^{OH}** in 65 % yield (28 mg), while the filtrated contained **PrS[5]^{OH}** that was recovered in 25 % yield (11 mg) after evaporation of the solvent under reduced pressure.

Derivative *c*-PrS[5]^{OH}:

M.p.: > 250 °C dec.; **^{1}H NMR** (400 MHz, DMSO-*d*$_6$, 298 K): δ 9.63 - 9.54 (*overlapped*, ArO*H*, 5H) 9.45 (*s*, ArO*H*, 1H), 9.19 (*s*, ArO*H*, 1H), 9.04 (*s*, ArO*H*, 1H), 8.80 (*d*, *J* = 9.3 Hz, Ar*H*, 1H), 8.65 (*d*, *J* = 9.3 Hz, Ar*H*, 1H), 8.60 (*d*, *J* = 9.4 Hz, Ar*H*, 1H), 8.55 (*d*, *J* = 9.2 Hz, Ar*H*, 1H), 8.36 - 8.33 (*overlapped*, Ar*H* + ArO*H*, 2H), 8.20 (*d*, *J* = 9.1 Hz, Ar*H*, 1H), 8.09 (*s*, ArO*H*, 1H), 8.02 (*overlapped*, Ar*H*, 2H), 7.39 (*d*, *J* = 2.2 Hz, Ar*H*, 1H), 7.07 - 6.78 (*overlapped*, Ar*H*, 9H), , 6.43 (*d*, *J* = 9.1 Hz, Ar*H*, 1H), 5.76 (*s*, Ar*H*, 1H), 4.57 - 4.14 (*overlapped*, ArC*H*$_2$Ar, 10H); **^{13}C NMR** {^{1}H} (100 MHz, DMSO-*d*$_6$, 298 K): δ 151.9, 150.7, 150.3, 149.0, 148.8, 148.7,147.7, 132.0, 129.6, 129.4, 129.0, 128.7, 128.4, 128.0, 127.4, 126.9, 124.9, 124.7, 124.3, 123.4, 122.8, 121.3, 120.4, 120.1, 119.8, 119.0, 118.5, 117.7, 117.5, 117.3, 116.9, 116.7, 104.6, 25.7, 21.6, 20.8, 20.4, 20.2; **HRMS** (FT-ICR MALDI) m/z $[M]^+$ calcd for $C_{55}H_{40}O_{10}$: 860.2622; found: 860.2622.

Derivative PrS[5]^{OH}:
M.p.: > 245 °C dec.; **^{1}H NMR** (600 MHz, CD_3OD, 298 K): δ 7.98 (*br s*, Ar*H*, 10H), 6.76 (*d*, *J* = 9.0 Hz, Ar*H*, 10H), 4.58 (*s*, ArC*H*$_2$Ar, 10H); **^{13}C NMR** {^{1}H} (100 MHz, CD_3OD, 298 K): δ 150.5, 130.5, 124.8, 121.0, 118.3, 22.0; **HRMS** (FT-ICR MALDI) m/z $[M]^+$ calcd for $C_{55}H_{40}O_{10}$: 860.2622; found: 860.2623.

Derivative PrS[6]^{OH}:
M.p.: > 250 °C dec.; **^{1}H NMR** (300 MHz, DMSO-*d*$_6$, 373 K): *δ* 7.86 (*d*, *J* = 8.7 Hz, Ar*H*, 12H), 6.87 (*d*, *J* = 8.7 Hz, Ar*H*, 12H), 4.53 (*s*, ArC*H*$_2$Ar, 12H); **^{13}C NMR** {^{1}H} (100 MHz, DMSO-*d*$_6$, 298 K): *δ* 148.8, 129.0, 123.3, 120.1, 117.4, 20.8; **HRMS** (FT-ICR MALDI) m/z $[M]^+$ calcd for $C_{66}H_{48}O_{12}$: 1032.3146; found: 1032.3148.

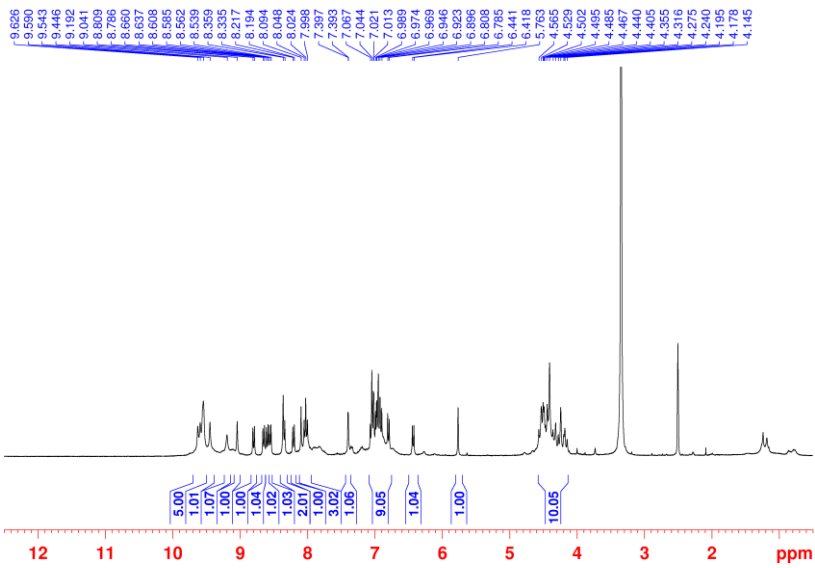

Figure 72. ^{1}H NMR spectrum of ***c*-PrS[5]^{OH}** (DMSO-*d*$_6$, 400 MHz, 298 K).

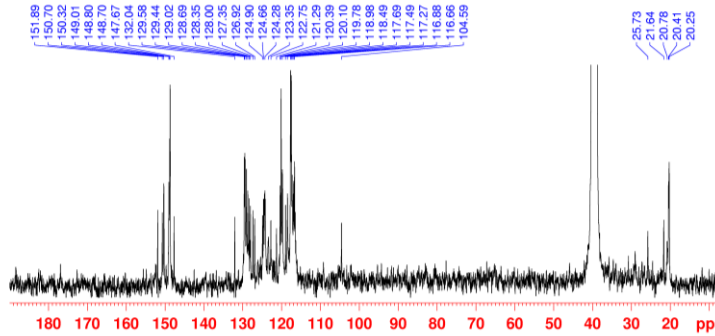

Figure 73. ^{13}C NMR spectrum of ***c*-PrS[5]^{OH}** (DMSO-d_6, 100 MHz, 298 K).

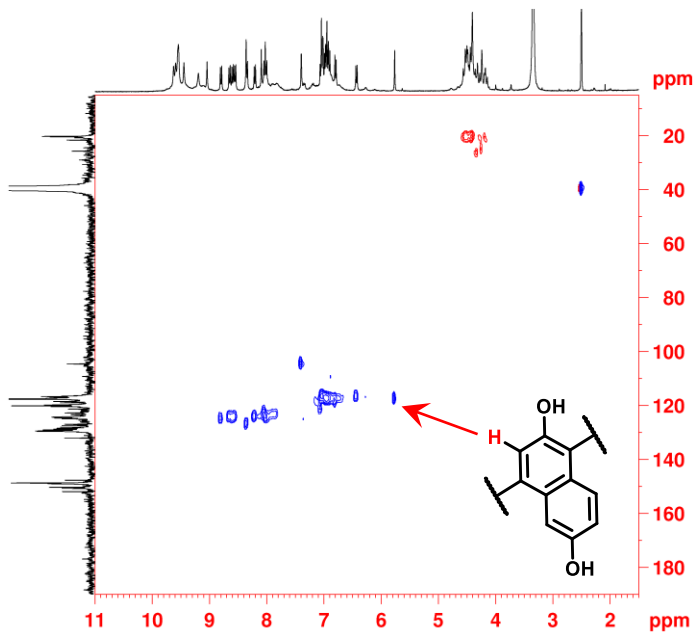

Figure 74. HSQC spectrum of ***c*-PrS[5]^{OH}** (DMSO-d_6, 400 MHz, 298 K).

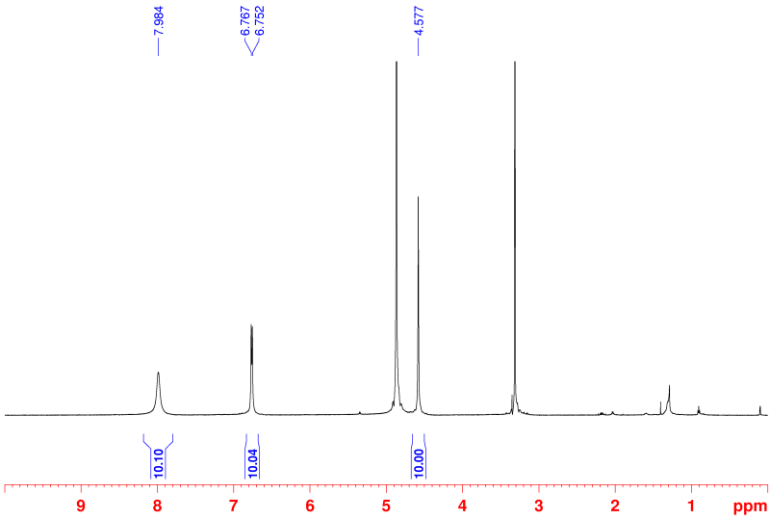

Figure 75. ^{1}H NMR spectrum of **PrS[5]^{OH}** (CD_3OD, 600 MHz, 298 K).

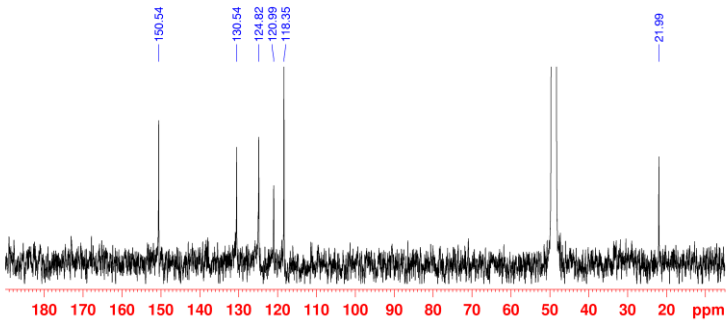

Figure 76. ^{13}C NMR spectrum of **PrS[5]^{OH}** (CD_3OD, 100 MHz, 298 K).

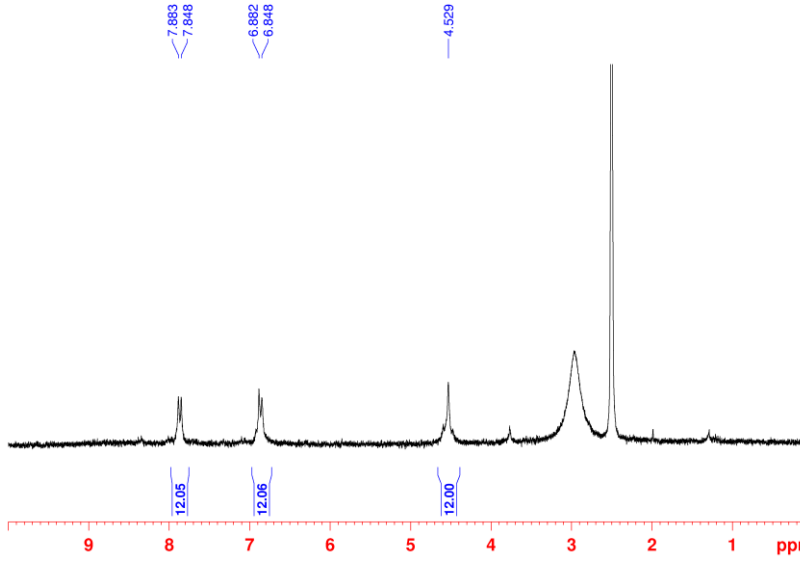

Figure 77. ^{1}H NMR spectrum of **PrS[6]^{OH}** (DMSO-d_6, 300 MHz, 373 K).

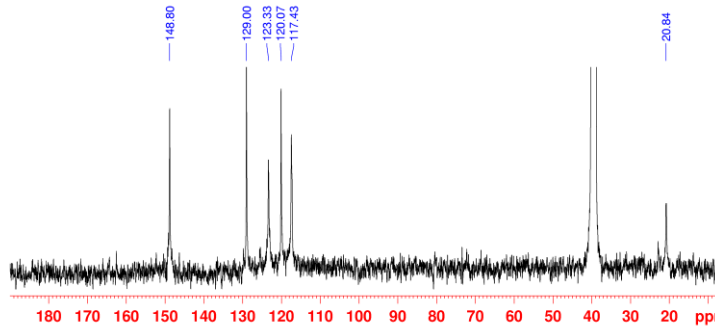

Figure 78. ^{13}C NMR spectrum of **PrS[6]^{OH}** (DMSO-d_6, 100 MHz, 298 K).

5.5.3 DFT Calculations[71]

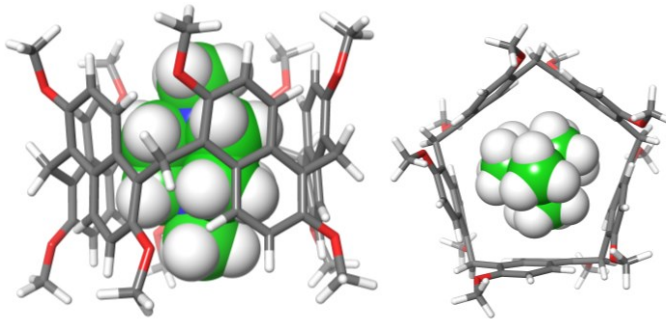

Figure 79. DFT-Optimized structure (GFN2-xTB) of **14^{2+}@PrS[5]^{Me}** complex.

6.0 Synthesis of Water-Soluble Carboxylato-Prismarenes and Study of Their Recognition Properties[73]

6.1 Synthesis of Water-Soluble Carboxylato-Prismarenes

per-Hydroxylated[71] prismarenes **PrS[5]^{OH}** and **PrS[6]^{OH}** can be considered as useful synthetic precursors to obtain novel hosts with intriguing supramolecular properties.

In recent years, water-soluble host[74] have shown amazing supramolecular properties. In fact, recently Wei Jiang[4a,55, 75] has reported water soluble naphthotube macrocycles which were able to recognize hydrophilic guests.

---

[73] Del Regno, R.; Santonoceta, G. D. G.; Della Sala, P.; De Rosa, M.; Soriente, A.; Talotta, C.; Spinella, A.; Neri, P.; Sgarlata, C.; Gaeta, C. *Org. Lett.* **2022**, *24*, 2711-2715.

[74] (a) Murray, J.; Kimoon, K.; Ogoshi, T.; Wei, Y.; Gibb, C. B. *Chem. Soc. Rev.* **2017**, *46*, 2479–2496; (b) Min, X.; Yong, Y.; Xiaodong, C.; Zibin, Z.; Feihe, H. *Acc. Chem. Res.* **2014**, *47*, 1925–1934; (c) Le, M.-Y.; Taghuo K., E. S.; Schrader, T. *Chem. Commun.* **2022**, *58*, 2954-2966; (d) Meiners, A.; Bäcker, S.; Hadrović, I.; Heid, C.; Beuck, C.; Ruiz-Blanco, Y. B.; Mieres-Perez, J.; Pörschke , M.; Grad, J.-N.; Vallet, C.; Hoffmann, D.; Bayer, P.; Sánchez-García, E.; Schrader, T.; Knauer, S. K. *Nat. Commun.* **2021**,*12*, 1505; (e) Grawe, T.; Schäfer, G.; Schrader, T. *Org. Lett.* **2003**, *5*, 1641–1644.

[75] (a) Huang, G.-B.; Wang, S.-H.; Ke, H.; Yang, L.-P.; Jiang, W. *J. Am. Chem. Soc.* **2016**, *138*, 14550–14553. (b) Yang, L.–P.; Ke, H.; Yao, H.; Jiang, W. *Angew. Chem. Int. Ed.* **2021**, *60*, 21404–21411.

During the third year of this PhD project, the synthesis of water-soluble prism[*n*]arenes (*n* = 5 and 6) bearing carboxylato anionic groups on the rims has been studied. In addition, the recognition properties of the **PrS[5]$^{COO-}$** and **PrS[6]$^{COO-}$** derivatives toward ammonium guests, in water, were investigated by NMR and calorimetry.[73]

Initially, the **PrS[5]^{OH}** and **PrS[6]^{OH}** were alkylated with ethyl bromoacetate to give ethoxycarbonylmethoxy groups-substituted prism[*n*]arene (**Scheme 8**). Subsequently, the **PrS[5]^{COOEt}** and **PrS[6]^{COOEt}** were hydrolysed to obtain the **PrS[5]^{COOH}** and **PrS[6]^{COOH}** in 95 % of yield.[73]

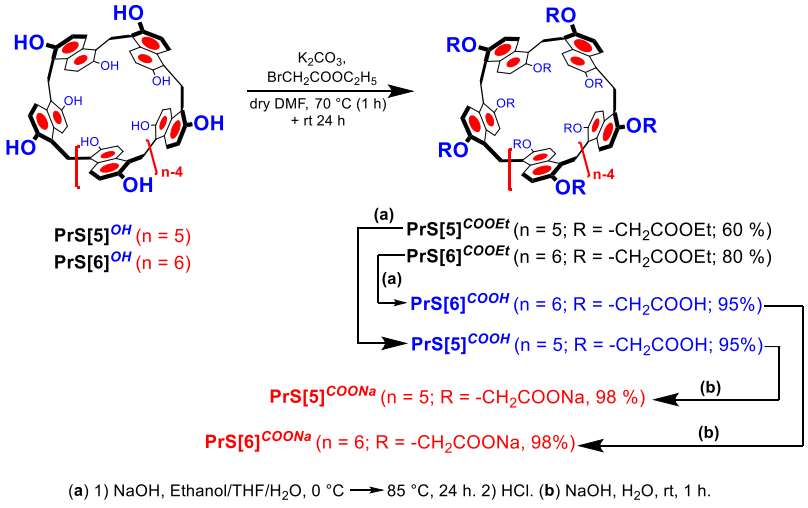

Scheme 8. Synthesis of water-soluble **PrS[n]^{COONa}**.[73]

Finally, the **PrS[5]^{COOH}** and **PrS[6]^{COOH}** were reacted with aqueous NaOH solution, obtaining **PrS[*n*]^{COONa}** salts in 98 % of yield - **Scheme 8**.

^{1}H NMR spectrum of the **PrS[5]$^{COO-}$** in D_2O solution (pH 7.6, phosphate buffer) at 298 K, evidenced a *D_5* symmetry of the molecule. An AX system was present at 7.89 and 6.88 ppm, attributable to the aromatic H-atoms of the macrocycle. Moreover, *OCH_2* groups resonated as an AB system at 4.25 and 4.14 ppm – **Figure 80**.[73]

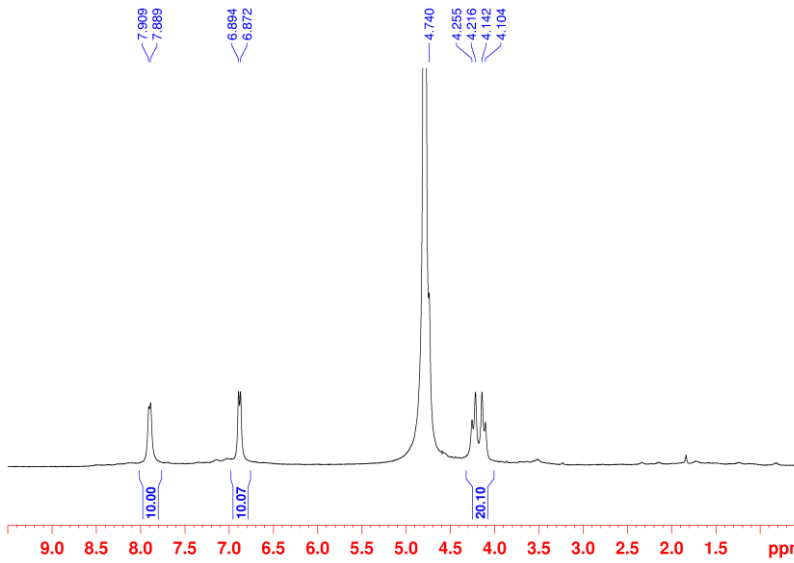

Figure 80. ^{1}H NMR spectrum of **PrS[5]^{COONa}** (buffered D_2O solution, pH 7.60, 400 MHz, 298 K).[73]

Similarly, the ^{1}H NMR spectrum of **PrS[6]$^{COO-}$** at 333 K was in agreement with a *D_6* symmetry – see **Figure 91** paragraph **6.4.2**. In detail, the spectrum showed the presence of two doublets at 8.42 and 7.43 ppm, attributable to the aromatic H-atoms of the macrocycle, while at 5.19 ppm a singlet was detected attributable to the methylene-bridged – see **Figure 91** paragraph **6.4.2**.[73]

6.2 Molecular Recognition Properties of Water-Soluble Prism[n]arenes[73]

At this point, it was interesting to study the recognition abilities in aqueous medium of **PrS[5]^{COONa}** and **PrS[5]^{COONa}** hosts toward cationic ammonium guests (**Scheme 9**).

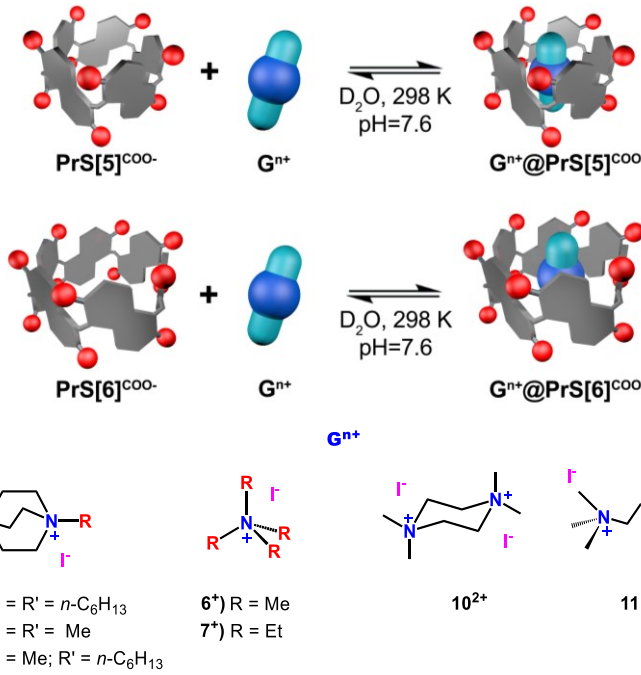

Scheme 9. Schematic complexation equilibrium of **PrS[5]^{COONa}** (top) and **PrS[6]^{COONa}** (bottom) with ammonium guests (PB buffer in D_2O, pH = 7.60, 298 K).[73]

In particular, when *N,N,N,N',N',N'*-hexamethylethylenediammonium salt **11^{2+}·$(I)_2$**, and **PrS[5]$^{COO-}$** were mixed in equimolar ratio in D_2O at pH

= 7.6 (**Scheme 9**), the formation of the *endo*-complex was observed by the presence of upfield shifted H-atoms signals of the guest to negative values of chemical shift – see **Figure 93c** paragraph **6.4.3**. In addition, similar results were obtained for the complexation of other ammonium guests (**Scheme 9**) with **PrS[5]$^{COO-}$**.[73]

Interestingly, an increase in distance between the signals of the aromatic H-atoms of the **PrS[5]$^{COO-}$** was observed upon inclusion of the guests inside the cavity of the carboxylato-prism[5]arene. As previously reported[46,47], these results are indicative of the inclusion of the guest inside the cavity of the host stabilized by C–H···π interactions.

Determination of the association constants of the **G^{n+}@PrS[n]$^{COO-}$** complexes (**Scheme 9**) by ^{1}H NMR spectra was not possible as the intensities of the host or guest free were found to be low compared to those of the complex. To overcome this problem, in collaboration with prof. Carmelo Sgarlata from *Università degli Studi di Catania*, we decided to perform calorimetric investigations[76].

In detail, calorimetry measurements confirm that **PrS[5]^{COONa}** host forms 1:1 complexes with all the mono- and bis-*N*-alkyl-ammonium – **Scheme 9**.[73] The complexes show affinity constant values ranging from 10^3 to 10^5 M^{-1}, which are smaller than those previously determined for the inclusion of some of these guests into the **PrS[5]^{R}** (R = Me, Et, *n*Pr) cavity in organic solvent.[46,47] Probably the drop in the constant values

[76] Arena, G.; Gans, P.; Sgarlata, C. *Anal. Bioanal. Chem*. **2016**, *408*, 6413–6422.

is due to the different complexation environment as water competes for hydrogen bonds and efficiently solvates charged species.[77]
Moreover, results in **Table 12** suggest that the stability of the host-guest complexes is significantly affected by the structural features of the differently charged guests.

	PrS[5]^{COONa}			**PrS[6]^{COONa}**		
Guest	*LogK*	ΔH^{0} [b]	ΔS^{0} [c]	*LogK*	ΔH^{0} [b]	ΔS^{0} [c]
6^{+}	4.51 (9)	-15.21 (2)	36 (2)	3.5 (2)	-1.33 (6)	63 (4)
7^{+}	3.50 (3)	-24.66 (1)	–15.8 (6)	3.3 (2)	-1.54 (6)	58 (4)
11^{2+}	5.1 (2)	-26.45 (2)	9 (3)	3.10 (5)	-7.95 (2)	32.7(9)
5^{2+}	4.5 (1)	-30.02 (2)	-14 (3)	3.41 (6)	-12.21 (2)	25 (2)
16^{2+}	4.5 (1)	-33.65 (3)	-27 (3)	3.29 (1)	-12.63 (1)	20.5(4)
14^{2+}	3.87 (6)	-18.53 (2)	13 (2)	2.91 (3)	-14.92 (1)	5.7 (6)
10^{2+}	5.3 (2)	-33.91 (3)	-12 (4)	3.05 (3)	-16.71 (1)	2.3 (6)

[a] σ in parentheses; [b] expressed in kJ·mol^{-1}; [c] expressed in J·deg^{-1}·mol^{-1}.

Table 12. Log K values and thermodynamic parameters[a] for host-guest complex formation at 25 °C in aqueous solution (pH 7.6, phosphate buffer 70 mM).[73]

In detail, the largest binding affinities were observed for **10^{2+}@PrS[5]$^{COO-}$** and **11^{2+}@PrS[5]$^{COO-}$**, with log *K* values of 5.3 (2) and 5.1 (2) respectively.[73] In fact, these guests meet the requirements to fill the host cavity volume and establish a larger number of favourable secondary interactions – **Table 12**. As concerns the singly-charged ammonium guests, **PrS[5]$^{COO-}$** displays a greater affinity for **6**$^{+}$ than **7**$^{+}$. The larger binding affinity for dicationic than for

[77] (a) Biedermann, F.; Vendruscolo, M.; Scherman, O. A.; De Simone, A.; Nau, W. M. *J. Am. Chem. Soc.* **2013**, *135* (39), 14879-14888; (b) Schneider, H. J. *Angew. Chem., Int. Ed. Engl.* **2009**, *48* (22), 3924-3977.

monocationic analogues suggests that Coulombic interactions between the carboxylate groups and the ammonium ions, along with cation-π interactions with the prismarene cavity, are fundamental for an efficient complexation as they contribute to enhance the free energy of binding of about 4 kJ·mol^{-1} – **Figure 81**.[73]

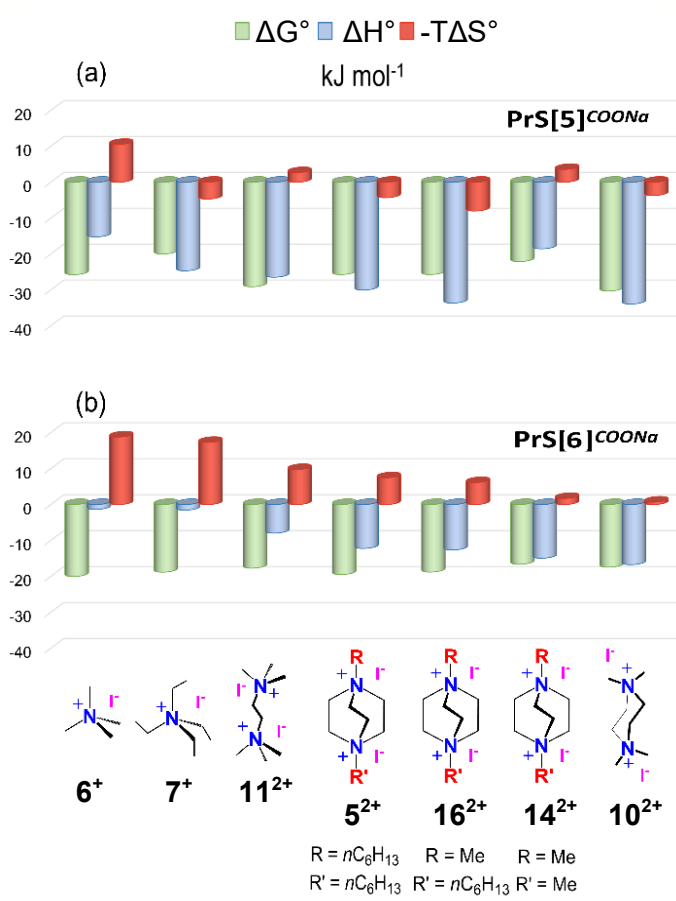

Figure 81. Thermodynamic parameters for host-guest complex formation of: (a) **PrS[5]**$^{COO-}$ and (b) **PrS[6]**$^{COO-}$ with positively charged guests at 25 °C in buffered aqueous solution (pH 7.6). [73]

The inclusion of all ammonium cations into the hydrophobic cavity of **PrS[5]$^{COO-}$** is due to enthalpically favourable attractive forces (including electrostatic, cation-π, and CH-π interactions), which balance the cost in energy needed for the desolvation of the host and guest – **Figure 81**. Moreover, the complexation of bulkier guests such as **10^{2+}** and **16^{2+}** is driven by larger enthalpy values because of a more favoured interaction with the host interior walls mostly due to CH-π interactions.[73]

Analogously, calorimetry measurements (**Figure 81**) indicated that **PrS[6]^{COONa}** forms only 1:1 inclusion complexes with all the charged guests . The association constant values for the formation of the **G^{n+}@PrS[6]$^{COO-}$** complexes, are all in the order of 10^3 M^{-1}, smaller than the analogous values measured for the complexes of the **PrS[5]$^{COO-}$** hosts, and these differences could be attributed to the greater conformational flexibility of the hexamer **PrS[6]$^{COO-}$**– **Table 12**.[73]

Unlike **PrS[5]$^{COO-}$**, the constant values determined for **PrS[6]$^{COO-}$** are quite comparable regardless of shape, size, charge and length of the aliphatic chains of the different guests – **Table 12**. Although binding free energies for all the complexes formed by **PrS[6]$^{COO-}$** are comparable (about -19 kJ·mol^{-1}, **Figure 81**), some differences can be revealed when the enthalpic and entropic contributions are determined (**Figure 81**). Firstly, the encapsulation of monocations **6$^+$** and **7$^+$**, into the **PrS[6]$^{COO-}$** cavity is an entropically favoured process ($T\Delta S^0$ is about 18 kJ·mol^{-1} on average, **Figure 81**). Desolvation of the **6$^+$** and **7$^+$** cations as well as the release of water molecules from the solvent-filled

cavity of **PrS[6]$^{COO-}$** to the bulk of the solvent account for the large entropic gain.[73]

The encapsulation of double charged guests **G^{2+}** (**10^{2+}**, **14^{2+}**, **16^{2+}**, **5^{2+}** and **11^{2+}**) inside the **PrS[6]$^{COO-}$** cavity is an process enthalpically driven by electrostatic interactions between the carboxylate and cationic groups, along with multiple cation-π and CH-π interactions with the π-electron rich **PrS[6]$^{COO-}$** cavity (**Figure 81**). But the structural features of the guests seem to heavily influence the enthalpic gain values for the complexation of the double-charged guests (ΔH^0 gain follows the order **14^{2+}** > **16^{2+}** > **5^{2+}**, **Figures 81**). In detail, longer side alkyl chains in **5^{2+}** confer larger hydrophobicity and a smaller charge to radius ratio resulting in a lower overall charge density. Accordingly, electrostatic and/or cation-π interactions are less efficient while the role of desolvation and CH-π interactions with the host cavity walls are enhanced – **Figure 81**.[73]

6.3 Conclusions[73]

In conclusion, the synthesis of water soluble carboxylato-prism[n]arenes (n = 5 and 6) was obtained. **PrS[5]^{COONa}** and **PrS[6]^{COONa}** were able to form complexes with organic ammonium cations **G^{n+}@PrS[n]$^{COO-}$** (n = 5 and 6) in water as confirmed by NMR titration experiments. ITC studies showed that the complexation processes, are driven by different thermodynamic factors depending on prismarene size and cation charge. The complexation of ammonium cations into the cavity of **PrS[5]$^{COO-}$** is

driven by enthalpically favourable attractive forces. Regarding the carboxylato-prism[6]arene, *endo*-cavity encapsulation of singly-charged ammonium guest is entropically favoured. Consequently, desolvation of the cations as well as the release of water molecules from the solvent-filled cavity of the hexamer account for the large entropic gain. Differently, the encapsulation of double charged guests inside the cavity of the **PrS[6]$^{COO-}$** is enthalpically driven by electrostatic interactions.

6.4 Experimental Section

6.4.1 General Section

See **Paragraph 2.4.1**

6.4.2 Procedures for the Synthesis of the Carboxylato-Prismarenes and Copies of NMR Spectra[73]

Ethoxycarbonylmethoxy-Substituted Prism[5]arene. Under a nitrogen atmosphere **PrS[5]^{OH}** (0.40 g, 0.46 mmol) and potassium carbonate (2.57 g, 18.58 mmol) were dissolved in dry DMF (46 mL). The reaction mixture was stirred for 1 h at 70 °C. Then, the reaction was reported to room temperature and an excess of ethyl bromoacetate (1.55 mL, 13.94 mmol) was added. The mixture was stirred at room temperature for 24 h. The reaction was stopped by adding a 10 % aqueous solution of NH_4Cl (50 mL). After removal of the solvent, the resulting solid was triturated with water (60 mL) and then,

the precipitate was filtered. The solid was washed with water (2 x 30 mL) and methanol (2 x 30 mL). The crude product was subject to chromatography on silica gel (CH_2Cl_2/ MeOH = 99:1, v/v) to give the pure product **PrS[5]^{COOEt}** (0.48 g, 60 %) as a white solid.

Carboxylic Acid Groups-Substituted Prism[5]arene. **PrS[5]^{COOEt}** (0.40 g, 0.23 mmol), and NaOH (0.70 g, 17.40 mmol), in THF (34 mL), H_2O (34 mL) and Ethanol (34 mL) was stirred for 24 h at 85 °C. After removal of the solvent, 100 mL of ethyl acetate and 50 mL of 1 N HCl solution were added at 0 °C. The aqueous layer was washed with ethyl acetate (5 x 50 mL). Then, the organic layer was washed with brine (50 mL), and it was dried with Na_2SO_4 and concentrated to give the derivative **PrS[5]^{COOH}** (0.31 g, 95 %) as a white solid.

Synthesis of Carboxylato-Prism[5]arene. To a suspension of **PrS[5]^{COOH}** (0.30 g, 0.21 mmol) in water (15 mL) was added an aqueous solution of NaOH (0.1 g, 2.10 mmol in 3 mL). The reaction mixture was stirred for 1 h at room temperature. The solution was evaporated and triturated with 20 mL of methanol to give the derivative **PrS[5]^{COONa}** as a white solid (0.34 g, 98 %).

Ethoxycarbonylmethoxy-Substituted Prism[6]arene. Under a nitrogen atmosphere **PrS[6]^{OH}** (0.370 g, 0.36 mmol) and potassium carbonate (2.38 g, 17.19 mmol) were dissolved in DMF (36 mL). The reaction mixture was stirred for 1 h at 70 °C. Then, the reaction was reported to room temperature and an excess of ethyl bromoacetate (1.44 mL, 12.89 mmol) was added. The mixture was stirred at room temperature for 24 h. The reaction was

stopped by adding a 10 % aqueous solution of NH_4Cl (50 mL). After removal of the solvent, the resulting solid was triturated with water (60 mL) and then, the precipitate was filtered. The solid was washed with water (2 x 30 mL) and methanol (2 x 30 mL). The crude product was purified through chromatographic column on silica gel (CH_2Cl_2/ MeOH = 98:2, v/v) to give the pure product **PrS[6]^{COOEt}** (0.59 g, 80 %) as a brown solid.

Carboxylic Acid Groups-Substituted Prism[6]arene. PrS[6]^{COOEt} (0.40 g, 0.19 mmol), and NaOH (0.70 g, 17.42 mmol), in THF (28 mL), H_2O (28 mL) and Ethanol (28 mL), was stirred for 24 h at 85 °C. After removal of the solvent, 100 mL of ethyl acetate and 50 mL of aqueous 1 N solution of HCl were added at 0 °C. The aqueous layer was washed with ethyl acetate (5 x 50 mL). Then, the organic layer was washed with brine (50 mL), and it was dried with Na_2SO_4 and concentrated to give the derivative **PrS[6]^{COOH}** (0.32 g, 95 %) as a brown solid.

Synthesis of Carboxylato-Prism[6]arene. To a suspension of **PrS[6]^{COOH}** (0.30, 0.17 mmol) in water (15 mL) was added an aqueous solution of NaOH (0.1 g, 2.10 mmol in 3 mL). The reaction mixture was stirred for 1 h at room temperature. The solution was evaporated and triturated with 20 mL of methanol to give the derivative **PrS[6]^{COONa}** as a white solid quantitatively (0.33 g, 98 %).

Derivative PrS[5]^{COOEt}:
M.p.: > 300 °C dec. **^{1}H NMR** (CD_2Cl_2, 600 MHz, 298 K): δ 8.02 (*d*, 10H, Ar-*H*, *J* = 9.6 Hz), 6.85 (*d*, 10H, Ar-*H*, *J* = 9.6 Hz), 4.83 (*s*, 10H, ArC*H*$_2$Ar), 4.37 and 4.31 (AB, 20H, O*CH*$_2$, *J* = 16.5 Hz), 4.07-3.96 (m, 20H, O*CH*$_2$CH$_3$), 1.05

(*t*, 30H, OCH_2CH_3, *J* = 7.2 Hz). **^{13}C NMR** {^{1}H} (CD_2Cl_2, 150 MHz, 298 K): *δ* 169.7, 152.0, 130.1, 125.7, 124.3, 114.6, 67.1, 61.4, 22.2, 14.2. **HRMS** (FT-ICR MALDI) *m*/*z* $[M]^+$ calcd for $C_{95}H_{100}O_{30}$: 1720.6299; found: 1720.6300.

Derivative PrS[5]^{COOH}:
M.p.: > 300 °C dec. **^{1}H NMR** (CD_3OD, 400 MHz, 298 K): *δ* 8.02 (*d*, 10H, Ar-*H*, *J* = 9.6 Hz), 6.91 (*d*, 10H, Ar-*H*, *J* = 9.6 Hz), 4.83 (overlapped to signal of H_2O, 10H, $ArCH_2Ar$), 4.35 and 4.20 (AB, 20H, OCH_2, *J* = 16.4 Hz). **^{13}C NMR** {^{1}H} (CD_3OD, 100 MHz, 298 K): *δ* 173.4, 153.1, 130.9, 126.5, 125.2, 115.6, 67.6, 22.7. **HRMS** (FT-ICR MALDI) m/z $[M]^+$ calcd for $C_{75}H_{60}O_{30}$: 1440.3169; found: 1440.3179.

Derivative PrS[5]^{COONa}:
M.p.: > 300 °C dec. **^{1}H NMR** (D_2O, 400 MHz, 298 K, **Figure 80**): *δ* 7.89 (*d*, 10H, Ar-*H*, *J* = 8.0 Hz), 6.88 (*d*, 10H, Ar-*H*, *J* = 8.8 Hz), 4.74 (overlapped to H_2O signal, 10H, $ArCH_2Ar$), 4.21 and 4.14 (AB, 20H, OCH_2, *J* = 15.4 Hz). **^{13}C NMR** {^{1}H} (D_2O, 100 MHz, 298 K): *δ* 177.9, 160.6, 151.8, 129.2, 125.1, 123.4, 114.6, 68.3, 21.8.

Derivative PrS[6]^{COOEt}:
M.p.: > 300 °C dec. **^{1}H NMR** (CD_2Cl_2, 400 MHz, 298 K): *δ* 8.04 (br, 12H, Ar-H), 6.94 (br, 12H, Ar-H), 4.82-4.67(overlapped, 36 H, $ArCH_2Ar$ and OCH_2), 4.21 (broad, 24H, OCH_2CH_3), 1.23 (broad, 36H, OCH_2CH_3). **^{13}C NMR** {^{1}H} (CD_2Cl_2, 100 MHz, 298 K): *δ* 169.6, 151.4, 130.4, 125.2, 125.0, 115.0, 67.1, 61.5, 22.1, 14.4. **HRMS** (FT-ICR MALDI) *m*/*z* $[M]^+$ calcd for $C_{114}H_{120}O_{36}$: 2064.7559; found: 2064.7565.

Derivative PrS[6]^{COOH}:
M.p.: > 300 °C dec. **^{1}H NMR** (DMSO-d_6, 300 MHz, 393 K): δ 7.98 (*d*, 12H, Ar-*H*, *J* = 9.0 Hz), 7.05 (*d*, 12H, Ar-*H*, *J* = 9.7 Hz), 4.80-4.69 (overlapped, 36H, ArCH_2Ar and OCH_2). **^{13}C NMR** {^{1}H} (DMSO-d_6, 75 MHz, 393 K): δ 169.5, 150.5, 129.1, 123.9, 123.4, 114.3, 66.0, 21.0. **HRMS** (FT-ICR MALDI) m/z $[M]^+$ calcd for $C_{90}H_{72}O_{36}$: 1728.3803; found: 1728.3813.

Derivative PrS[6]^{COONa}:
M.p.: > 300 °C dec. **^{1}H NMR** (D_2O, 250 MHz, 333 K): δ 8.42 (*d*, 12H, Ar-*H,* *J* = 6.5 Hz), 7.43 (*d*, 12H, Ar-*H*, *J* = 8.5 Hz), 5.19 (*s*, 12H, ArCH_2Ar), 4.59 (overlapped to signal of H_2O, 24H, OCH_2). **^{13}C NMR** {^{1}H} (D_2O, 75 MHz, 333 K): δ 177.0, 152.0, 129.4, 125.0, 124.1, 116.6, 69.4, 22.3.

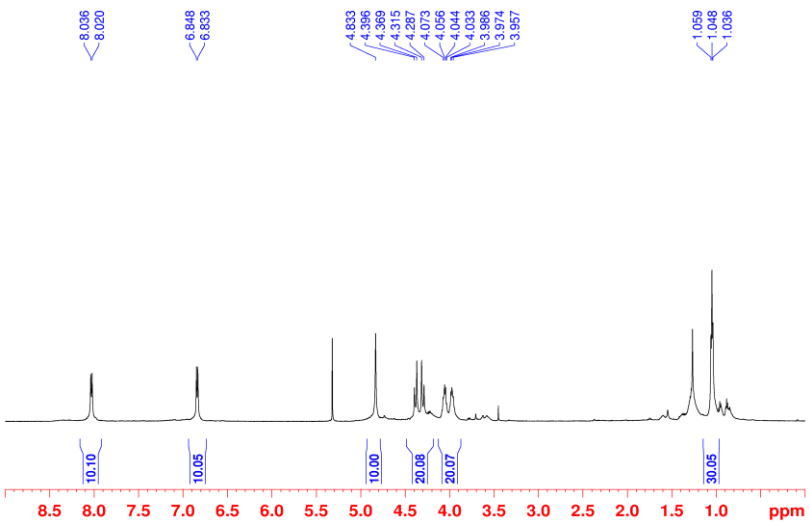

Figure 82. ^{1}H NMR spectrum of **PrS[5]^{COOEt}** (CD_2Cl_2, 600 MHz, 298 K).

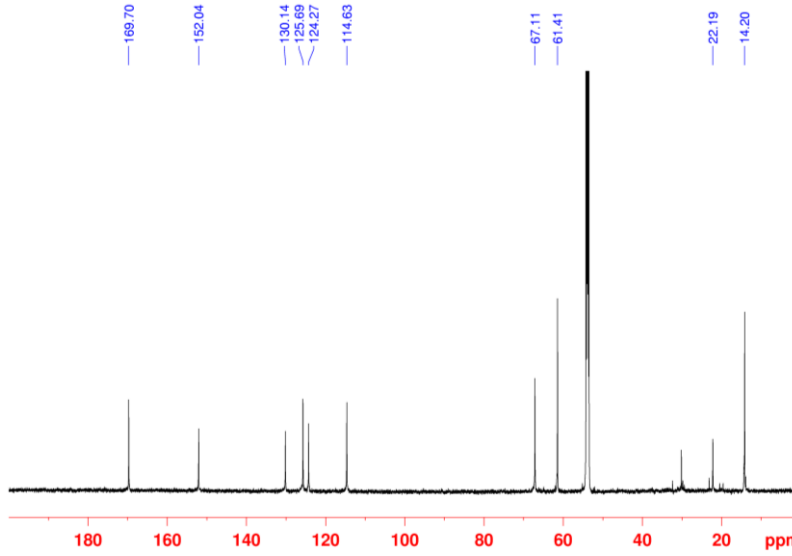

Figure 83. ^{13}C NMR spectrum of **PrS[5]**^{COOEt} (CD_2Cl_2, 150 MHz, 298 K).

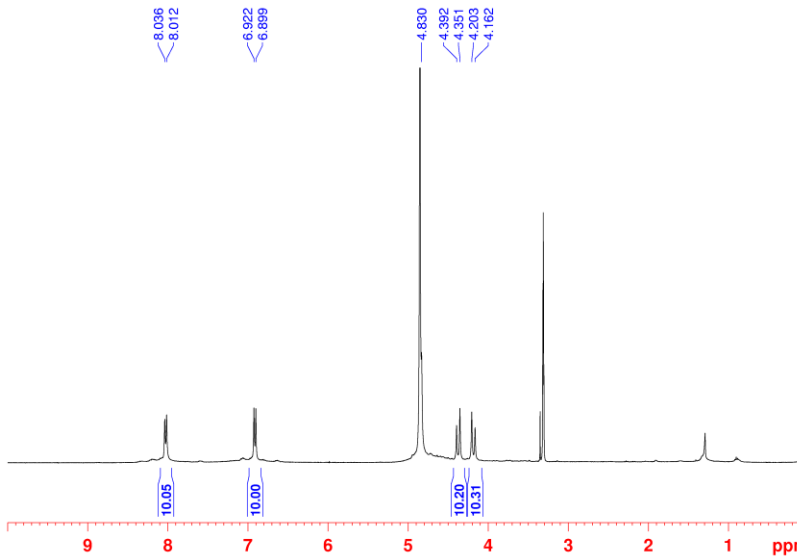

Figure 84. ^{1}H NMR spectrum of **PrS[5]**^{COOH} (CD_3OD, 400 MHz, 298 K).

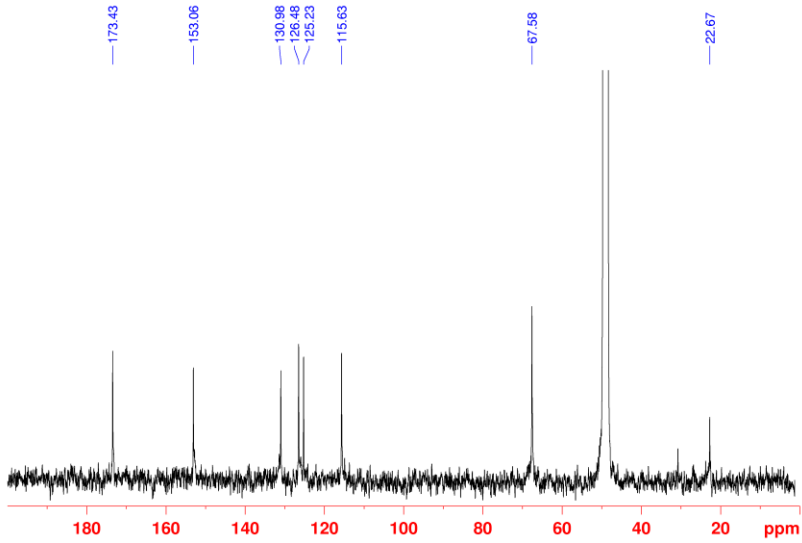

Figure 85. ^{1}H NMR spectrum of **PrS[5]**^{COOH} (CD_3OD, 100 MHz, 298 K).

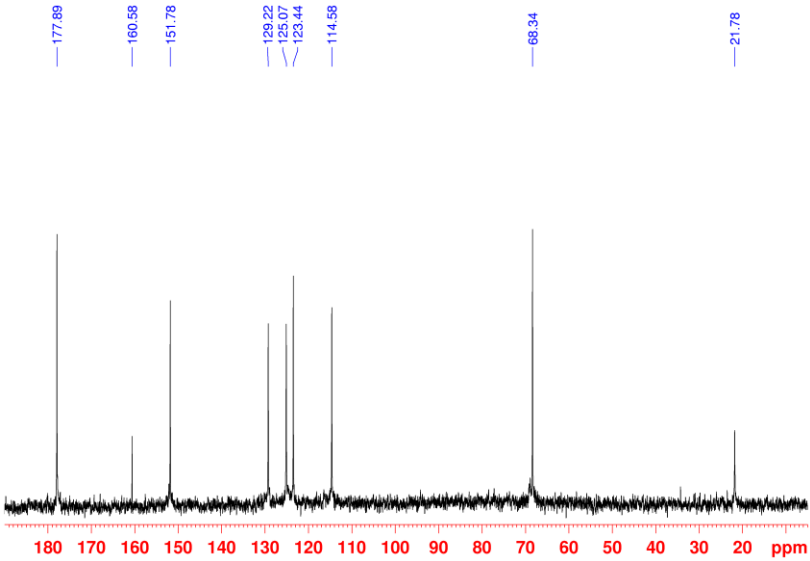

Figure 86. ^{13}C NMR spectrum of **PrS[5]**^{COONa} (D_2O, 100 MHz, 298 K).

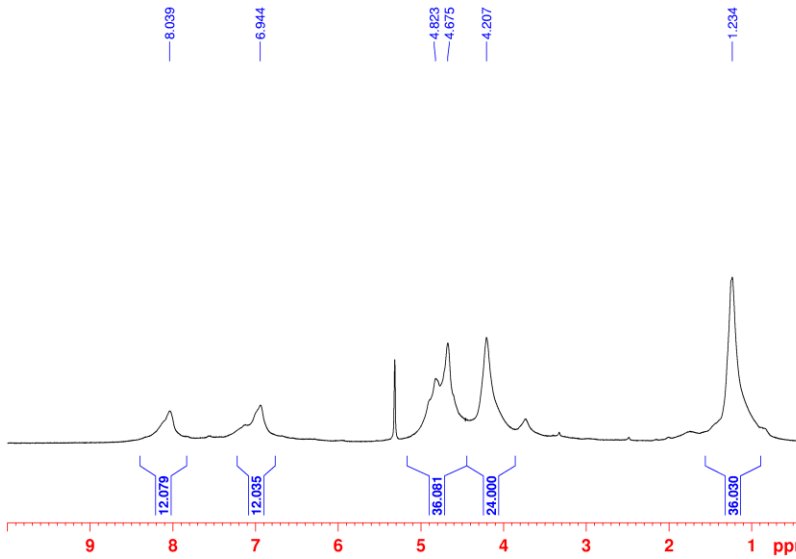

Figure 87. ^{1}H NMR spectrum of **PrS[6]**^{COOEt} (CD_2Cl_2, 400 MHz, 298 K).

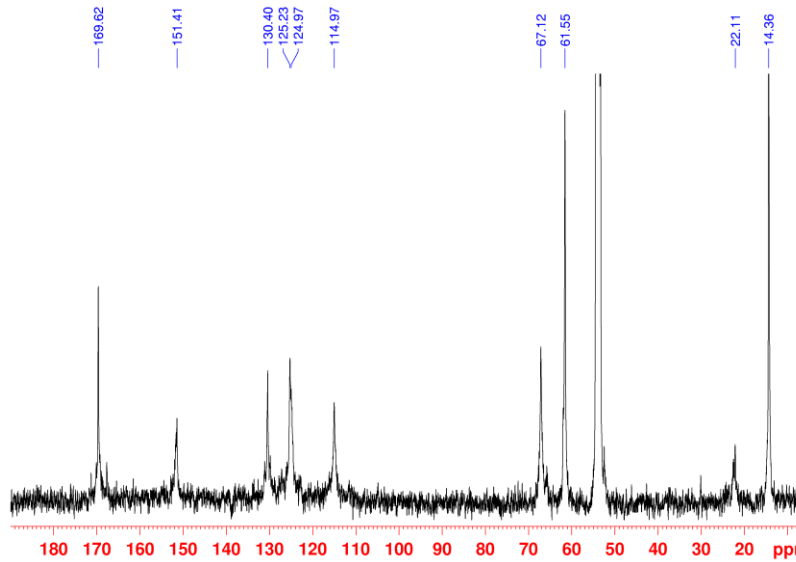

Figure 88. ^{13}C NMR spectrum of **PrS[6]**^{COOEt} (CD_2Cl_2, 100 MHz, 298 K).

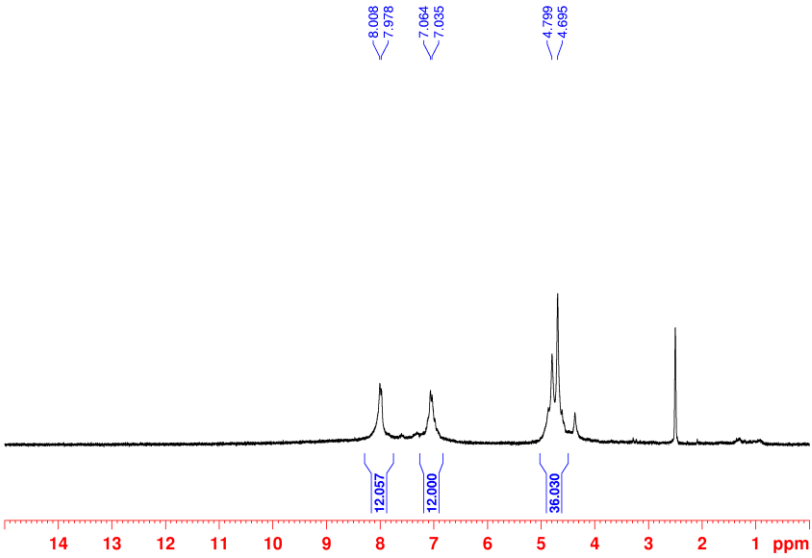

Figure 89. ^{1}H NMR spectrum of **PrS[6]^{COOH}** (DMSO-d_6, 300 MHz, 393 K).

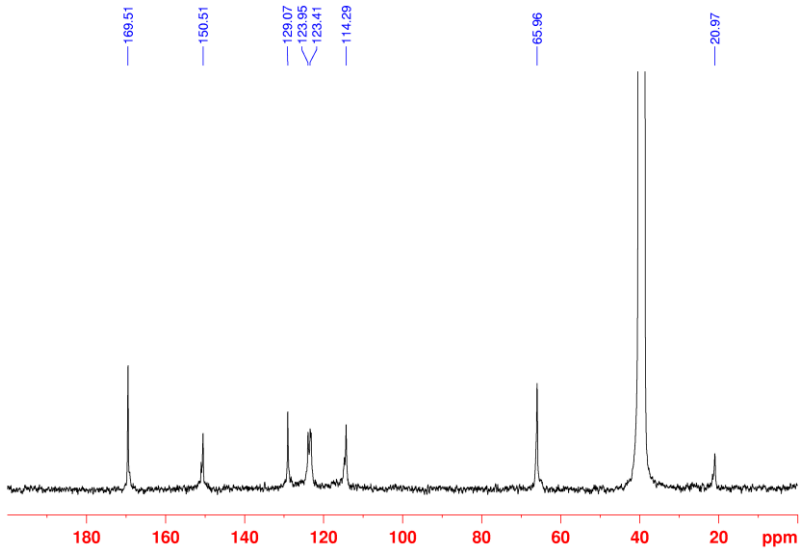

Figure 90. ^{13}C NMR spectrum of **PrS[6]^{COOH}** (DMSO-d_6, 75 MHz, 393 K).

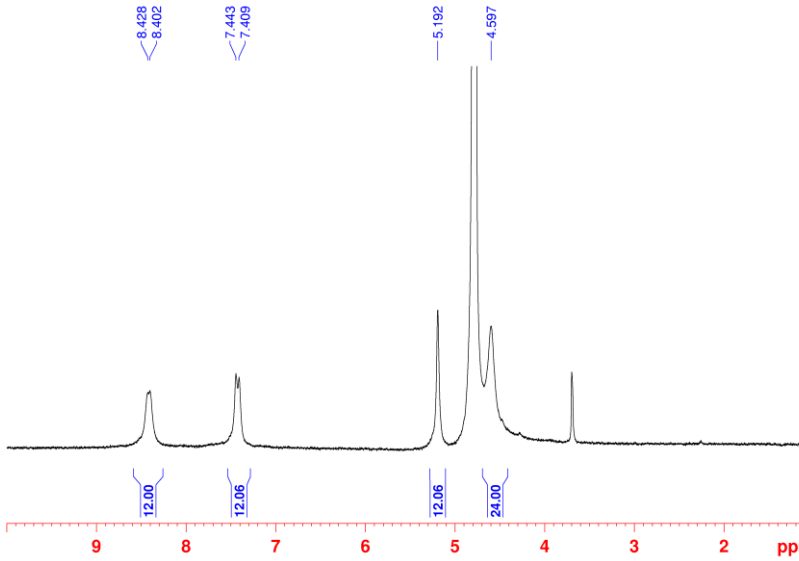

Figure 91. ^{1}H NMR spectrum of **PrS[6]^{COONa}** (D_2O, 250 MHz, 333 K).

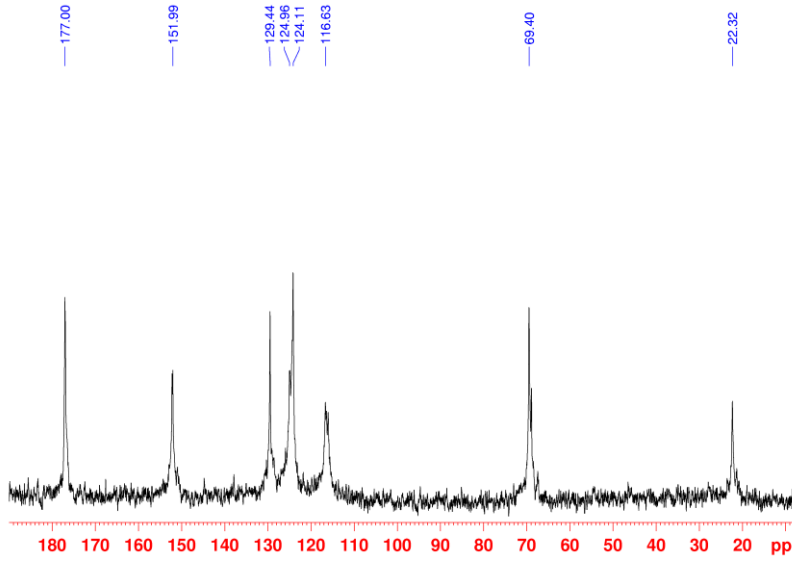

Figure 92. ^{13}C NMR spectrum of **PrS[6]^{COONa}** (D_2O, 75 MHz, 333 K).

6.4.3 Copies of 1D NMR Spectra of PrS[n]$^{COO-}$ Complexes[73]

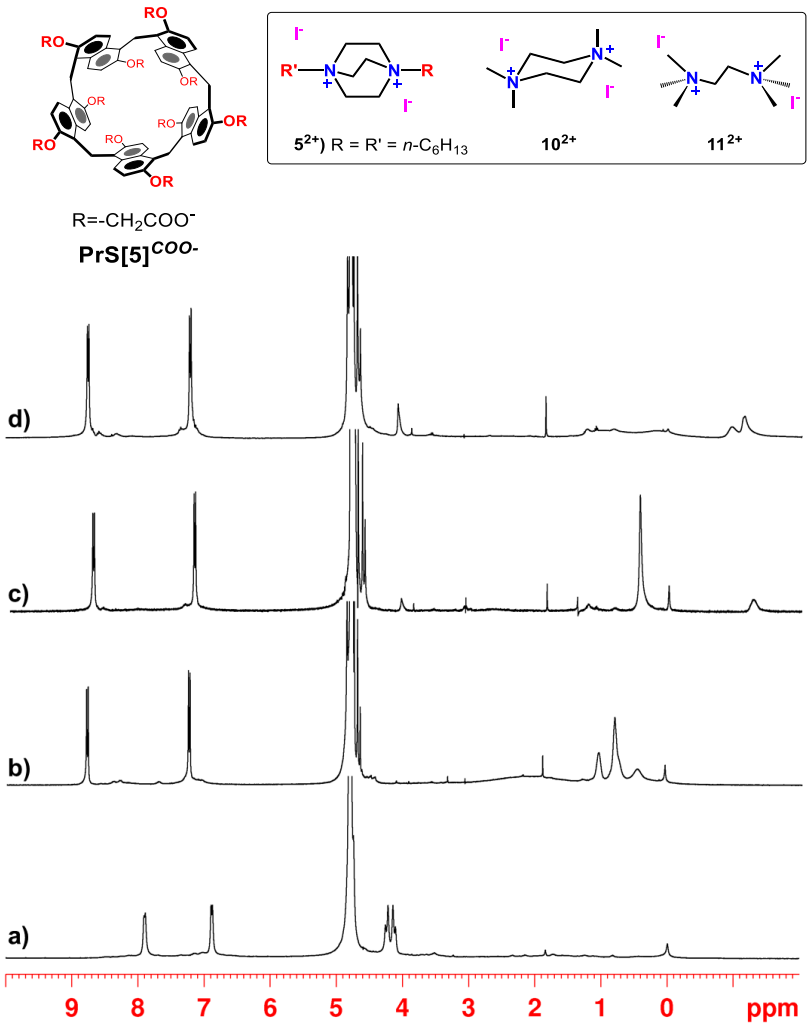

Figure 93. ^{1}H NMR spectra in an aqueous deuterated phosphate buffer (68 mM), 400 MHz at 298 K of: (a) **PrS[5]$^{COO-}$** ; 1:1 mixture of **PrS[5]$^{COO-}$** (6.02 mM) and, respectively: (b) **5^{2+}· 2I^{-}**; (c) **11^{2+}· 2I^{-}**; (d) **10^{2+}· 2I^{-}**.

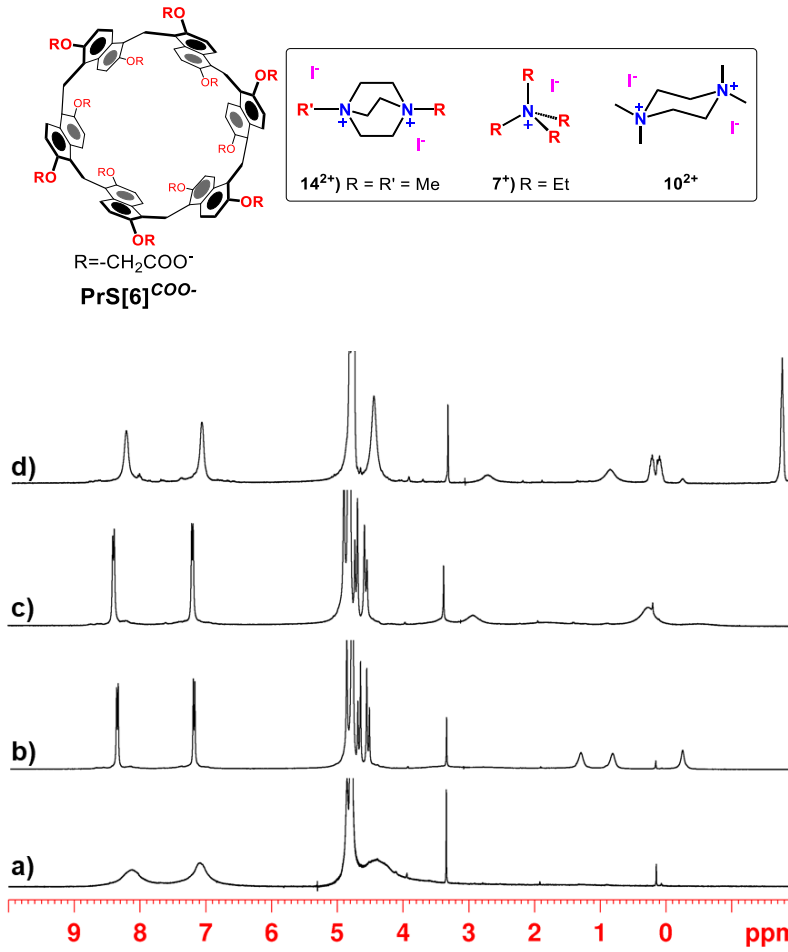

Figure 94. ^{1}H NMR spectra in an aqueous deuterated phosphate buffer (68 mM), 400 MHz at 298 K of: (a) **PrS[6]$^{COO-}$** ; 1:1 mixture of **PrS[6]$^{COO-}$** (6.02 mM) and, respectively: (b) **14^{2+}· 2I^{-}**; (c) **10^{2+}· 2I^{-}**, (d) **7^{+}· 2I^{-}**.

6.4.4 ITC Titrations Experiments[73]

Calorimetric titrations were carried out at 25 °C with a nano-isothermal titration calorimeter (Nano-ITC, TA Instruments, USA) having an active cell volume of 0.988 mL and a 250 µL injection syringe. Injection time intervals were chosen to guarantee equilibrium conditions before each subsequent addition. The reaction mixture in the sample cell was stirred at 250 rpm during the titration. The reference cell was always filled with ultrapure water. All solutions were stirred and degassed under vacuum for about 15 min before each run. Measurements were run in the overfilled mode. The power curve was integrated by NanoAnalyze (TA Instruments, USA) to obtain the gross heat of reaction. The calorimeter was calibrated chemically by a test HCl/TRIS reaction according to the procedure previously described.[78] The instrument was also checked through electrical calibrations.

ITC measurements were conducted by titrating an aqueous buffered solution of each guest (2.5÷20.0 mM) into an aqueous buffered solution of **PrS[*n*]**$^{COO^-}$ (0.25÷1.2 mM) host. All solutions were prepared in 70 mM phosphate buffer (pH 7.6). Typically, three independent experiments were run for each host-guest system. Heats of dilution were determined in separate "blank" experiments by titrating solutions of each guest into phosphate buffer (pH 7.6, 70 mM) only. The net heats of reaction were obtained by subtracting the heat evolved/absorbed in the blank experiments. Calorimetric data obtained from different titrations were analyzed

[78] Sgarlata, C.; Zito, V.; Arena, G. *Anal. Bioanal. Chem*. **2013**, *405*, 1085–1094.

simultaneously by HypCal software,[76] which allows for the determination of both equilibrium constants and enthalpies of complex formation through a non-linear least-squares minimization procedure.

PrS[5]^{COONa}

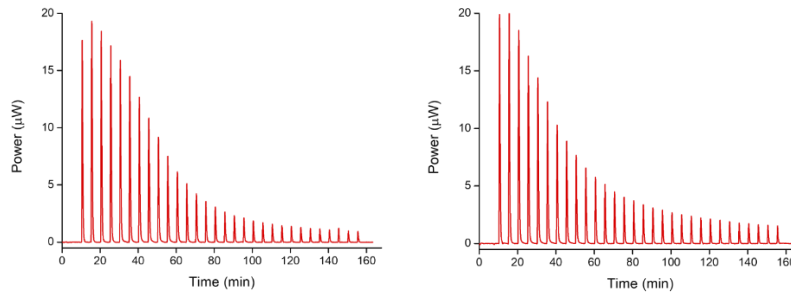

Figure 95. Typical ITC titration of **6**$^{+}$ (5.03 mM) into a **PrS[5]**$^{COO-}$ (0.47 mM) solution at 25 °C and pH 7.6 (Left); Typical ITC titration of **14**$^{2+}$ (6.45 mM) into a **PrS[5]**$^{COO-}$ (0.42 mM) solution at 25 °C and pH 7.6 (Right)

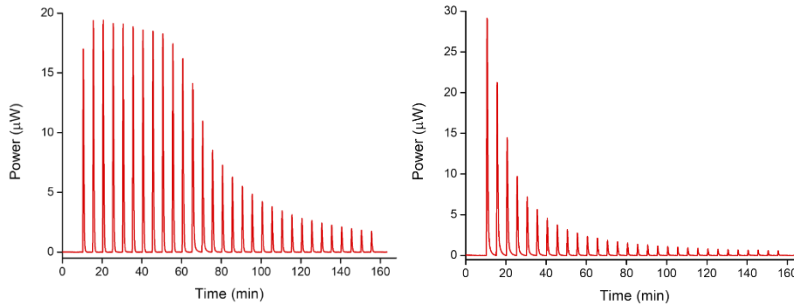

Figure 96. Typical ITC titration of **16**$^{2+}$ (2.99 mM) into a **PrS[5]**$^{COO-}$ (0.34 mM) solution at 25 °C and pH 7.6 (Left); Typical ITC titration of **7**$^{+}$ (19.68 mM) into a **PrS[5]**$^{COO-}$ (0.26 mM) solution at 25 °C and pH 7.6 (Right).

PrS[6]^{COONa}

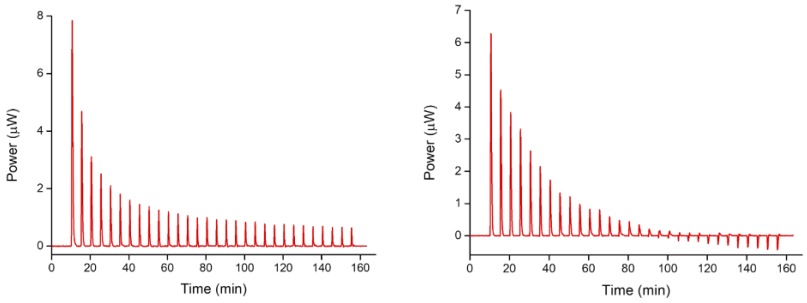

Figure 97. Typical ITC titration of **6**$^{+}$ (11.0 mM) into a **PrS[6]**$^{COO-}$ (0.75 mM) solution at 25 °C and pH 7.6 (Left); Typical ITC titration of **11**$^{2+}$ (10.5 mM) into a **PrS[6]**$^{COO-}$ (0.51 mM) solution at 25 °C and pH 7.6 (Right).

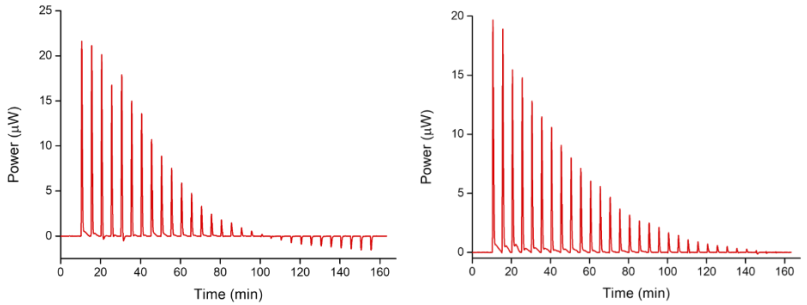

Figure 98. Typical ITC titration of **5**$^{2+}$ (14.34 mM) into a **PrS[6]**$^{COO-}$ (0.98 mM) solution at 25 °C and pH 7.6 (Left); Typical ITC titration of **16**$^{2+}$ (12.92 mM) into a **PrS[6]**$^{COO-}$ (0.82 mM) solution at 25 °C and pH 7.6 (Right).

7.0 Applications of Prismarenes by Other Groups

During this PhD project a novel class of naphthol-based macrocycle has been obtained and studied for the first time: the ***prismarenes***.[46,47,71,73] Since 2020,[46] this novel class of macrocycles has already attracted a lot of interest in the scientific community as shown by a recent highlight of prof. Wei Jiang (South University of Science and Technology, Shenzhen, China): Yang, L.-P.; Jiang, W. Prismarene: An Emerging Naphthol-Based Macrocyclic Arene. *Angew. Chem. Int. Ed.* **2020**, *7*, 15794–15796.[79]
In addition, very recently, the prismarenes have shown interesting applications as photoinitiators for polymerization[80, 81] and as nonpourous adaptive crystals for aromatic VOCs adsorption in the solid state.[82]

7.1 Prism[5]arene-Based Photoinitiator

Yincheng Chang[80] has developed a photoinitiator based on **PrS[5]*Me***. In detail, they obtained linear oligomer biradicals irradiating the **PrS[5]*Me*** under the LEDs light (365–405 nm), breaking the bond between methylene and naphthalene.[80]

---

[79] Yang, L.-P.; Jiang, W. *Angew. Chem. Int. Ed.* **2020**, *59*, 15794-15796.
[80] Song, Q.; Shang, K.; Xue, T.; Wang, Z.; Pei, D.; Zhao, S.; Nie, J.; Chang, Y. *Macromol. Rapid Commun.* **2021**, *42*, 2100299.
[81] Song, Q.; Zhao, K.; Xue, T.; Zhao, S.; Pei, D.; Nie, J.; Chang, Y. *Macromolecules.* **2021**, *54*, 8314-8320.
[82] Pei, D.; Guo, W.; Liu, P.; Xue, T.; Meng, X.; Shu, X.; Nie, J.; Chang, Y. *Chem. Eng. J.* **2022**, *433*, 134463.

This process initiate, thus, a polymerization of monomers such as acrylate – **Scheme 10**.[80] With respect to most common photoinitiators, **PrS[5]*Me*** shows a strong light absorption between 365–405 nm. In addition, there is no small molecule fragment generated during prism[5]arene fracture, so **PrS[5]*Me*** photoinitiators show much lower migration rate and cytotoxicity.

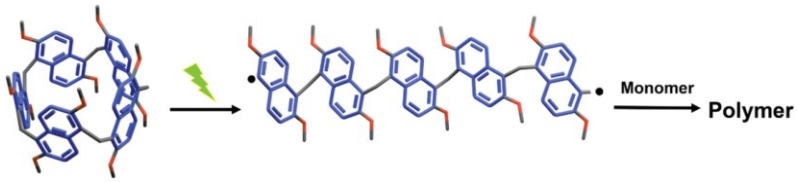

Scheme 10. Schematic diagram of free radical photopolymerization initiated by **PrS[5]*Me*** fracture, reported in **reference 80**.

7.2 Nondiffusion-Controlled Photoelectron Transfer Induced by Host−Guest Complexes of Prism[n]arenes

As previously described,[46,47] the prism[n]arenes show a good affinity for ammonium guests and form pseudorotaxane architectures stabilized by cation···π and $^{+}$NC−H···π interactions with high association constants.[46,47] On the basis of these recognition proprieties, the first prismarene-based supramolecular photoinitiators (supra-photoinitiators) were obtained and studied.[81]

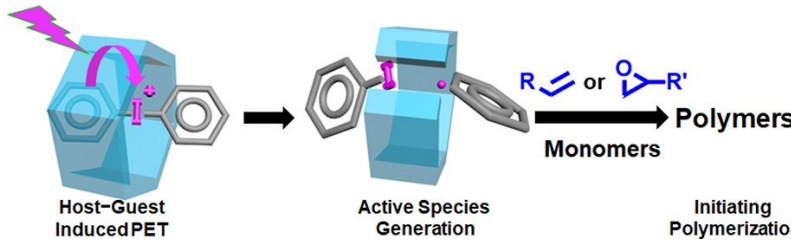

Scheme 11. Proposed mechanism for the transfer electrons to the guest with the subsequent conversion of the **PrS[5]*Me*** in linear oligomers, reported in **reference 81**.

In detail, the endo-cavity complex of **diphenyl-iodonium@PrS[5]*Me*** in **Scheme 11** was excited under light irradiation transferring electrons to the guest.[81] Subsequently the **PrS[5]*Me*** was converted in linear oligomers, releasing the active species produced by the decomposition of the guest and starting the photopolymerization – **Scheme 11**.[81]
Finally, this electron transfer results in a much higher photopolymerization rate and high conversion of epoxy resin, respect to commercial activators.[81]

7.3 Prism[5]arene-based Nonporous Adaptive Crystals

Recently, nonporous adaptive crystals (NACs) based on prism[5]arene[46] macrocycle were obtained.[82] The **PrS[5]*Me***-based NACs showed high potential in the capture of different aromatic VOCs molecules, such as toluene (**Figure 99**) and benzene, through C-H---π and C-H---O interactions between host and guest - **Figure 99**.[82]
In addition, heating the **PrS[5]*Me*** crystals, it is possible to remove the VOCs from nonpourous adaptive crystals.

This means that these crystals can be recycled and reused for further studies.[82]

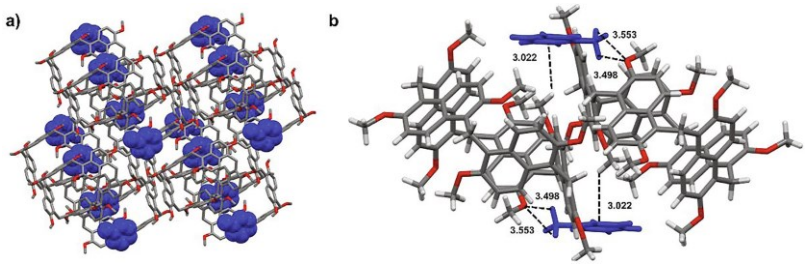

Figure 99. a) Single crystal structure of **Toluene@PrS[5]*Me***; b) The interactions between **PrS[5]*Me*** and Toluene, reported in **reference 82**.

8.0 Calix[2]naphth[2]arene: A Novel Class of Hybrid Macrocycles[83]

Among the macrocycles studied in supramolecular chemistry, many interest has been focused on hybrid systems which are
constituted by different aromatic monomers – **Figure 100**.[83, 84,85]

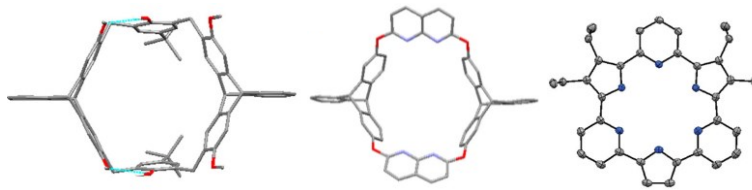

Figure 100. Single crystal X-ray structure of: (a) Triptycene-Derived Calix[6]resorcinarene-like[84a, 85]; b) Triptycene-Derived Oxacalixarene[84b, 85]; (c) Cyclo[m]pyridine[n]pyrroles[84c].

Calixarenes[12] macrocycles are constituted by *p-tert*-butylphenol rings bridged by methylene units. They show high conformational versatility; for example, the smallest

[83] Del Regno, R; Della Sala, P.; Spinella, A.; Talotta, C.; Iannone, D.; Geremia, S.; Hickey, N.; Neri, P.; Gaeta, C. *Org. Lett*. **2020** , *22,* 6166–6170.

[84](a) Li, P.-F.; Chen, C.-F. *Chem. Commun.* **2011**, *47*, 12170– 12172; (b) Hu, S.-Z.; Chen, C.-F. *Chem. Commun.* **2010**, *46*, 4199– 4201; (c) Zhang, Z.; Lim, J. M.; Ishida, M.; Roznyatovskiy, V. V.; Lynch, V. M.; Gong, H.-Y.; Yang, X.; Kim, D.; Sessler, J. L. *J. Am. Chem. Soc.* **2012**, *134*, 4076–4079.

[85] (a) Chen, C.-F.; Han, Y. *Acc. Chem. Res.* **2018**, *51*, 2093−2106. (b) Ma, Y.-X.; Han, Y.; Chen, C.-F. *J. Incl. Phenom. Macrocycl. Chem.*, **2014**, *79*, 261–281.

term of the series, namely calix[4]arene, can adopt an all-syn cone conformation,[12] which possesses a hydrophobic cavity capable of hosting a variety of species, and three other ones (partial cone, 1,3-alternate and 1,2-alternate) with one or two anti-oriented phenol rings.[12]

Recently, Chen[85] and co-workers showed that the fragment coupling strategy can be used to obtain hybrid-macrocycles constituted by different aromatic units, such as triptycene-based macrocycles, which have exhibited specific fixed conformations and molecular recognition abilities toward small organic molecules.[85]

8.1 Synthesis of Calix[2]naphth[2]arene: An Hybrid Naphthalene-Phenol Based Macrocycles [83]

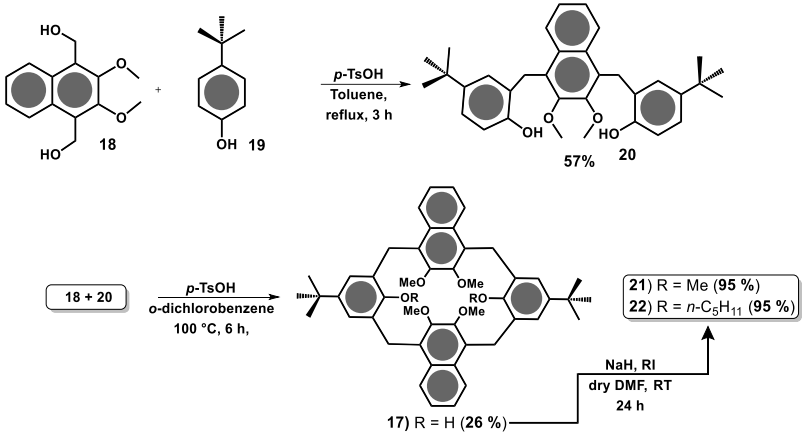

Scheme 12. Fragment coupling synthesis (FCS) of Calix[2]naphth[2]arene.[83]

Prompted by these considerations, during the second year of this PhD project, the synthesis of a hybrid naphthalene/phenol macrocycle, named calix[n]naphth[m]arene (in which n and m indicate the number of phenol and naphthalene units), by a Fragment Coupling Synthesis (FCS) has been studied - **Scheme 12**.[83]

In detail, the synthesis of calix[2]naphth[2]arene **17** was obtained by a fragment-coupling reaction between **18**[86] (already described in literature) and **20** (**Scheme 12**).[83] Derivative **20** was obtained by reaction between the derivative **18**[86] and an excess of *p-tert*-butylphenol **19**, in the presence of *p*-toluenesulfonic acid as catalyst, in toluene at reflux.[83]

Like calix[4]arene[12], the calix[2]naphth[2]arene **17** can adopts different conformations. In detail the derivative **17** can assumes the following conformations: cone, partial-cone-1 (paco1), partial-cone-2 (paco2), 1,3-alternate (1,3-alt), and 1,2-alternate (1,2-alt) (**Figure 101**).[83, 41b]

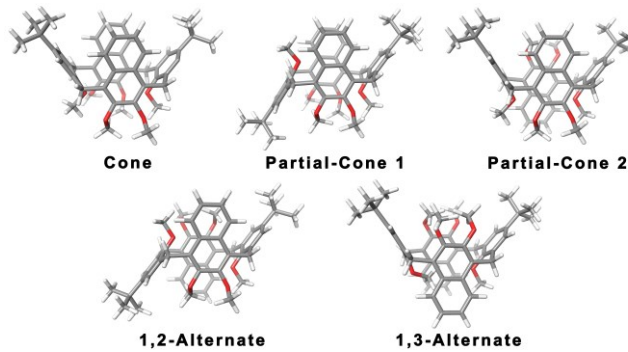

Figure 101. The five possible conformations for the Calix[2]naphth[2]arene.[83]

[86] Miller, D. O.; Georghiou, P- E. *J. Org. Chem*. **2005**, *70*, 1115–1121.

By X-ray analysis, (in collaboration with prof. Silvano Geremia and Dr. Neal Hickey from the *Università di Trieste*) the derivative **17** adopts a 1,2-alternate conformation (**Figure 102**), with C_i point symmetry. Moreover, intramolecular hydrogen bonding interactions are observed, between the OH functions and the methoxy oxygen atoms, with O···O distances of 2.78 Å (**Figure 102**).[83]

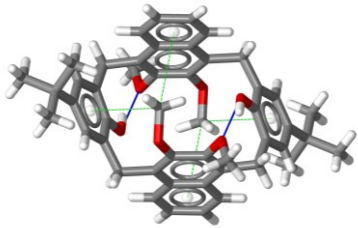

Figure 102. X-ray structure of calix[2]naphth[2]arene **17**.[83]

^{1}H VT NMR analysis reported in **Figure 104** indicates clearly that the derivative **17**[83] shows conformational mobility due to *O-through-the-annulus* passage – **Figure 103**[12].

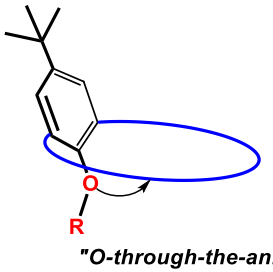

Figure 103. Chemical drawing of *O-through-the-annulus* passage.[12]

At room temperature the conformational mobility of **17** is fast with respect to the NMR time scale (600 MHz) but lowering the temperature a broadening of the methylene-bridged signals was observed at 213 K (**Figure 104a**), while at 193 K the ^{1}H NMR spectrum of **17** (**Figure 104b**) indicated clearly that it was frozen in the 1,2-alternate conformation (**Figure 104**). An energy barrier of 9.7 kcal/mol,[83] was calculated for this conformational process by Kurland-Rubin-Wise method[87].[83]

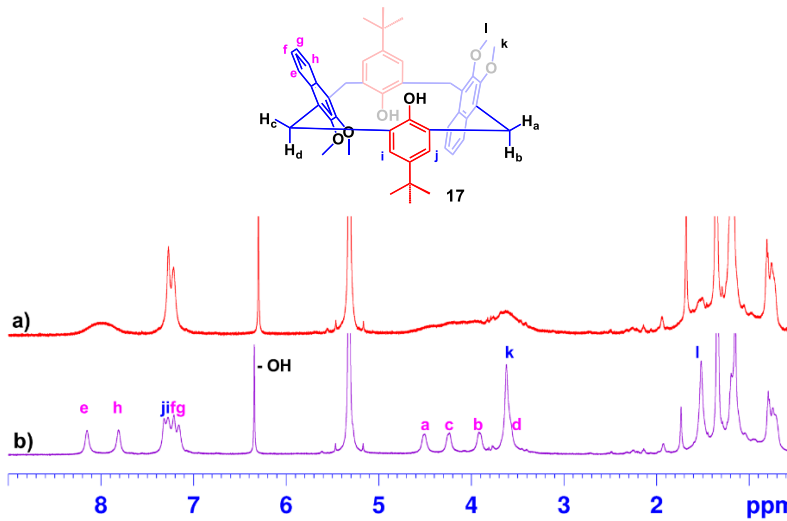

Figure 104. ^{1}H NMR spectra (600 MHz, CD_2Cl_2) of **17** at: (a) 213 K; (b) 193 K.[83]

Subsequently the derivative **17** was alkylated under the conditions reported in **Scheme 12**, the hexamethoxy-calixnaphtharene **21** was obtained in 95 % yield. Also in

[87] Kurland, R. J.; Rubin, M. B.; Wise, M. B. *J. Chem. Phys.* **1964**, *40*, 2426.

this case, the ^{1}H NMR spectrum of **21** in CD_2Cl_2 at 298 K (**Figure 105a**) shows a broad $ArCH_2Ar$ signal at 4.00 ppm, indicative of its conformational mobility due to the *OMe-through-the-annulus* passage (energy barrier of 12.3 kcal/mol[87]).[83] But lowering the temperature at **193 K**, also the derivative **21** is frozen in the 1,2-alternate conformation (**Figure 105b**).[83]

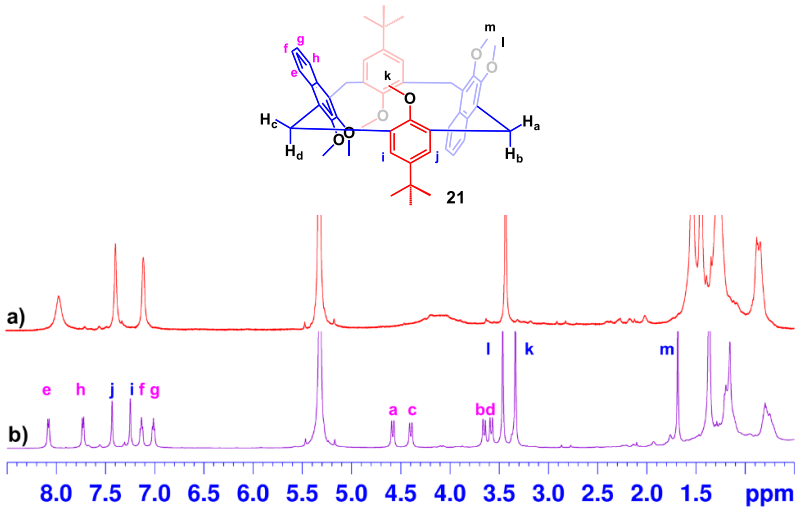

Figure 105. ^{1}H NMR spectra (600 MHz, CD_2Cl_2) of **21** at: (a) 298 K; (b) 193 K.[83]

An exhaustive 1D (**Figure 105b**) and 2D NMR studies at 193 K supported by DFT calculations[83] have confirmed the 1,2-alternate conformation of **21**. NOESY spectrum (see **Figure 116** paragraph **8.4.2**), clearly shows the anti-orientation of the couples of anisole and naphthalene rings, confirming the 1,2-alternate conformation of **17**. In fact, at 193 K, the NOESY spectrum shows the presence of a dipolar coupling between the anisole OMe singlet at 3.33 ppm and the naphthalene H signal at 8.09 ppm. [83]

Analogously, when the derivative **17** was alkylated in the presence of 1-iodopentane and NaH as base, in dry DMF (**Scheme 12**), the derivative **22** was obtained in 95 % yield. Surprisingly, the ^{1}H NMR spectrum of **22** in CD_2Cl_2 at 298 K (see **Figure 117** paragraph **8.4.2**) shows the 1,2-alternate conformation of derivatives **17** and **21** observed at low temperature. Moreover, by increasing the temperature, the ^{1}H NMR spectrum does not change; probably because the pentyl groups block the 1,2-alternate conformation, preventing the *OR-through-the-annulus* passage.[83]

8.2 Molecular Recognition Properties of Calix[2]naphth[2]arene[83]

At this point, it was interesting to study the recognition abilities of hexamethoxy-calixnaphtharene **21** host toward alkali metal cations.[83] In detail, when **Na^+ $BArF^-$** was added to the solution of **21** in CD_2Cl_2, the formation of the supramolecular complex **Na^+@21** was evidenced by ^{1}H NMR analysis. Interestingly, the ^{1}H NMR spectrum of the **Na^+@21** complex at 298 K in CD_2Cl_2, indicated the presence of the hexamethoxy-calixnaphtharene **21** in 1,2-alternate conformation (**Figure 106d**), already observed for the host free **21** at 193 K (**Figure 106b**). Similarly, the ^{1}H NMR spectrum of a 1:1 mixture of the hexamethoxy-calixnaphtharene and **K^+ $BArF^-$** or **Li^+ $BArF^-$** shows the same features (**Figures 106c** and **106e**).[83]

These results clearly indicate that in the presence of alkali metal cations such as Na^+, K^+, or Li^+ cations a conformational templation occurs, which blocks the 1,2-

alternate conformation of **21** already at room temperature (with respect to the NMR time scale).[83]

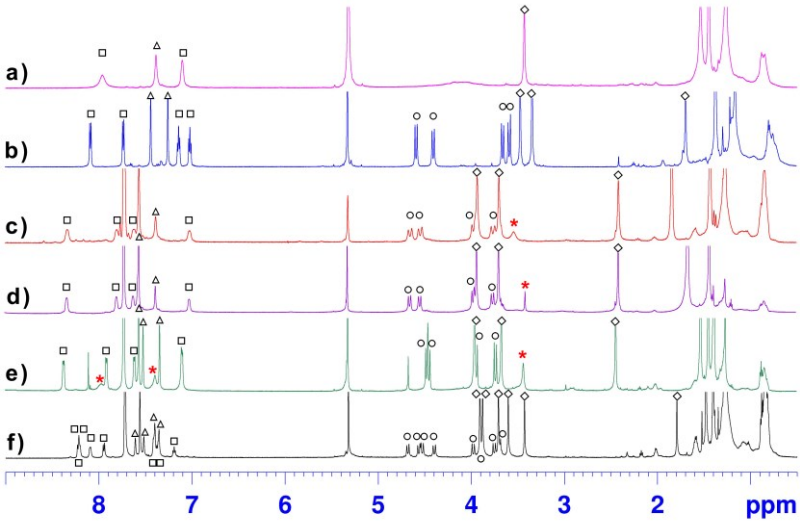

Figure 106. ^{1}H NMR spectra of **21** in CD_2Cl_2, 600 MHz: (a) at 298 K; (b) at 193 K; (c-f), 298 K, 1:1 mixture (5.3 mM) of **21** and, respectively: (c) **Li$^+$BArF$^-$**, (d) **Na$^+$BArF$^-$**, (e) **K$^+$BArF$^-$**, (f) **Cs$^+$BArF$^-$**. Marked with (*) the signals of free 5. Marked with (□ and △) the signals of the aromatic H-atoms of the naphthalene and phenol rings; (○ and ◇) the signals of the $ArCH_2Ar$ and OMe groups.[83]

In fact, the DFT-optimized structure (**Figure 107a**) of the complex **Na$^+$@21** shows that the sodium cation is inside the macrocycle cavity (**Figure 107a**) between the two naphthalene rings; the complex is stabilized by cation$\cdots\pi$ and ion-dipole interactions (MeO$\cdots$Na$^+\cdots$OMe), the latter between the OMe of the anisole rings and Na$^+$.[83] Finally, an association constant value of 2.2×10^3 M^{-1} (see **Table**

13 paragraph **8.4.3**) was calculated[88] for the **Na⁺@21** complex by integration of the ^{1}H NMR signals of the free host and complex.[83]

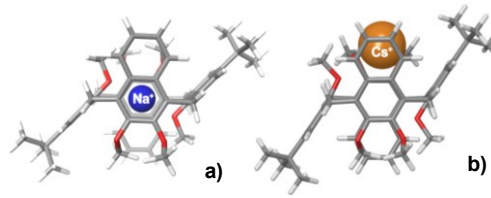

Figure 107. DFT-Optimized structures of the (a) **Na⁺@21** and (b) **Cs⁺@21** complexes at B3LYP/6-31G(d,p) and B3LYP/SDD level of theory.[83]

Similarly, the values of 2.5×10^3 M^{-1} and 2.0×10^3 M^{-1} were calculated, respectively, for the **K⁺** and **Li⁺** complexes of **21** (see **Table 13** paragraph **8.4.3**).[83]

Surprisingly, the ^{1}H NMR spectrum of the **Cs⁺@21** complex shows very different features. In fact, the pattern of signals in **Figure 106f** is only compatible with the formation of a chiral **Cs⁺@21** complex ($K_{ass} = 3.0\times10^3$). In detail the ^{1}H spectrum shows 4 AX systems (8 doublets), 12 aromatic signals and 6 OMe singlets – **Figure 106f**. DFT-optimized structure of the **Cs⁺@21** complex (**Figure 107b**), shows that the larger **Cs⁺** cation is nested on one side of the macrocycle, stabilized by cation···π interactions with a pair of naphthalene and anisole rings.[83] In this structure the macrocycle **21** is devoid of the inversion center present in the other **M⁺@21** complexes.

[88] Hirose, K. *In Analytical Methods in Supramolecular Chemistry*; Schalley, C. A., Ed.; Wiley-VCH: Weinheim, Germany, **2007**; Chapter 2, pp 17−54.

An analogous behavior was observed for the complexes of the macrocycle **22**.[83]

8.3 Conclusions[83]

In conclusion, we synthesised a new hybrid macrocycles named calix[2]naphth[2]arenes, through a fragment coupling synthesis.
Surprisingly, these macrocycles show, at 193 K and in a presence of alkali metal cations, a 1,2-alternate conformation. This conformation is rare both in the solid state and in solution for the calix[4]arene. Moreover, this conformation is also observed when alkali metal cations are added to the solution of **21** or **22** in CD_2Cl_2 at room temperature. But surprisingly, with the cation $\mathbf{Cs^+}$, the formation of chiral complexes of **21** and **22** were observed with the cation nesting on one of the two equivalent faces. Finally, these complexes are mainly stabilized by cation···π interactions between cationic guests and naphthalene rings.

8.4 Experimental Section

8.4.1 General Section

See **Paragraph 2.4.1**

The derivative **18** was synthesized according to literature procedures.[86] The ^1H and ^{13}C NMR spectra of **18** are in accord with those reported in literature.[86]

8.4.2 Procedures for the Synthesis of derivatives 17, 20, 21, and 22 and Copies of NMR Spectra[83]

Synthesis of derivative 20: A mixture of **18**[86] (3.00 g, 12.10 mmol), *p-tert*-butylphenol **19** (18.16 g, 120.90 mmol) and *p*-toluenesulfonic acid *p*-TsOH (2.30 g, 12.10 mmol) in toluene (1200 mL) was stirred at reflux, 110 °C, in an oil bath, for 3 h. After cooling at room temperature, a saturated solution of $NaHCO_3$ (500 mL) was added and the aqueous layer was extracted with $CHCl_3$ (3 x 150 mL). Then, the organic layer was washed with water (100 mL), dried over Na_2SO_4, filtered and the solvent was evaporated under vacuum. The crude product was purified through chromatographic column on silica gel (petroleum ether/ EtOAc = 9:1, v/v) to give the pure product **20** (3.50 g, 57 %) as a white solid.

Synthesis of derivative 17: To a solution of *p*-TsOH (0.02 g, 0.11 mmol) in *o*-dichlorobenzene (32 mL) was added a solution of **18** (0.05 g, 0.21 mmol) and **20** (0.11 g, 0.21 mmol) in *o*-dichlorobenzene (64 mL) under nitrogen atmosphere at 100 °C (oil bath). The mixture was stirred at 100 °C for 6 h. The solution was evaporated in vacuum and then the mixture was separated by chromatographic column on silica gel (petroleum ether/ CH_2Cl_2 = 6:4, v/v) to give the pure product **17** (0.040 g, 26 %).

Synthesis of derivatives 21 and 22: To a solution of **17** (15.00 mg, 0.02 mmol) in dry DMF (7 mL) was added NaH (8.30 mg, 60% dispersion in mineral oil, 0.21 mmol) under nitrogen atmosphere at 0 °C. The mixture was stirred for

1 h at room temperature. Then alkyl iodide (1.03 mmol) was slowly added and the resulting solution was stirred for 24 h at room temperature. After, 10 mL of 1 M solution of HCl was added. The mixture was extracted with $CHCl_3$ (3 x 20 mL), and the organic layer was dried over Na_2SO_4, filtered, and concentrated under reduced pressure. The crude product was purified through chromatographic column on silica gel (petroleum ether/ CH_2Cl_2 = 6:4, v/v).

Derivative 20:

M.p.: 180.2-181.2 °C; **^{1}H NMR** (600 MHz, $CDCl_3$, 298 K): δ 8.30 (m, ArH, 2H), 7.46 (m, ArH, 2H), 7.43 (d, *J* = 2.4 Hz, ArH ,2H), 7.34 (s, O*H*, 2H), 7.09 (m, ArH, 2H), 6.74 (d, *J* = 8.4 Hz, ArH, 2H), 4.33 (s, ArC*H*$_2$Ar, 4H), 4.08 (s, OC*H*$_3$, 6H), 1.25 (s, *t*-Bu,18H); **^{13}C NMR** {^{1}H} (150 MHz, $CDCl_3$, 298 K): δ 152.6, 147.8, 142.7, 131.1, 128.2, 127.4, 125.6, 125.3, 124.9, 124.2, 116.1, 62.2, 34.1, 31.7, 27.5; **HRMS** (FT-ICR MALDI) m/z $[M]^+$ calcd for $C_{34}H_{40}O_4$: 512.2927; found: 512.2926.

Derivative 17:

M.p.: > 300 °C dec.; **^{1}H NMR** (400 MHz, $CDCl_3$, 298 K): δ 8.04 (m, ArH, 4H), 7.32 (s, ArH, 4H), 7.22 (m, ArH, 4H), 6.05 (s, O*H*, 2H), 4.25 and 4.06 (AB system, *J* = 14.8 Hz, ArC*H*$_2$Ar, 8H), 2.73 (s, OC*H*$_3$, 12H), 1.44 (s, *t*-Bu, 18H); **^{13}C NMR** {^{1}H} (150 MHz, $CDCl_3$, 298 K): δ 151.9, 148.8, 141.3, 130.3, 127.2, 127.1, 126.5, 124.9, 123.9, 60.0, 34.1, 32.0, 29.4; **HRMS** (FT-ICR MALDI) m/z $[M]^+$ calcd for $C_{48}H_{52}O_6$: 724.3764; found: 724.3761.

Derivative 21: The macrocycle **21** was obtained in 95% yield (15 mg) as a white solid.
M.p.: > 300°C dec.; **^{1}H NMR** (300 MHz, TCE-d_2, 373 K): δ 7.80 (m, ArH, 4H), 7.22 (s, ArH, 4H), 6.94 (m, ArH, 4H), 4.06 and 3.96 (AB system J = 14.4 Hz, ArCH_2Ar, 8H), 3.30 (s, OCH_3, 6H), 2.67 (s, OCH_3, 12H), 1.33 (s, *t*-Bu,18H); **^{13}C NMR** {^{1}H} (75 MHz, TCE-d_2, 373 K): δ 157.0, 150.8, 145.2, 134.7, 130.2, 128.0, 127.1, 124.7, 122.7, 61.3, 59.5, 34.3, 31.9, 29.8; **HRMS** (FT-ICR MALDI) m/z $[M]^+$ calcd for $C_{50}H_{56}O_6$: 752.4077; found: 752.4082.

Derivative 22: The macrocycle **22** was obtained in 95 % yield (17 mg) as a white solid.
M.p.: > 300°C dec.; **^{1}H NMR** (600 MHz, TCE-d_2, 298 K): δ 7.87 (d, J = 8.4 Hz, ArH, 2H), 7.67 (d, J = 9.0 Hz, ArH, 2H), 7.25 (br s, ArH, 2H), 7.11 (br s, ArH, 2H), 7.00 (m, ArH, 2H), 6.90 (m, ArH, 2H), 4.44 (d, J = 13.8 Hz, ArCH_2Ar, 2H), 4.23 (d, J = 14.4 Hz, ArCH_2Ar, 2H), 3.52-3.41 (overlapped, ArCH_2Ar + OCH_2(CH$_2$)$_3$CH$_3$, 8H), 3.33 (s, OCH_3, 6H), 1.79 (s, OCH_3, 6H), 1.26 (s, *t*-Bu,18H), 1.09-1.11 (overlapped, OCH$_2$(CH_2)$_3$CH$_3$, 12H), 0.72 (m, OCH$_2$(CH$_2$)$_3$CH_3, 6H); **^{13}C NMR** {^{1}H} (100 MHz, CD_2Cl_2, 298 K): δ 156.1, 150.8, 150.4, 144.8, 135.7, 134.1, 130.6, 129.6, 128.9, 128.4, 128.1, 126.5, 124.8, 124.8, 123.3, 122.8, 75.1, 60.1, 59.2, 34.4, 31.8, 30.2, 29.3, 23.1, 14.3; **HRMS** (FT-ICR MALDI) m/z $[M]^+$ calcd for $C_{58}H_{72}O_6$: 864.5329; found: 864.5318.

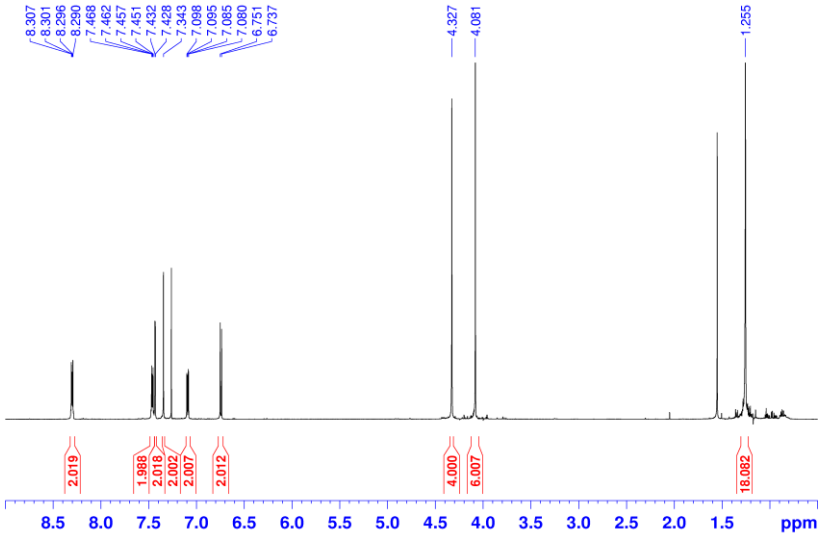

Figure 108. ^{1}H NMR spectrum of **20** ($CDCl_3$, 600 MHz, 298 K).

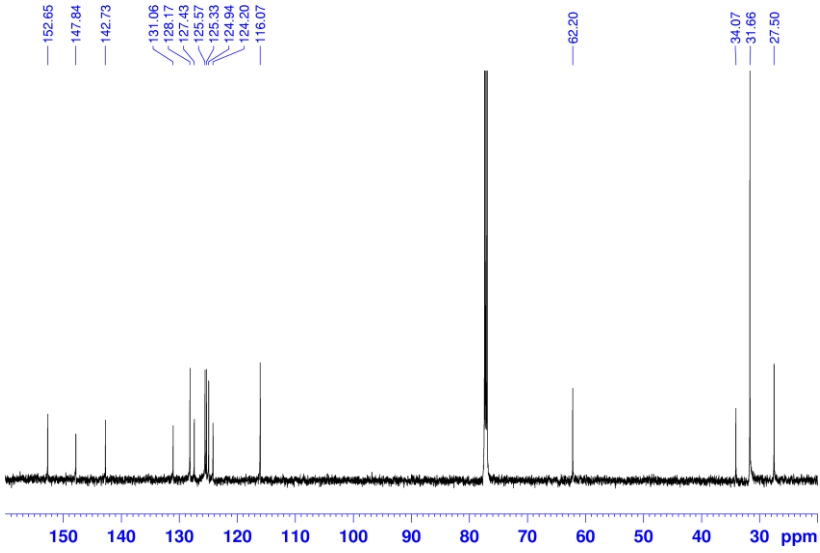

Figure 109. ^{13}C NMR spectrum of **20** ($CDCl_3$, 150 MHz, 298 K).

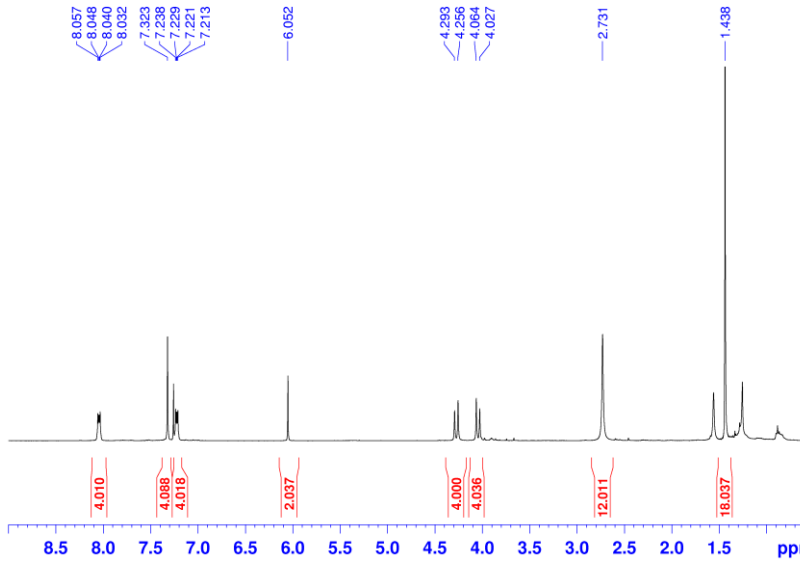

Figure 110. ^{1}H NMR spectrum of **17** ($CDCl_3$, 400 MHz, 298 K).

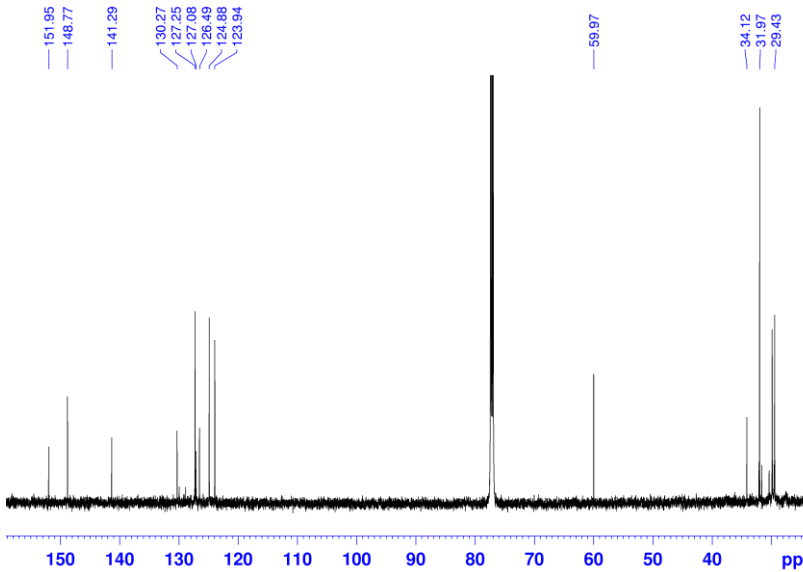

Figure 111. ^{1}C NMR spectrum of **17** ($CDCl_3$, 150 MHz, 298 K).

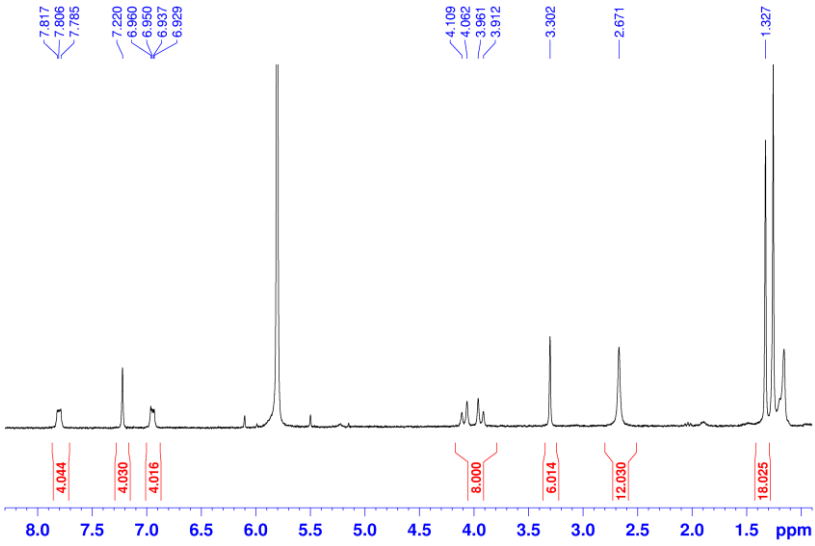

Figure 112. ^{1}H NMR spectrum of **21** (TCE-d_2, 300 MHz, 373 K).

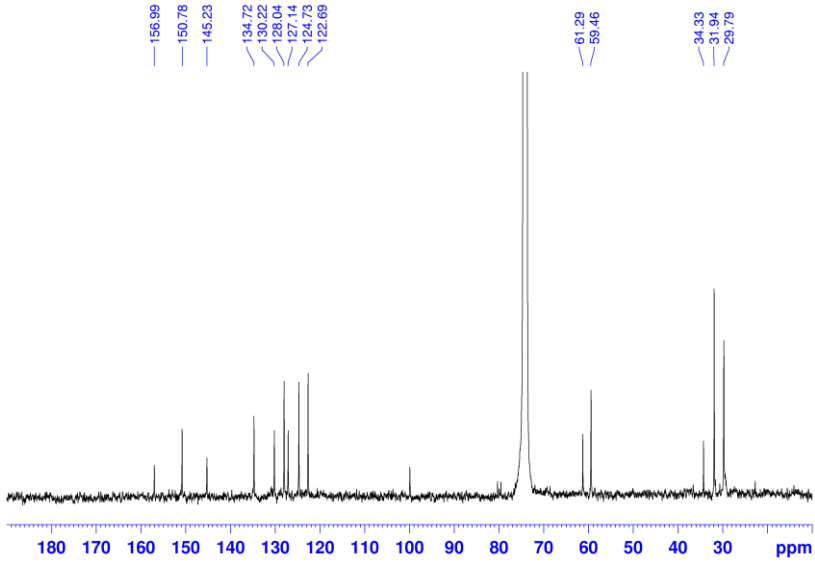

Figure 113. ^{13}C NMR spectrum of **21** (TCE-d_2, 75 MHz, 373 K).

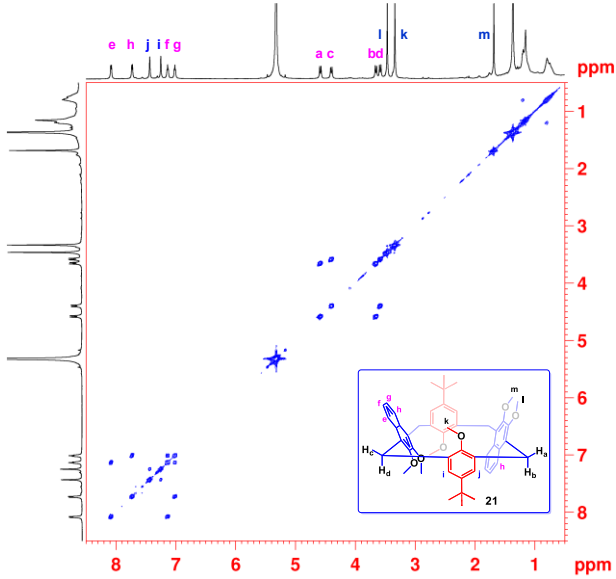

Figure 114. 2D-DQF COSY spectrum of **21** (CD_2Cl_2, 600 MHz, 193 K).

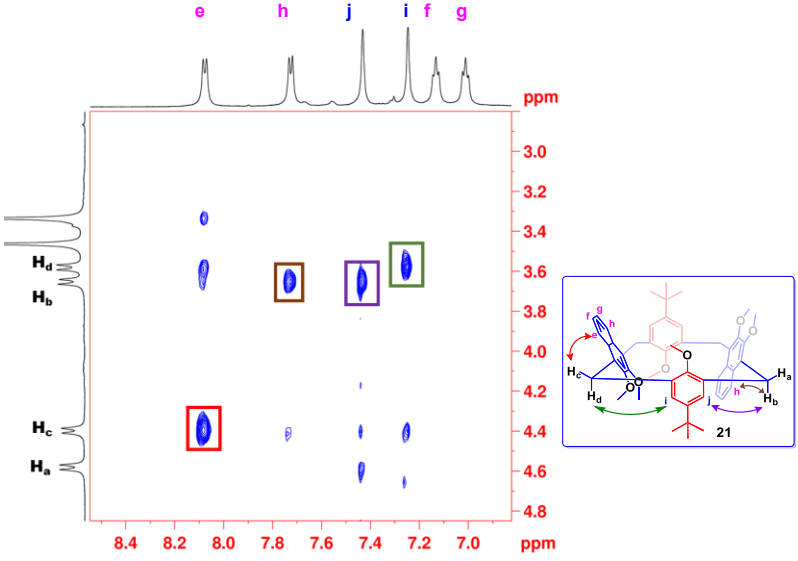

Figure 115. Significant portion of the NOESY spectrum of **21** (CD_2Cl_2, 600 MHz, 193 K).

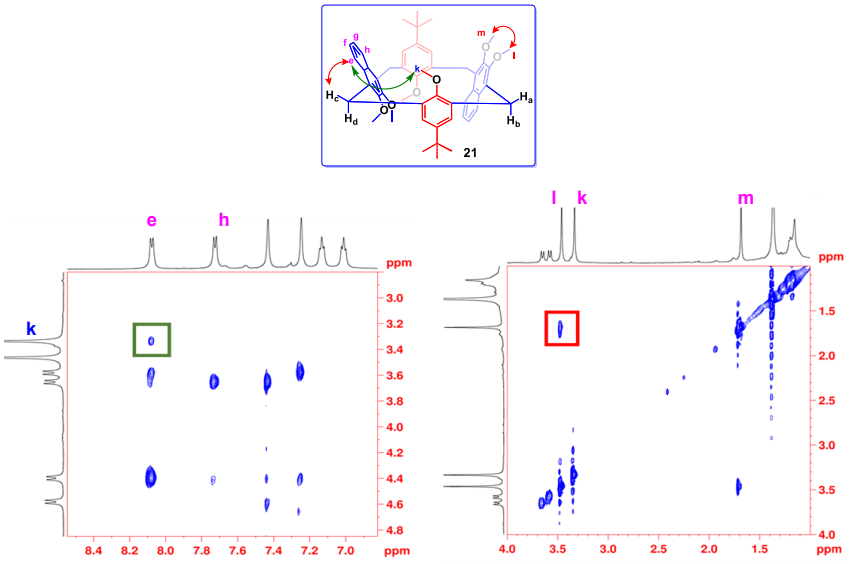

Figure 116. Significant portions of the NOESY spectrum of **21** (CD_2Cl_2, 600 MHz, 193 K).

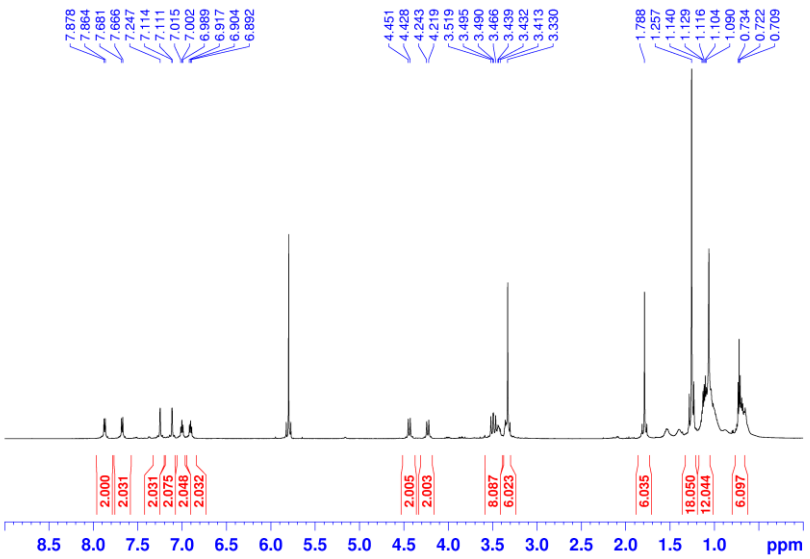

Figure 117. ^{1}H NMR spectrum of **22** (TCE-d_2, 600 MHz, 298 K).

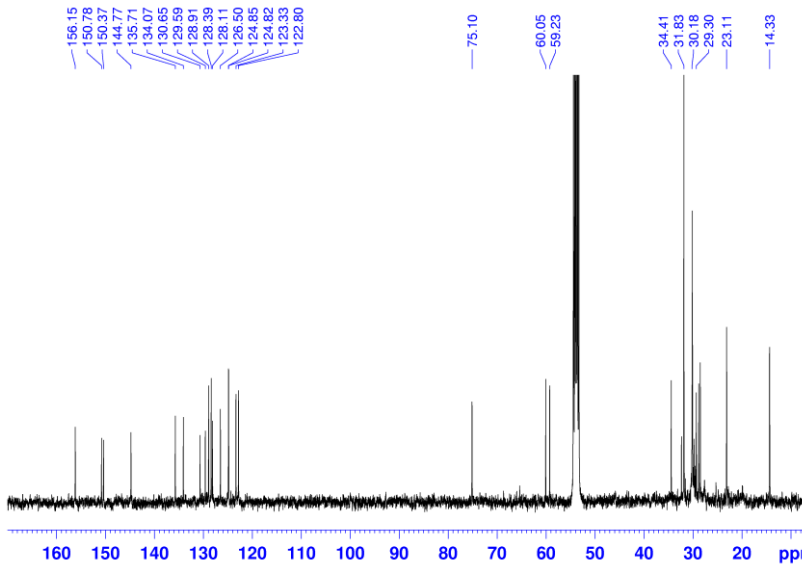

Figure 118. ^{13}C NMR spectrum of **22** (CD_2Cl_2, 100 MHz, 298 K).

8.4.3 ^1H NMR determination of K_{ass} values[83, 62]

The association constant values of the complexes were calculated by means of three methods:

a) ^1H NMR competition experiments. In this case, was performed an analysis of a 1:1:1 mixture of host, and two guests in an NMR tube.
b) Integration of free and complexed ^1H NMR signals of host. In this case, an equimolar quantity of host and guest was solubilized in CD_2Cl_2.
c) Quantitative ^1H NMR experiments using TCE as the internal standard[5]. In this case, ^1H NMR experiments were carried out on a 1:1 mixture of host and guest containing a known amount of 1,1,2,2-tetrachloroethane. (d= 1.59 g/mL) as internal standard.

	21	22
Li^+TFPB^-	$2.0\pm0.3\times10^3$ [b]	$1.5\pm0.3\times10^3$ [c]
Na^+TFPB^-	$2.2\pm0.2\times10^3$ [a]	$3.7\pm0.3\times10^3$ [c]
K^+TFPB^-	$2.5\pm0.3\times10^3$ [b]	$5.1\pm0.6\times10^3$ [c]
Cs^+TFPB^-	$3.0\pm0.2\times10^3$ [c]	$1.7\pm0.2\times10^3$ [d]

Table 13. Association constant (K_{ass}, M^{-1}) values for the formation of the complexes between the sodium and potassium cations as **BArF**$^-$ salts and the derivatives **21** and **22**. Determined by ^1H NMR experiments in CD_2Cl_2 (400 and 600 MHz).

[a] Calculated by competition experiment at 298 K with **K$^+$ BArF**$^-$. [b] Calculated at 298 K by integration of ^1H NMR signals of free host and complexed species. [c] Calculated by quantitative ^1H NMR spectroscopy at 298 K analysis using TCE as internal standard. [d] Calculated by quantitative ^1H NMR study at 253 K analysis using TCE as internal standard.

8.4.4 Determination of the Crystallographic Structures of Calix[2]naphth[2]arene[83]

These studies were performed in collaboration with prof. Silvano Geremia and Dr. Neal Hickey from the *Università di Trieste*.

Derivative **17** crystallized in the centrosymmetric triclinic P-1 space group. The asymmetric unit contains a ½ molecule of **17** which lies on a centre of inversion and one co-crystallized $CHCl_3$ solvent molecule located outside of the ring. All non-hydrogen atoms of the well-ordered structure were anisotropically refined with hydrogen atoms placed at the geometrically calculated positions using the

riding model. Crystal data and final refinement details for the structures are reported in **Table 14.**

Small colourless single crystals of **17** suitable for X-ray structure determination were analysed using synchrotron radiation and cryo-cooling techniques.

The molecule crystallized in the centrosymmetric triclinic P-1 space group. The cyclic molecules lie on crystallographic centres of inversion (C_i molecular point symmetry) and the asymmetric unit contains a ½ molecule of **17**, and one $CHCl_3$ solvent molecules located outside of the macrocycle (**Figure 119a**).

The mean planes of the oppositely oriented naphthalene moieties are almost orthogonal with respect to the mean plane defined by the four bridging methylene groups (dihedral angles of 84°); while the oppositely oriented phenyl ring t-butyl groups of are tilted outwards from the centre of the molecule (dihedral angles between phenyl and methylene bridges of 57°). Interestingly, the mean planes of the naphthalene and phenyl moieties are near orthogonal (dihedral angle of 87°) and the aromatic walls define an oblique quadrangular prism (**Figure 119b**). The distances between parallel phenyl rings and parallel naphthalene moieties are 5.3 Å and 5.0 Å respectively. Important intramolecular hydrogen bond interactions are observed between the hydroxy group donors and the adjacent methoxy oxygen acceptors with O•••O distances of 2.782 Å. The prismatic structure is closed above and below by methoxy and methyl groups which protrude towards the centre of the macrocycle (**Figure 119c**). The chloroform solvent molecules form interesting symmetric intermolecular C−H···π H-bonds with the arene moieties of **17** (**Figure 119a**). The distance between the H atom of $CHCl_3$ and the barycentre of aromatic ring is 2.3 Å**.**

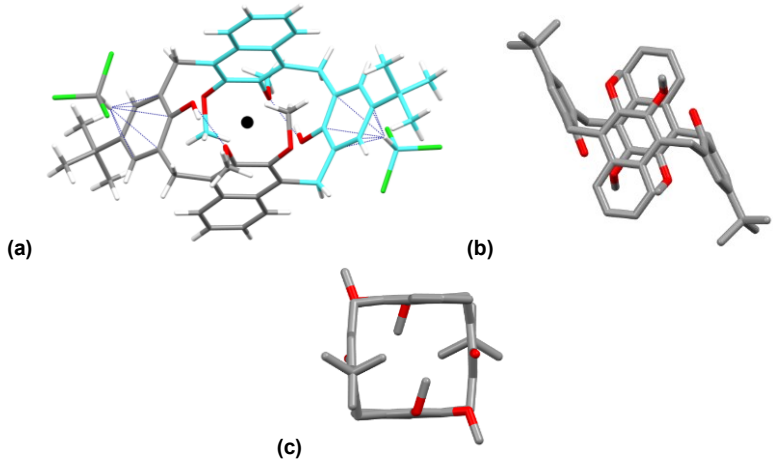

Figure 119. X-ray structure of **17**. (a) Capped stick model of the unit cell which contains one molecule of **17** and two $CHCl_3$ molecules. The centre of crystallographic symmetry is indicated as black dot and the symmetry related carbon atoms are shown in grey/cyan colours. H-bonds are shown as dotted lines. (b) View of the **17** molecule evidencing the oblique rectangular prism geometry of the molecule. (c) View of **17** along the direction of the central prism axis.

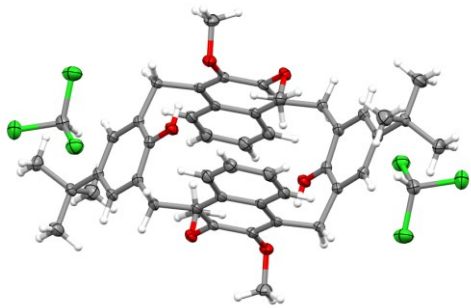

Figure 120. X-ray structure of **17**. The unit cell contains one centrosymmetric molecule of **17** and two $CHCl_3$ molecules. The asymmetric unit is half of the unit cell. Thermal ellipsoids at 50% probability.

Empirical formula	$C_{48}H_{52}O_6$, 2($CHCl_3$)
Formula weight	963.63
Temperature (K)	100(2)
Wavelength (Å)	0.7
Crystal system	Triclinic
Space group	P-1
Unit cell dimensions (Å, °)	a = 9.767(5) b = 10.215(3) c = 13.129(4) α = 77.68(2) β = 76.179(19) γ = 66.86(3)
Volume (Å^3)	1159.1(8)
Z	1
ρ_{calcd} (g/cm^3)	1.38
μ (mm^{-1})	0.415
F(000)	504.0
Reflections collected	18053
Independent reflections	5259
Data / restraints / parameters	5259 / 0 / 286
GooF	1.022
R_1 / wR_2 [I>2σ(I)]	0.069 / 0.189
R_1 / wR_2 all data	0.0886 / 0.2047
Largest. Diff. peak/hole (e Å^{-3})	0.984 / -0.709
CCDC code	1991495

Table 14. Crystal data and structure refinement for **17.**

8.4.5 Conformational Studies by DFT Calculations[83]

The lowest energy structures for the 5 conformations of **21** in **Figure 121** were obtained by molecular mechanics calculations. Successively, the structures were optimized by DFT calculations (Gaussian 16) at B3LYP/6-31G(d,p) level of theory. Finally, single point energies were calculated at B3LYP/6-31G(d,p) level of theory, **Table 15**.

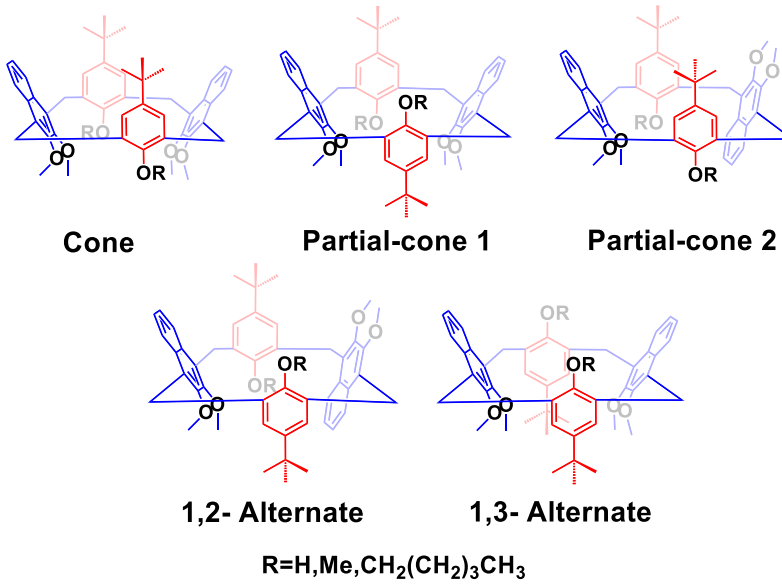

Figure 121. Possible conformations of the Calix[2]naphth[2]arene.

	B3LYP/6-31G(d,p) Single point energy (hartree)	ΔE in kcal/mol	Z_i	*Fractional Population*
21$^{1,2\text{-}alt}$	-2390.43096	-	1.0000	99.39
21^{cone}	-2390.42759	2.11	0.0040	0.40
21^{paco2}	-2390.42700	2.48	0.0015	0.15
21^{paco1}	-2390.42632	2.91	0.0005	0.05
21^{1,3alt}	-2390.41353	10.94	-	0.01

Table 15. Single point energies of the five conformations of **21** and Boltzmann populations at 193 K for the conformers of **21.**

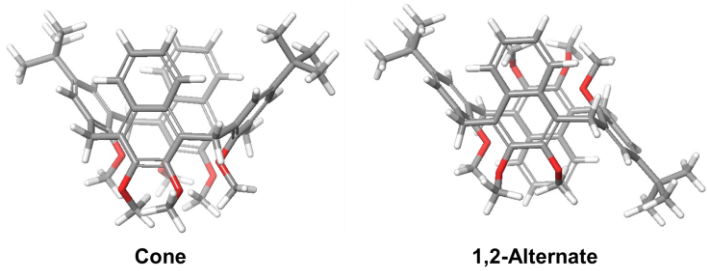

Figure 122. DFT-optimized structures (B3LYP/6-31G(d,p)) of the cone and 1,2-Alternate conformations of **21**.

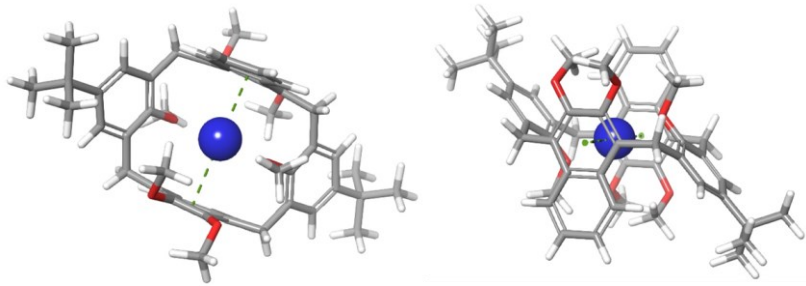

Figure 123. DFT-optimized structures (B3LYP/6-31G/(d,p)) of the **Na^+@21** complex.

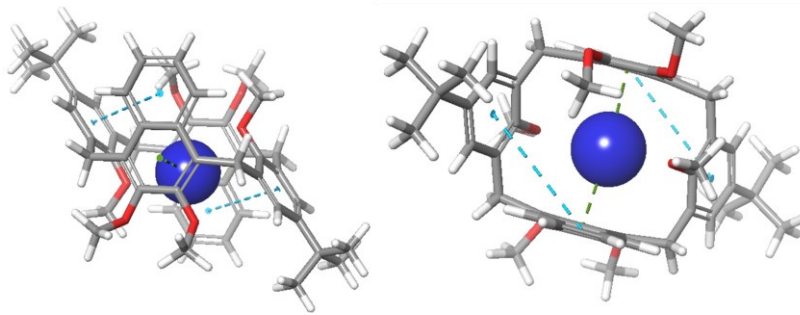

Figure 124. DFT-optimized structures (B3LYP/6-31G/(d,p)) of the **K^+@21** complex.

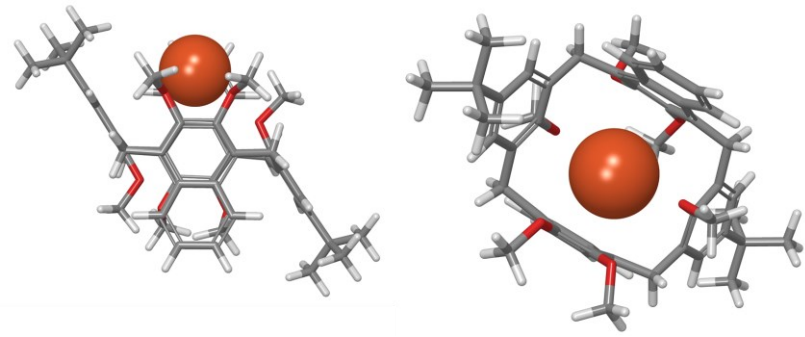

Figure 125. DFT-optimized structures (B3LYP/SDD) of the **Cs^+@21** complex.

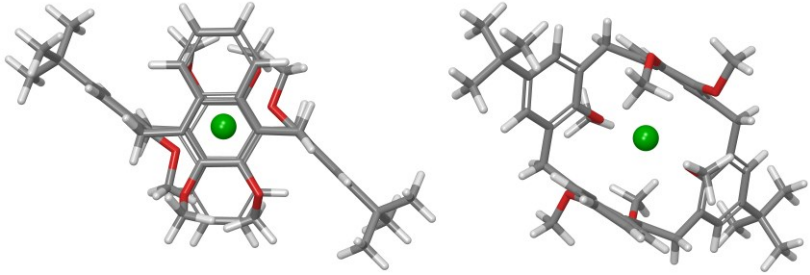

Figure 126. DFT-optimized structures (B3LYP/6-31G/(d,p)) of the **Li^+@21** complex.

Publications Relative to this Ph.D. Project

- Paolo Della Sala, **Rocco Del Regno**, Carmen Talotta, Amedeo Capobianco, Neil Hickey, Silvano Geremia, Margherita De Rosa, Aldo Spinella, Annunziata Soriente, Placido Neri and Carmine Gaeta "Prismarenes: A New Class of Macrocyclic Hosts Obtained by Templation in a Thermodynamically Controlled Synthesis" *J. Am. Chem. Soc.* **2020**, *142*, 1752-1756. **DOI**: 10.1021/jacs.9b12216.

- **Rocco Del Regno**, Paolo Della Sala, Aldo Spinella, Carmen Talotta, Dalila Iannone, Silvano Geremia, Neal Hickey, Placido Neri and Carmine Gaeta "Calix[2]naphth[2]arene: A Class of Naphthalene-Phenol Hybrid Macrocyclic Hosts" *Org. Lett*. **2020**, *22*, 6166–6170. **DOI**: 10.1021/acs.orglett.0c02247.

- Paolo Della Sala[89], **Rocco Del Regno**[89], Luca Di Marino, Carmela Calabrese, Carmine Palo, Carmen Talotta, Silvano Geremia, Neil Hickey, Amedeo Capobianco, Placido Neri and Carmine Gaeta "An intramolecularly self-templated synthesis of macrocycles: self-filling effects on the formation of Prismarenes" *Chem. Sci.*, **2021**, *12*, 9952-9961. **DOI**: 10.1039/D1SC02199K.

- **Rocco Del Regno**, Paolo Della Sala, Davide Picariello, Carmen Talotta, Aldo Spinella, Placido Neri and Carmine Gaeta "*per*-Hydroxylated Prism[n]arenes: Supramolecularly Assisted Demethylation of Methoxy-Prism[5]arene" *Org. Lett.*

[89] P. D. S. and R. D. R. contributed equally to this work.

2021, *23*, 8143−8146. **DOI**: 10.1021/acs.orglett.1c02800.

- **Rocco Del Regno**, Giuseppina D. G. Santonoceta, Paolo Della Sala, Margherita De Rosa, Annunziata Soriente, Carmen Talotta, Aldo Spinella, Placido Neri, Carmelo Sgarlata and Carmine Gaeta "Molecular Recognition in an Aqueous Medium Using Water-Soluble Prismarene Hosts" *Org. Lett.* **2022**, *24*, 2711-2715. **DOI**: 10.1021/acs.orglett.2c00819.

Contribution to National and International Conferences

Poster Presentation

- **Rocco Del Regno**, Paolo Della Sala, Carmen Talotta, Placido Neri, Silvano Geremia, Neal Hickey, Amedeo Capobianco, Luca Di Marino, Carmela Calabrese, Carmine Palo, Aldo Spinella, Carmine Gaeta *"Prism[n]arene Macrocycles: A New Tool in Supramolecular Chemistry"* **Poster** in XXVII Congresso Nazionale della Società Chimica Italiana – **2021** – Virtual Edition.

- **Rocco Del Regno**, Paolo Della Sala, Davide Picariello, Carmen Talotta, Aldo Spinella, Placido Neri, Carmine Gaeta *"Supramolecularly Assisted Synthesis of per-Hydroxylated Prism[n]arenes"* **Poster** in Supramolecular Chemistry Days for Young Researchers – **2021** – Virtual Edition.